High Frequency Oscillations (HFOs: 80-500 Hz), ictogenesis and epileptogenesis

PARIYA SALAMI

Integrated Program in Neuroscience (IPN)
McGill University
Montreal, QC, Canada

April, 2015

A thesis submitted to McGill University in partial fulfillment of the requirements of the degree of Doctor of Philosophy

Acknowledgements

I would have not been able to accomplish my research goals without the support and contribution of many people to whom I am truly grateful. Although I will not be able to thank everyone, I want to take the time to acknowledge all their help and support.

First of all, I would like to express my deepest gratitude to my supervisor Dr. Massimo Avoli for believing in me and accepting me in his laboratory without any prior background in the field. The experience I acquired in his lab and everything I learned from him is something I can never forget. I cannot thank him enough for all the support he provided me with throughout the course of my PhD.

I am thankful to Dr. Jean Gotman for his very useful feedback and for patiently teaching me how my findings can be applied in clinical settings.

I am grateful to my committee member Dr. David Ragsdale for his guidance and valuable advices in the field.

I would like to take this opportunity to thank Maxime Lévesque who guided me through my research with great patience. He is not only the best mentor but also an amazing friend with whom I laughed a lot. Without his help and support I would have not been able to accomplish my goals.

I am deeply grateful to all my colleagues at the lab, Ruba, Charles, Gabriella, Rochelle, Shabnam, Zahra, and all my friends at the MNI for making a very friendly and supportive environment. You all made these years the most joyful years ever.

I am truly thankful to Toula Papadopoulos for all her assistance whenever I came to her. I would also like to thank the IPN administration (Dr. Josephine Nalbantoglu, Katherine Vanka, Safiya Simon, Micha Chemali); Neuro Media services (specially Jean-Paul Acco and Susan Kaupp) and everyone at the MNI Animal Care Facility (specially Cathy Hunt and Benoit Chambaron) for their readiness and all their help.

I would like to take this opportunity to acknowledge the support I received from all my dearest friends and relatives all around the world. Thank you for laughing with me, encouraging me, and always being there for me.

Lastly, I would like to thank my family, my biggest supporters of all time. First, I must thank my amazing parents, for having trust and confidence in me and for all their endless support. Finally, to my beloved brother: I always miss our long talks and laughs, your sincere love means a lot to me; I love you so much and you are always with me even though distance keeps us apart.

Contributions of authors

Chapter 2: Salami P, Lévesque M, Gotman J, Avoli M. A comparison between automated methods of high-frequency oscillations (80-500 Hz) during seizures. *Journal of Neuroscience Methods*, 2012 211(2):265-71.

PS and MA designed the study. PS performed the experiments, developed the methods, analyzed the data, and wrote the first draft of the manuscript. PS, ML, JG and MA reviewed the manuscript.

Chapter 3: Lévesque M, Salami P, Gotman J, Avoli M. Two seizure-onset types reveal specific patterns of high-frequency oscillations in a model of temporal lobe epilepsy. *Journal of Neuroscience*, 2012 32(38):13264-72.

ML, PS and MA designed the study. ML and PS performed the experiments and analyzed the data. ML wrote the first draft of the manuscript. PS, ML, JG and MA reviewed the manuscript.

Chapter 4: Lévesque M, Salami P, Behr C, Avoli M. Temporal lobe epileptiform activity following systemic administration of 4-Aminopyridine in rats. *Epilepsia*, 2013 54(4):596-604.

ML, PS and MA designed the study. ML and PS performed the experiments. ML, PS, and CB analyzed the data. ML wrote the first draft of the manuscript. PS, ML, CB, JG and MA reviewed the manuscript.

Chapter 5: Salami P, Lévesque M, Gotman J, Avoli M. Distinct EEG seizure patterns reflect different seizure generation mechanisms. *Journal of Neurophysiology*, 2015 113(7):2840-4.

PS and MA designed the study. PS performed the experiments, analyzed the data, and wrote the first draft of the manuscript. PS, ML, JG and MA reviewed the manuscript.

Chapter 6: Salami P, Lévesque M, Benini R, Behr C, Gotman J, Avoli M. Dynamics of interictal spikes and high-frequency oscillations during epileptogenesis in temporal lobe epilepsy. *Neurobiology of Disease*, 2014 67:97-106.

PS and MA designed the study. PS, RB, and BC performed the experiments, PS analyzed the data and wrote the first draft of the manuscript. PS, ML, JG and MA reviewed the manuscript.

Abstract

Mesial temporal lobe epilepsy (MTLE), one of the most common forms of focal epilepsy, is characterized by recurrent seizures that originate from limbic structures such as the hippocampus, the amygdala or the entorhinal cortex. Around 30% of MTLE patients do not benefit from antiepileptic drug therapy and are, thus, potential candidates for surgical removal of the epileptogenic zone but approximately 30% of them do not become seizure free. Therefore, it is of paramount importance to understand the mechanisms underlying MTLE to develop new therapeutical interventions.

Interictal spikes, and more recently high-frequency oscillations (HFOs, 80-500 Hz), recorded from MTLE patients and in animal models mimicking this disorder are markers of abnormal patterns of neural network activity. In addition, studies of HFOs and interictal spikes can reveal information about the mechanisms underlying ictogenesis and epileptogenesis. In my thesis, by employing the pilocarpine model of MTLE and the systemic administration of either 4-Aminopyridine (4AP) or picrotoxin. I addressed the role of interictal spikes and HFOs in ictogenesis, and epileptogenesis.

The main findings of my studies can be summarized as follows:

I first developed an automated method for detecting HFOs during pre-ictal, ictal, and post-ictal periods; this method, which employs a reference period before the seizure onset for signal normalization, provides results that are more similar to visual analysis in detecting HFOs compared to other automated methods.

Employing this method, I discovered that two main types of seizure onsets in pilocarpine treated rats, namely low-voltage fast and hypersynchronous onset patterns, are associated with different HFO types.

The results obtained in the pilocarpine treated rats were confirmed and replicated with the systemic injection of 4-aminopyridine (4AP) or picrotoxin. Specifically, I discovered that 4AP-induced low-voltage fast seizures are mostly associated to ripples, whereas hypersynchronous seizures induced with picrotoxin are mostly associated to fast ripples.

Finally, I identified specific changes in interictal spikes and HFOs during the transition from latent to chronic period; these changes may indeed reflect pathophysiological modifications occurring in limbic structures that are implicated in epileptogenesis.

Altogether, my findings demonstrated that: (i) there are specific changes in network excitability occurring during low-voltage fast-onset and hypersynchronous-onset seizures, and that these differences can be pinpointed *in vivo* by analyzing HFOs, and (ii) possible changes in synaptic plasticity in limbic structures during epileptogenesis are reflected by alterations in interictal spikes and HFOs. I anticipate that my findings will open new perspectives in epilepsy diagnostic approaches as well as in developing new antiepileptic drugs for controlling epileptic seizures.

Résumé

L’épilepsie mésiale temporale (EMT), l'une des formes les plus courantes d’épilepsie focale, se caractérise par des crises récurrentes dont l’origine se situe dans les structures limbiques telles que l'hippocampe, l'amygdale ou le cortex entorhinal. Environ 30% des patients ayant l’EMT demeurent réfractaires au traitement et sont donc des candidats potentiels à l'ablation chirurgicale de la zone épileptogène. Cependant, 30% de ces patients demeurent toujours épileptiques après la chirurgie. Par conséquent, il est d'une importance primordiale de comprendre les mécanismes sous-jacents à l’EMT, afin de développer de nouvelles interventions thérapeutiques.

Les pointes intericales, et plus récemment les oscillations à haute fréquence (OHF, 80-500 Hz), enregistrées chez les patients atteints d’EMT et dans les modèles animaux reproduisant ce trouble, sont considérées comme marqueurs d’une activité pathologique des réseaux neuronaux. En effet, les OHF et les pointes intericales révèlent des informations sur les mécanismes sous-jacents à l’ictogenèse et l’épileptogenèse. Dans ma thèse, à l’aide du modèle animal de l’EMT à la pilocarpine et par l'administration systémique de 4-aminopyridine (4AP) ou de picrotoxine, j'ai adressé le rôle des pointes intericales et des OHF au cours de l’ictogenèse et de l'épileptogénèse. Les principales conclusions de mes études peuvent être résumées comme suit:

J’ai d'abord développé une méthode automatisée pour détecter les OHF lors de la période pré-ictale, ictale et post-ictale; cette méthode, qui emploie une période de référence avant le début de la crise pour la normalisation du signal, donne des résultats

davantage similaires à ceux obtenus par l'analyse visuelle que les autres méthodes automatisées.

Grâce à cette méthode, j'ai découvert que deux types principaux de crises chez des rats traités à la pilocarpine, à savoir les crises à bas voltage haute fréquence et hypersynchrone, sont associées à différents patrons d'occurrence des OHF (80-500 Hz).

Les résultats obtenus chez les rats traités à la pilocarpine ont été confirmés et reproduits par l'injection systémique de 4-aminopyridine (4AP) ou par l'injection de picrotoxine. Plus précisément, j'ai découvert que les crises à bas voltage haute fréquence induites par la 4AP sont souvent associées à des oscillations entre 80-200 Hz, alors que les crises hypersynchrone induites par la picrotoxine sont principalement associées aux oscillations entre 250-500 Hz.

Enfin, j'ai identifié des changements spécifiques dans les pointes interictales et dans les OHF lors du passage de la période de latence à la période chronique. Ces changements pourraient refléter les modifications physiopathologiques qui se produisent dans les structures limbiques impliquées dans l'épileptogénèse.

Dans l'ensemble, les résultats ont démontré que: (i) il existe des changements spécifiques de l'excitabilité des réseaux neuronaux survenant durant les crises à bas voltage et à haute fréquence ainsi que durant les crises hypersynchrones, et que des différences existent *in vivo* en analysant les OHF, et (ii) les modifications possibles de la plasticité synaptique dans les structures limbiques au cours de l'épileptogénèse sont reflétées par des altérations dans l'occurrence des pointes interictales et des OHF. Je pense que mes résultats ouvriront de nouvelles perspectives dans le diagnostic de l'épilepsie ainsi

que dans le développement de nouveaux traitements antiépileptiques pour contrôler les crises récurrentes.

Table of contents

Abbreviations

4AP	4-aminopyridine
EC	Entorhinal cortex
HYP	Hypersynchronous
IPSP	Inhibitory Post Synaptic Potentials
LFP	Local Field Potential
LVF	Low-voltage fast
MTLE	Mesial Temporal Lobe Epilepsy
SE	Status Epilepticus
TLE	Temporal Lobe Epilepsy

1. Chapter 1

General Introduction

In chapter 1, a general introduction to the content of this thesis is provided, consisting of a brief introduction to epilepsy and in particular to mesial temporal lobe epilepsy (MTLE), followed by an introduction to the known electrophysiological biomarker of this disorder. In this chapter, the related articles are reviewed and a broad overview of the contents of this thesis can be found.

1.1. Mesial temporal lobe epilepsy

Epilepsy, one of the most frequent neurological disorders (Pitkänen and Sutula, 2002; Holden et al., 2005), is characterized by sudden periods of hypersynchronous neuronal activity. Several brain disorders arising from injury, malformations or genetic mutations can underlie the occurrence of epileptic seizures. Seizures present different characteristics depending on the involvement of the entire brain or parts of the brain, and based on these characteristics, they can be classified in two main groups: generalized and focal epilepsies (Engel, 2005; Jefferys, 2010).

Mesial temporal lobe epilepsy (MTLE) is one of the most common forms of focal epilepsy, in which recurrent seizures originate from temporal limbic structures, and in particular the hippocampus, amygdala or the entorhinal cortex (EC). Seizures often occur after a latent period, the seizure free period, many years following an initial brain insult (such as complicated febrile convulsions, encephalitis, or *status epilepticus*). This latent period is presumably associated with reorganization of neural networks and changes in cellular excitability (i.e. epileptogenesis) (Pitkänen and Sutula, 2002; Ono and Galanopoulou, 2012).

Antiepileptic drugs are employed as the primary therapy for epileptic disorders, but approximately 30% of patients with MTLE often do not benefit from antiepileptic drugs, thereby becoming potential candidates for surgical removal of the epileptogenic zones. Pre-surgical evaluation, including localizing seizure onset zone, must be performed before the surgery, with paroxysmal brain activities and oscillations serving as biomarkers to localize the epileptogenic region(s) (Engel, 1996, 2008). Unfortunately, in spite of the progress in

diagnostic techniques, approximately 30% of patients undergoing surgery do not become seizure free. Thus, it is of paramount importance to understand the mechanisms underlying epileptic disorders, and in particular MTLE, to prevent their occurrence as well as to find new treatments.

Animal models, presenting similar features as those seen in patients suffering from MTLE, have been established to help us understand the mechanisms of this disorder and to develop therapeutic options (Löscher, 2002; Avanzini et al., 2008). Human studies are much more limited than animal studies, whereas the latter can provide information about the mechanisms underlying epileptogenesis, ictogenesis as well as information about the efficacy of medications. However, it should be kept in mind that information obtained from animal models can only be used if they are subsequently validated by human studies. A brief introduction to animal models that were developed to shed more light on MTLE, is provided below.

1.2. Animal models of mesial temporal lobe epilepsy

Over the past few decades, animal studies have been the valuable sources for collecting information on the mechanisms leading to epileptic disorders. Around mid-twentieth century, many animal models of epilepsy were developed with the help of different physical or chemical insults as well as genetic manipulations (Jefferys, 2010).

Both acute and chronic models of epilepsy are helpful in order to advance our knowledge in epileptic disorders. Acute models mostly provide information about the mechanisms underlying ictogenesis. Chemoconvulsants such as 4-aminopyrdine (4AP),

penicillin, and picrotoxin as well as electrical stimulations can be used to acutely provoke epileptic seizures (Engel and Schwartzkroin, 2006). In chapter 4 and chapter 5 of this thesis, seizures were induced acutely by systemic administration of 4AP or picrotoxin. 4AP is a K^+ channel blocker and has been used *in vitro* to initiate seizure-like events. In chapter 4, I report a descriptive introduction to this model as well as its behavioral and electrophysiological features *in vivo*. Picrotoxin is a $GABA_A$ antagonist that induces seizures by blocking the $GABA_A$ receptor Cl^- channels. The rats who receive picrotoxin systemically are reported to start having seizures within 30 min after the injection (Velíšek, 2006).

Chronic models were developed in order to help epileptologists study the mechanisms of epileptogenesis and interictal abnormalities. For instance, hippocampal sclerosis, the most common pathophysiology feature of MTLE, can be induced by applying an initial injury such as *status epilepticus*, defined as a period of seizure activity that lasts more than 10 minutes. After the termination of the *status epilepticus*, animals progress into a seizure-free latent period, before the occurrence of the first spontaneous seizure. These spontaneous seizures start mostly in the limbic areas.

The preferred chemoconvulsants to induce *status epilepticus* are kainic acid and pilocarpine, either of which can be injected systemically or locally into a specific limbic region (Dudek et al., 2006; Engel and Schwartzkroin, 2006; Curia et al., 2008; Lévesque and Avoli, 2013). These models are highly isomorphic to MTLE in humans since: (i) the animals are experiencing a latent period before the occurrence of the first seizure; (ii) the recurrent spontaneous seizures are refractory to medications; and (iii) the induced lesion shows high similarity to hippocampal sclerosis in patients, which is associated with neuronal loss in CA1/CA3 region of the hippocampus as well as mossy fiber sprouting in the dentate gyrus.

Electrical stimulation, the other method to induce recurrent seizures in animals, is used less often as a model of MTLE. It is more time consuming in terms of animal preparation and it may not be the best representative of this disorder. The electrical model for induction *status epilepticus* consists of administrating repeated electrical stimulation to hippocampal afferents, the hippocampus or the amygdala. This method of stimulation has been reported by Vicedomini and Nadler (1987). Structural rearrangements similar to chemoconvulsant models are seen in the neuronal network of stimulated regions; however, depending on the pulse intensity and the stimulated region, the damage can be different (Avanzini et al., 2008).

In chapter 2, 3, and 6 of this thesis, the pilocarpine model of MTLE is used to study both epileptogenesis and ictogenesis. Specifically, pilocarpine was administered systemically and the *status epilepticus* was terminated after 1 h. Pilocarpine is an M1 muscarinic receptor agonist, and its use as a chemoconvulsant was first described by Turski et al. (1983). Pilocarpine administration causes an imbalance between excitatory and inhibitory signaling and a massive activation of hippocampal neurons, which results in the generation of behavioral seizures leading to *status epilepticus*. Similarly to kainic acid, there is an induction of neuropathological lesions following the seizures. The lesions reported in the pilocarpine model are mostly widespread and consist of changes in the hippocampus, amygdala, thalamus, piriform and entorhinal cortices. These regional modifications may continue to occur during the chronic period and cell loss and mossy fiber sprouting is also evidence (Avanzini et al., 2008).

Neuropathological changes as well as electroencephalographic and behavioral modifications are similar following the systemic administration of both kainic acid and

pilocarpine models, although pilocarpine induces more damage in the neocortex, while kainic acid induces more damage in the hippocampus (Clifford et al., 1987). Overall, pilocarpine is a more reliable animal model; almost 100% of the rats who display *status epilepticus* for 30 min to 2 h develop spontaneous seizures, whereas rats that are injected with kainic acid need more time in the *status epilepticus* to develop spontaneous seizures, something which is very time consuming (Lévesque and Avoli, 2013).

1.3. Electrophysiological biomarkers of mesial temporal lobe epilepsy

The advent of recording tools and advances in recording techniques were significant breakthroughs in neuroscience, and more specifically in epileptology. Brain oscillations recorded from the scalp or using depth electrodes can reveal information about the brain activities in normal and pathologic brain. However, their association to a specific mechanism requires more extensive research. EEG, the first introduced tool of measuring the cerebral function, reflects synaptic activity with different underlying mechanisms and can provide information about the epilepsy disorder in general, as well as its type in particular (Worrell et al., 2012).

Interictal spikes, and more recently high-frequency oscillations (HFOs, 80-500 Hz), recorded from the limbic structures and neocortex of patients with MTLE and in animal models mimicking this disorder, have been considered markers of abnormal patterns of neural network activity (Jacobs et al., 2008, 2009a; Bragin et al., 2010; Crépon et al., 2010; Staba and Bragin, 2011; Jefferys et al., 2012b). In addition, studies of HFOs and interictal spikes can reveal information about the mechanisms underlying epileptogenesis and

ictogenesis. Below, a brief introduction to possible physiological biomarkers of MTLE as well as some mechanisms believed to be involved in their generation is provided.

1.3.1. Interictal spike as a marker of mesial temporal lobe epilepsy

Interictal spikes are brief discharges of less than 250 ms in duration, arising from the synchronous activation of neurons (de Curtis and Avanzini, 2001), which can be detected between seizures on the EEG of epileptic patients and in animal models of epilepsy, however, they are not accompanied by clinical symptoms. After the discovery of epileptic spikes on the EEG (Berger, 1933), EEG oscillations and more specifically epileptic spikes, were used as specific markers of epileptic seizures. Jasper and Gibbs along with their respective teams were among the pioneers who established interictal spikes as the most reliable marker of epilepsy (Avoli, 2012). Their value as a predictive indicator has been proved in many later studies, with the help of new recording and analyzing approaches. It was shown in these studies that they are diagnostic markers for epilepsy; however, they may not be specific biomarkers of epileptogenic areas (Staba and Bragin, 2011), meaning that they cannot precisely pinpoint the epileptogenic area.

Despite the fact that epileptic spikes are manifestations of epilepsy, their specific roles are unclear: studies performed in epileptic patients undergoing removal surgeries indicated that interictal spikes can be generated in areas other than the seizure onset zones, and therefore they are not the best biomarkers of seizure onset zones in focal seizures (Jacobs et al., 2008; Zijlmans et al., 2012). In support of this view, *in vitro* studies also showed that focal seizures are generated independently of interictal spikes (Jensen and Yaari, 1988). In addition, it was shown that interictal spikes in CA3 can control the

occurrence of the ictal events in EC, thus proposing an anti seizure effect of these interictal events; however, interictal spikes may also precede and initiate ictal discharges (Avoli, 2014). Antiepileptic drugs also did not necessarily have an effect on the rate of their occurrence, but may change the morphology of interictal spikes (Smith and Swann, 1987; Gotman, 1991; Avoli et al., 2006; Zijlmans et al., 2009a; Staley et al., 2011). Altogether, the findings of these studies propose that the exact role of interictal spikes in epilepsy remains unclear.

Although the role of interictal spikes in seizure control and generation is still under investigation, animal studies showed that interictal spikes can be detected during the latent period (Huneau et al., 2010; Chauvière et al., 2012). More investigation on the interictal spikes occurring during both the latent and chronic periods could be of great interest in better understanding their role in epilepsy. The proposed role for interictal spikes is further discussed in the section 1.4.1. and chapter 6 of this thesis.

1.3.2. High Frequency Oscillations (HFOs)

The development of recording and analyzing techniques led to the discovery of a higher frequency bands on the EEG. These oscillations were first discovered in the normal and pathologic brains of animal models, and then in patients going through pre-surgical evaluation of MTLE. HFOs can coincide with the interictal spikes or can occur independently (Jacobs et al., 2012).

HFOs are classified as ripples (80-200 Hz) and fast ripples (250-500 Hz), both of which were detected in patients suffering from MTLE that are known to be associated with epileptogenesis (Jefferys et al., 2012b; Zijlmans et al., 2012). A large number of clinical

studies proved that HFOs are localized specifically to the regions generating seizures (Jacobs et al., 2008, 2009a; Crépon et al., 2010; Akiyama et al., 2011), and a better surgery outcome was seen in patients who had removal of regions that were generating HFOs. HFOs were shown to occur at high rates in the seizure onset and epileptogenic zones rather than in lesioned areas (Jacobs et al., 2009a). Recent studies proposed that HFOs can be better markers of seizure onset zones than interictal spikes (Urrestarazu et al., 2006; Wu et al., 2010; Engel and da Silva, 2012; Jefferys et al., 2012b) while at the same time proposing a promising role for HFOs as a biomarker of epileptogenicity.

1.3.2.1. HFO detection

HFOs are oscillations in the range of frequencies from 80 to 500 Hz that were first detected with the use of micro-electrodes in the brain of control animals, of animal models of MTLE, and eventually, in the epileptic human brain. The first detection of HFOs using clinical electrodes (macro-electrodes) was reported by Jirsch et al. (2006) in the hippocampus as well as the neocortex, as they were mostly recorded in the epileptic regions and they were highly correlated with the seizure onset zone. Following the finding of HFOs using macro-electrodes, more studies reported their occurrence in the epileptogenic areas and their high correlation with the successive results of surgery resection (Jirsch et al., 2006; Urrestarazu et al., 2006; Jacobs et al., 2008, 2009b; Crépon et al., 2010; Wu et al., 2010).

Although it was shown that the size of the recording electrodes does not affect the capacity to detect HFOs (Châtillon et al., 2011), it still needs to be investigated that they are identical whether they are detected using micro- or macro- electrodes. For years, HFOs could only be detected in depth recordings but some recent studies reported their

occurrence on the scalp EEG in adults (Andrade-Valenca et al., 2011; Melani et al., 2013), and in children during infantile spasms (Kobayashi et al., 2004). The detection of HFOs on the scalp EEG is of great interest, in particularly for patients at risk of developing epilepsy.

The visual detection of HFOs is the gold standard method for their analysis; however, this is a very time-consuming and subjective process, thus making the development of automated methods inevitable. In the past decade, several computational methods for analyzing HFOs were proposed (Zelmann et al., 2012), whose algorithms filter the raw signal in the appropriate frequency band and then apply different methods of energy comparison in order to detect HFOs from the background signal (Worrell et al., 2012). In chapter 2 of my thesis, three different methods of detecting HFOs are proposed and compared in order to find the best automated method for our dataset. The proposed method, which was validated by visual analysis, has been widely used to detect and analyze HFOs in our laboratory, both *in vitro* and *in vivo* (Lévesque et al., 2012a; Panuccio et al., 2012; Salami et al., 2015; Shiri et al., 2015).

1.3.2.2. HFO mechanisms

Brain synchronization at different scales is important for normal brain function, and different oscillations mirror the underlying synchronization, although this becomes excessive and pathologic in epileptic disorders. Several mechanisms can contribute to these changes in synchronization including imbalance between synaptic excitation and inhibition, as well as non-synaptic activities such as gap junction coupling and changes in the extracellular K^+ (Engel, 1996; Jefferys et al., 2012a).

Ripples associated to the HFOs in the lower frequency band (i.e., 80-200 Hz) are believed to reflect the synchronized IPSPs regulated by interneurons activation (Buzsáki et al., 1992; Ylinen et al., 1995). HFOs in the ripple frequency range can be recorded in the hippocampus during both physiological and pathological conditions. Physiological ripples in the hippocampus were first reported during behavioral immobility and slow-wave sleep by Buzsáki and colleagues in 1992, and are believed to be involved in learning and memory (Buzsáki et al., 1992; Buzsáki and Draguhn, 2004). Later, their association with epilepsy was shown in the kainic acid model of MTLE, as they were detected in the dentate gyrus, where normal ripples are absent (Bragin et al., 2004).

Higher oscillations in the fast ripple range (i.e., 250-500 Hz) have been recorded in the somatosensory cortex of healthy brains of both animals and humans, and are believed to be involved in sensory information processing (Worrell et al., 2012). In 1999, Bragin and colleagues reported the existence of fast ripples in the hippocampal region of epileptic patients and kainic acid treated-rats (Bragin et al., 1999b). Fast ripples have been proposed to arise from local clusters of pyramidal cells and independently from inhibitory activities (Dzhala and Staley, 2004; Bragin et al., 2011).

The difference between the mechanisms underlying physiological and pathological HFOs is still an active area of research. Recently, it was shown by different groups that the mechanisms of generation of ripples recorded during interictal periods vary from the mechanisms of those occurring before the onset of the seizure or during the seizure (Matsumoto et al., 2013; Alvarado-Rojas et al., 2015). Alvarado-Rojas et al. (2015) demonstrated that ripples recorded in epileptic tissue obtained from human brain rise from different populations when they occur during the interical periods compared to when

they appear in the preictal period. Specifically, they proposed that interictal ripples are associated with GABAergic and glutamatergic signaling, whereas preictal ripples are associated with the activity of bursting pyramidal cells. In another study, Matsumoto et al. (2013) compared the physiological and pathological HFOs in patients during pre-surgical evaluation, and reported that pathological HFOs have a higher amplitude and duration, and a lower frequency than normal physiological HFOs (Matsumoto et al., 2013).

It has been suggested that HFOs in the ripple frequency range reflect the synchronous activity of interneurons in an area larger than the one involved in fast ripple generation (Jefferys et al., 2012b). Fast ripples that are only occurring in seizure generating areas may reflect bursts of population spikes generated by the activity of a synchronous principal cell cluster (Staba et al., 2014). On the other hand, oscillations in the ripple frequency band that are believed to be pathologic (because they are generated in regions that do not generate normal ripples), have also been shown to be a burst of clustering spikes (Bragin et al., 2004). *In vitro* data from animal models suggested a reduction in interneuron activity and an increase in pyramidal cell discharge during pathologic HFOs, whose frequency exceeds the limited firing rate of an individual neuron, which is suggested by *in vitro* and *in vivo* experiments to be of 300 Hz. Therefore, it was proposed that higher-frequency HFOs that are above the maximal firing frequency of most principal cells, reflect the out-of-phase firing of synchronous principal cells (Foffani et al., 2007; Ibarz et al., 2010; Menendez de la Prida and Trevelyan, 2011). This can be achieved through ephaptic field effects, neuronal loss, synaptic reorganization or other modifications in network organization (Jefferys et al., 2012b).

In addition to synaptic mechanisms, non-synaptic mechanisms can also contribute to HFO generation. Recent studies have proposed that ephaptic effects as well as gap junctions can contribute to HFO generation in the absence of synaptic transmission (Draguhn et al., 1998; Jiruska et al., 2010a; Köhling and Staley, 2011). In addition to these *in vitro* studies, computational simulations also postulate a role for gap junctions during fast ripple generation (Traub et al., 2010). Interneuronal cell loss and synaptic reorganization can change the field potentials dramatically, but are not necessary for the generation of HFOs according to Jiruska et al. (2010b). A more recent study by (Demont-Guignard et al., 2012) has shown that fast ripples and interictal spikes share some mechanisms, but that the size of the network involved in their generation and their firing patterns are different (Demont-Guignard et al., 2012). It is important to consider that the aforementioned mechanisms can all contribute to some degree to the generation and maintenance of HFOs.

1.3.2.3. HFOs and ictogenesis

In vivo and *in vitro* studies of normal brains revealed significant information about the mechanisms involved in the excessive excitation and synchronization during seizures. The physiological and anatomical characteristics of the limbic system make the neuronal synchronization in its structures more likely. There are two types of events that can emerge from the synchronous activity of the neuronal networks in epilepsy: interictal and ictal events (Behr et al., 2014). HFOs detected during both interictal and ictal periods were shown to be associated with seizure onset zones and were detected in the regions ipsilateral to the seizure generation region (Jacobs et al., 2012; Jefferys et al., 2012b). Despite the appearance of HFOs in both ictal and interictal periods, it is not yet clear if they have different diagnostic value to mark the epileptogenic zone. Following their discovery,

HFOs were detected in epileptic rodents in areas close to the lesioned region as well as during pre-surgical evaluations in patients suffering from MTLE using micro- and macro-electrodes (Bragin et al., 1999c; Jirsch et al., 2006; Jacobs et al., 2008; Zijlmans et al., 2009b; Wu et al., 2010).

The first study of HFO detection at the onset of seizures was reported by Fisher et al., (1992) as a significant increase in power in the 80-120 Hz frequency range (Fisher et al., 1992). Later on, such a spectrum power increase was identified during seconds before the onset of the seizure at the transition from preictal to the ictal period in an *in vitro* low Mg^{2+} model of epileptiform discharges (Khosravani et al., 2005). However, no increase in the HFO was identified in minutes preceding seizure onset (Jacobs et al., 2009b). An increase in the amplitude, frequency and duration of HFOs was also presented at the seizure onset in the dentate gyrus of kainic acid treated rats (Bragin et al., 2005). HFOs are seen at the transition from the interictal to ictal periods (Jacobs et al., 2009b; Zijlmans et al., 2009a), and as mentioned earlier, these oscillations are believed to originate from various neuronal populations. The analysis of the relationship between HFOs and seizure onsets can reveal more information on the cellular mechanisms underlying different seizure patterns.

There are two common types of seizure onset patterns seen in the patients of MTLE: the low-voltage fast (LVF) onset and the hypersynchronous (HYP) onset. The former is characterized by a positive or negative-going spike followed by low-amplitude high-frequency activity, whereas the latter is characterized by a pattern of spiking of around 2Hz at the onset of the seizure. LVF onset seizures were shown to have widespread origins, to involve a broader network , and to be mostly correlated with diffuse atrophy, whereas HYP seizures mostly originate more locally and are seen more specifically in patients with

hippocampal sclerosis (Lieb et al., 1981; Spencer et al., 1992; Velasco et al., 2000; Perucca et al., 2014).

Animal studies presented an association between different HFO generation patterns and different seizure onset patterns. More specifically, ripples are shown to increase at the onset of LVF seizures (Bragin et al., 2005), with a suggested role of $GABA_A$ receptor signaling (Lopantsev and Avoli, 1998a, 1998b) and interneuronal synchronization (Grasse et al., 2013). On the other hand an increase in pyramidal cells firing has been reported at the onset of HYP seizures, and fast ripples occur at higher rates at the beginning of this seizure onset pattern (Huberfeld et al., 2011). In chapter 3 and chapter 5 of this thesis, we address the correlation between the seizure onset patterns and the occurrence of the HFOs.

1.4. Mechanisms in epileptogenesis

Epileptogenesis, the process by which a brain becomes epileptic, is not fully understood in humans. During epileptogenesis, the brain undergoes molecular, cellular and morphological changes that are thought to lead to hyperexcitability. Studies in animal models of MTLE as well as in epileptic patients undergoing surgical removal of the epileptogenic zone reported anatomical changes associated with this disorder. Selective neuronal loss, gliosis and mossy fiber sprouting are shown to be the hallmark changes occurring during epileptogenesis in MTLE (Houser et al., 1990; Cavazos et al., 1991; Sutula et al., 1992; Houser, 1999), and any of these modifications could be detected using advanced imaging techniques. Because of the limitations that come with human brain recordings, most of the studies in this field are coming from animal models - for example,

some presented that there are changes in the electrophysiological signal of animal models of MTLE during epileptogenesis that can also serve as a potential biomarker for the underlying structural changes (Bortel et al., 2010; Chauvière et al., 2012).

Several studies show significant changes in the EEG of animal models that have become epileptic after different methods of the insult initiation, such as the induction of *status epilepticus* (Bragin et al., 2004; Bortel et al., 2010; Lévesque et al., 2011; Chauvière et al., 2012). Discovering electrographic biomarkers not only can make it possible to detect epileptogenesis in advance, but can also shed a light on our understanding of the changes occurring during epileptogenesis and may help to better understand the effects of antiepileptic drugs and their possible advantages.

1.4.1. Interictal spikes and epileptogenesis

Animal studies showed that interictal spikes characteristics can serve as a biomarker of epileptogenesity. Huneau et al. (2010) reported that there is an increase in the frequency of occurrence of interictal spikes in the rats that developed epilepsy compared to controls, and also proposed that the alterations in spike features, such as their amplitude and duration, reflect plasticity changes during epileptogenesis (Huneau et al., 2010). The study of Bortel et al. (2010) in our laboratory also suggested that interictal spikes are recorded in all rats that developed spontaneous seizures after experiencing different duration of *status epilepticus* induced by pilocarpine. In this study, it was shown that interictal spikes characteristics change from the latent to the chronic period (Bortel et al., 2010).

A more recent study by Chauvière et al. (2012) described two types of interictal discharges following pilocarpine- or kainic acid-induced *status epilepticus* in the

hippocampal CA1 area: the first (type 1) consisting of a spike followed by a long-lasting wave, and the second (type 2) characterized by a spike without wave. These authors also found that the amount of type 1 events progressively decreased while type 2 events increased during the latent period (Chauvière et al., 2012).

Reports in developmental systems suggested that interictal spikes may play a role in the guidance of axon sprouting. During epileptogenesis, the interneuronal loss could have an important effect in the hyperexcitability of neurons as well as the generation of spikes leading to axonal sprouting and making new connections. This process would make a strong locally-connected network, and helps the initiation of epileptogenic focus (Staley et al., 2011).

In chapter 6 of this thesis, I am looking at the changes in the morphology and the characteristics of interictal spikes at the transition from the latent to the chronic period in the CA3 region of the hippocampus and EC, in order to further investigate their role in epileptogenesis.

1.4.2. HFOs and epileptogenesis

One piece of evidence that supports a role for fast ripples during epileptogenesis comes from the study of Bragin et al., (2004). These investigators found that fast ripples were only detected in rats who manifested spontaneous seizures, but not in those not developing epilepsy. They also proposed a role for ripples in epileptogenicity as they were only seen in the dentate gyrus of rats who presented with epilepsy and there is not enough substantial evidence of their existence in the normal dentate gyrus (Bragin et al., 1995). It is also presented that the shorter time to the appearance of the first HFO leads to a shorter time to

the appearance of the first spontaneous seizure (Bragin et al., 2004). The location of these HFOs persists over time and can serve as a biomarker for epileptogenicity in those sites (Staba and Bragin, 2011).

A study by (Lévesque et al., 2011) in our laboratory determined that there is a high correlation between the regions generating HFOs and the seizure onset zones. More specifically, in pilocarpine treated rats, the seizures were mostly generated in the CA3 region of the hippocampus and there was a high correlation between the occurrence of the seizures and the rate of interictal spikes associated with fast ripples in this region (Lévesque et al., 2011).

Despite all the studies investigating the electrophysiological changes during epileptogenesis, no study has addressed the changes of HFOs along with interictal spikes and their role in epileptogenesis. In chapter 6 of my thesis, I am presenting data showing the changes in interictal spikes and their associated HFOs during epileptogenesis as well as their potential role to serve as a biomarker of epileptogenicity.

1.5. Aim of my thesis

My graduate studies have focused on establishing the participation of HFOs during ictogenesis, and on identifying their role, along with that of interictal spikes, the main electrophysiological biomarker of MTLE, during epileptogenesis. To achieve my goals, (i) I improved an automated method for detecting HFOs during seizures (Salami et al., 2012); (ii) then employing the proposed method, I showed that the two most common seizure onset patterns in MTLE are associated to different HFO types (Lévesque et al., 2012). (iii)

The results obtained in the previous study were confirmed and replicated by increasing both GABAergic and glutamatergic mechanisms or by blocking GABAergic signaling (Lévesque et al., 2013; Salami et al., 2015). (iv) Finally interictal and HFO changes were analyzed during latent and chronic periods to see how their changes contribute to epileptogenesis (Salami et al., 2014).

1.5.1. Aim 1: HFO analysis

HFOs are believed to serve as biomarkers for seizure onset zones, and over the past decade, an increasing number of studies have analyzed HFOs *in vitro*, *in vivo* and in the EEG of epileptic patients, with a specific emphasis on analyzing HFOs during interictal events or at the seizure onset. Therefore, in my study (Salami et al., 2012), I compared three different automated methods of HFO detection to two methods of visual analysis, during the pre-ictal, ictal and post-ictal periods on multiple channels in the rat pilocarpine model of MTLE, in order to find a reliable method for detecting HFOs. According to our findings, we proposed a reliable automated method to analyze the HFOs in large data sets (Salami et al., 2012). This method was later used to analyze HFOs occurring during interictal and ictal periods.

1.5.2. Aim 2: HFOs during ictogenesis

In order to study the temporal changes of HFOs during seizures, we recorded from the hippocampal CA3 subfield, subiculum, EC, and dentate gyrus of pilocarpine treated rats to quantify the occurrence of ripples (80–200 Hz) and fast ripples (250–500 Hz). It was found that the temporal distribution of HFOs during pre-ictal and ictal periods highly depends on seizure onset types. As mentioned earlier, seizures in MTLE have different onset patterns,

characterized mostly as LVF-onset seizures or HYP-onset seizures (Velasco et al., 2000). We discovered in the rat pilocarpine model of MTLE that these two typical seizure onset patterns, the LVF onset seizures and the HYP onset seizures, are related to distinct types of HFOs occurrences. Specifically, LVF seizures showed high rates of HFOs at 80-200 Hz (ripples frequency band) in all recorded regions, whereas HYP seizures were associated with high rates of HFOs at 250-500 Hz (fast ripples frequency band) in more localized seizure onset zones (Lévesque et al., 2012).

These findings led us to speculate that HFOs mirror different functional properties of neural networks during ictogenesis. More specifically, we hypothesized that during ictogenesis, fast ripples reflect hypersynchronized bursting of principal (glutamatergic) neurons at HYP seizure onset zones, whereas ripples during LVF seizures reflect summated IPSPs generated by pyramidal cells in response to inhibitory interneuron firing (Lévesque et al., 2012).

1.5.3. Aim 3: Seizure patterns and their mechanisms

The hypothesis formulated in the previous section was further tested by inducing seizures acutely by systemic injections of 4AP, a substance that blocks K^+ channels, or of the $GABA_A$ receptor antagonist picrotoxin *in vivo.* The effect of the former on local field potentials has been substantially investigated in our laboratory *in vitro* (Avoli and de Curtis, 2011). In chapter 4 of this thesis, it is presented that 4AP administration can induce seizures in hippocampal region as well as in the cortex; however, the onset of the epileptiform activities in hippocampus precedes those in the cortex (Lévesque et al., 2013). The seizures

recorded in this study mostly showed an LVF pattern, thereby confirming our hypothesis that there are more LVF seizures following the injection of 4AP.

In order to further confirm our hypothesis, we analyzed HFOs during seizures following 4AP and picrotoxin administration. Based on previous experiments, it was hypothesized that there are more LVF seizures following the injection of 4AP, and that these seizures are characterized by more ripples than fast ripples, whereas seizures following picrotoxin would display more HYP seizures and fast ripples. A second set of experiments further confirmed that most seizures induced by 4AP were LVF seizures. The analysis of HFOs also revealed that the ripple occurrence increases in recorded LVF seizures shortly before the initiation of ictal activity (Salami et al., 2015). These results and also the morphology of the seizures can be related to an increase in GABAergic inhibition and interneuronal activities (Avoli and de Curtis, 2011; Lévesque et al., 2013).

In contrast, after the systemic administration of picrotoxin, all recorded seizures were characterized by HYP onset pattern (Salami et al., 2015). HFO analysis revealed that the rate of occurrence of fast ripples was higher than that of ripples during HYP seizures recorded in the CA3 region and subiculum after the administration of picrotoxin. Since HFOs are believed to reflect neuronal network activity in epileptic regions, these findings indicate that different mechanisms underlie the two seizure-onset patterns.

1.5.4. Aim 4: Interictal spikes, HFOs and epileptogenesis

HFO analysis may help in identifying different mechanisms underlying seizures thus helping patients to benefit from different treatments. The roles of HFOs and interictal spikes and the changes in their characteristics may also bring us information about the

modifications that the neural networks undergo during the latent period. As mentioned earlier, previously studies in our laboratory (Bortel et al., 2010) showed that the duration and frequency of interictal spikes is modified in pilocarpine treated rats following the appearance of the first seizure. More recently, Chauvière et al. (2012), suggested a role for the changes in interictal spike morphology to serve as a biomarker of epileptogenicity. However, no study addressed the dynamic changes that characterize HFOs during the latent period.

HFOs occur in the EEG of epileptic patients and animals in coincidence with interictal spikes, but also in their absence. We used the pilocarpine model of MTLE to analyze the evolution of interictal spikes and the occurrence of HFOs in two limbic structures during the latent and chronic periods, in an attempt to further elucidate the mechanisms leading to the establishment of epileptic networks (Salami et al., 2014). As addressed earlier, MTLE is characterized in humans as well as animal models mimicking this disorder, by a latent period associated to plastic changes in temporal lobe structures. In the last part of my thesis (Chapter 6), I have investigated the changes in the occurrence of interictal spikes and HFOs in the two most epileptogenic limbic regions: EC and CA3 of the hippocampus. Two types of interictal spikes were classified in these regions and their changes from latent to the chronic period were then compared. I found a switch in the distribution of both types of interictal spikes at the transition from the latent to the chronic period. Besides describing the changes in interictal spikes, HFOs associated with interictal spikes as well as independent HFOs were analyzed. I found higher rates of fast ripples associated with type 2 spikes in EC compared to CA3 during the latent period, whereas they occurred at similar rates in both regions in the chronic period. The rate of occurrence of

fast ripples outside of spikes was also higher in EC compared to CA3 during the latent period. These findings demonstrate that, at the transition from the latent to the chronic phase, there is a dynamic change in the occurrence of interictal spikes and HFOs in EC and CA3.

These changes reflect the progressive pathological reorganization of limbic neuronal networks during epileptogenesis, may shed light in understanding the progression of epileptogenicity, and can serve as biomarkers of an epileptogenic network in human patients at risk of developing epilepsy.

2. Chapter 2

A comparison between automated detection methods of high-frequency oscillations (80–500 Hz) during seizure

Salami P, Lévesque M, Gotman J, Avoli M. *Journal of Neuroscience Methods*, 2012 211(2):265-71.

For the past two decades, HFOs have attracted the attention of epileptologists as a promising biomarker of epileptogenic zones. Several studies have analyzed HFOs during interictal periods as well as at the initiation of the ictal periods visually or by the use of an automated method. Visual HFO analysis is highly time consuming and an automated method to detect HFOs is necessary. However, there remains a lack of standardized methods to detect HFOs. In this chapter, I am presenting a comparison between three proposed methods of detecting HFOs during seizures. This study was published in 2012 in the *Journal of Neuroscience Methods* with the title "A comparison between automated detection methods of high-frequency oscillations (80-500 Hz) during seizures".

2.1. Abstract

High-frequency oscillations (HFOs, ripples: 80-200 Hz, fast ripples: 250-500 Hz) recorded from the epileptic brain are thought to reflect abnormal network-driven activity. They are also better markers of seizure onset zones compared to interictal spikes. There is thus an increasing number of studies analyzing HFOs *in vitro*, *in vivo* and in the EEG of human patients with refractory epilepsy. However, most of these studies have focused on HFOs during interictal events or at seizure onset, and few have analyzed HFOs during seizures. In this study, we are comparing three different automated methods of HFO detection to two methods of visual analysis, during the pre-ictal, ictal and post-ictal periods on multiple channels using the rat pilocarpine model of temporal lobe epilepsy. The first method (method 1) detected HFOs using the average of the normalized period, the second (method 2) detected HFOs using the average of the normalized period in 1 s windows and the third (method 3) detected HFOs using the average of a reference period before seizure onset. Overall, methods 2 and 3 showed higher sensitivity compared to method 1. When dividing the analyzed traces in pre-, ictal and post-ictal periods, method 3 showed the highest sensitivity during the ictal period compared to method 1, while method 2 was not significantly different from method 1. These findings suggest that method 3 could be used for automated and reliable detection of HFOs on large data sets containing multiple channels during the ictal period.

2.2. Introduction

High-frequency oscillations (HFOs, ripples: 80-200 Hz, fast ripples: 250-500 Hz) have been recorded in experimental epilepsy models and in patients with refractory epilepsy (Engel and da Silva, 2012; Jefferys et al., 2012b). HFOs are thought to reflect abnormal network-driven activity and may help to locate seizure onset zones (Jacobs et al., 2008, 2009a; Crépon et al., 2010; Lévesque et al., 2011).

Using automated algorithms to detect HFOs is preferable, since using visual analysis is time consuming and requires experienced reviewers. Moreover, one needs to consider inter-rater reliability and come to an agreement between reviewers on what has to be considered as HFOs (Gardner et al., 2007; Zelmann et al., 2012). Thus, multiple automated methods of HFO detection have been developed in recent years. However, most of these studies focused on the detection of HFOs during interictal periods (Staba et al., 2002; Bragin et al., 2004; Jacobs et al., 2009a; Lévesque et al., 2011). Few studies have explored HFOs during seizures. In this paper, we are comparing three automated methods to detect HFOs during the pre-ictal, ictal and post-ictal periods of seizures in the rat pilocarpine model of temporal lobe epilepsy. We report here that an automated method that uses a reference period before seizure onset for signal normalization produces results that are similar to what is detected with visual analysis.

2.3. Materials and Methods

2.3.1. Animal preparation

Sprague-Dawley rats (250-300 g) were injected with scopolamine methylnitrate (1 mg/kg i.p.; Sigma-Aldrich, Canada) and 30 min later with a single dose of pilocarpine hydrochloride (380 mg/kg, i.p.; Sigma-Aldrich, Canada) (Bortel et al., 2010; Lévesque et al., 2011). Their behavior was scored according to the Racine scale (Racine, 1972), and *status epilepticus* (SE) was defined as continuous stage 5 seizures. *Status epilepticus* was terminated after 1 h by injection of diazepam (5 mg/kg, i.p.; CDMV, Canada) and ketamine (50 mg/kg, i.p.; CDMV, Canada) (Martin and Kapur, 2008). The mortality rate was 13 %. Surviving animals were allowed to recover for 72 h before surgery. Four stainless steel screws (2.4 mm length) were fixed to the skull and 4 small holes were drilled to allow the implantation of bipolar electrodes (20-30 kΩ; 30-50 mm length; distance between exposed tips: 500 μm) made by twisting and gluing two 0.1524 mm resin-insulated copper wires. Contacts consisted of the cut edge of the wire (0.018 mm^2) (Châtillon et al., 2011). Electrodes were implanted in the CA3 subfield of the ventral hippocampus (AP: -4.4, ML: ±4, DV: -8.8), medial entorhinal cortex (AP: -6.6, ML: ±4, DV: -8.8), ventral subiculum (AP: -6.8, ML: ±4, DV: -6) and dentate gyrus (AP: -4.4, ML: ±2.4, DV: 3.4). Screws and electrode pins were connected with a pin connector and fastened to the skull with dental cement. A cortical screw placed in the frontal bone was used as reference, and a second screw, placed on the opposite side of the frontal region, was used as ground (For more details see: (Lévesque et al., 2011).

2.3.2. Local field potential recordings

After surgery, rats were housed individually in custom-made Plexiglas boxes (30 x 30 x 40 cm) and let habituate to the environment for 24 h. The pin connector was then connected to a multichannel cable and electrical swivel (Slip ring T13EEG, Air Precision, France; or Commutator SL 18C, HRS Scientific, Canada) and LFP-video monitoring (24 h per day) was performed. LFPs were amplified via an interface kit (Mobile 36ch LTM ProAmp, Stellate, Montreal, QC, Canada), low-pass filtered at 500 Hz and sampled at 2 kHz per channel. Infrared cameras were used to record day/night video files that were time-stamped for integration with the electrophysiological data using monitoring software (Harmonie, Stellate, Montreal, QC, Canada). Throughout the recordings, animals were placed under controlled conditions (22 ± 2 ˚C, 12 h light/dark schedule) and provided with food and water *ad libitum.* LFP-video recordings were performed up to 15 days after *status epilepticus*.

2.3.3. Selection of samples for HFO analysis

Only seizures with good quality signals were selected for analysis. A total of 43 seizures (n = 6 animals) were thus extracted during the chronic period, on average 5.5 (± 2.3) days after SE. These periods were then exported to Matlab 7.9.0 (Mathworks, Natick, MA) using custom-built routines, and analyzed off-line.

Seizures were analyzed from 60 s before the onset until 50 seconds after the end of the seizure. Then, 1 s sample traces from each seizure were randomly selected from one of the 4 regions recorded (n = 100, 25 traces from each region). Of the 100 selected traces, 43 % were extracted from the pre-ictal period, 44 % from the ictal period and 13 % from the

post ictal period. Every 1s trace was analyzed using 2 methods of visual analysis and 3 automated methods, as described in the following sections (see Sections 2.2.5 and 2.2.6).

2.3.4. Filtering of signals

Raw LFP recordings were band-pass filtered in the 80-200 Hz and in the 250-500 Hz frequency range using an FIR filter; zero-phase digital filtering was used to avoid phase distortion. Figure 2.1 shows a seizure from the CA3 region of hippocampus with the filtered signals in the ripple (80-200 Hz) and fast ripple frequency band (250-500 Hz). Every automated method employed a multi-parametric algorithm using routines based on standardized functions in Matlab 7.9.0.

2.3.5. Visual analyses of HFOs

For the first method of visual analysis, four reviewers trained in electrophysiology and HFO analysis marked events in every 1 s selected traces (n = 100). Reviewers were provided with the raw LFP signal (1 s in duration) as well as the filtered signals in the ripple (80-200 Hz) and fast ripple (250-500 Hz) frequency band. Reviewers were asked to mark oscillations as HFOs if they could clearly see oscillations having 3 consecutive cycles with amplitude higher than the average of the background. Every event detected by at least 3 reviewers was then considered as HFOs and the remaining oscillations were excluded from the analysis. Figure 2.2D shows oscillations detected by at least 3 of 4 reviewers in one sample trace. The parameters of this visual analysis were similar to the parameters used by the automated method 2 (see Section 2.2.6.2).

Four different reviewers identified HFOs using the second method of visual analysis. They were provided with a 10 s filtered time-reference trace and with a 1 s filtered trace in

each frequency band (ripples and fast ripples). The 10 s time-reference trace corresponded to a period ranging from 50 s to 40 s before seizure onset. Reviewers were asked to identify oscillations as HFOs if they could clearly see oscillations having 3 consecutive cycles higher than the average of the reference period. Again, HFOs detected by at least 3 reviewers were included in the analysis and the remaining detected oscillations were excluded from the study. The parameters of this visual analysis were similar to the parameters used by the automated method 3 (see Section 2.2.6.3).

2.3.6. Automated methods

2.3.6.1. Automated method 1

The first method used to detect HFOs was built to be similar to what is used to detect HFOs during interictal periods (Staba et al., 2002; Bragin et al., 2004; Lévesque et al., 2011). The filtered traces in each frequency band are normalized using their own average and standard deviation. Thus, for each channel the average of the filtered signal, from 60 s before the start of the seizure to 50 s after the end of the seizure, was computed. Then, the signal was normalized according to the average so that the normalized signal had an average (Avg) of 0 and standard deviation (SD) of 1.

$$Normalized\ LFP = \frac{Raw\ (LFP) - \ Avg(LFP)}{SD(LFP)}$$

HFOs had to show more than three consecutive cycles (Bragin et al., 2004; Lévesque et al., 2011) higher than a standard threshold (3 SD above the background mean). Moreover, the time lag between two consecutive cycles in the ripple frequency range had to be between 5 and 12.5 ms for ripples, and between 2 and 4 ms for fast ripples. Figure 2.2A shows a sample trace with HFOs detected by method 1.

2.3.6.2. Automated method 2

The selected traces of every seizure were first divided in 1 s trace. Every 1 trace was then normalized using its own root mean square (RMS), where:

$$Normalized \;\; 1\ s\ LFP\ sample\ = \frac{Raw\ (1\ s\ LFP\ sample)}{RMS(1\ s\ LFP\ sample)}$$

After having normalised traces for each frequency band, oscillations with 3 consecutive cycles having an amplitude above 4 SD of the background mean were detected. As in method 1, the time lag between two consecutive cycles in the ripple frequency range had to be between 5 and 12.5 ms for ripples, and between 2 and 4 ms for fast ripples. Figure 2.2B shows a sample trace with the detected oscillations using method 2.

2.3.6.3. Automated method 3

The third method detected HFOs in each frequency band according to a reference period. A 10 s artifact-free period (50 to 40 seconds before the start of the seizure) was selected as a reference period for signal normalization. LFP in the pre-ictal, ictal and post-ictal periods were normalized using the average and SD of the reference.

$$Normalized\ LFP = \frac{Raw\ (LFP) - \ Avg(Ref)}{SD(Ref)}$$

Oscillatory events in each frequency band were considered as HFOs if they showed at least three consecutive cycles above a standard threshold (3 SDs above the mean of the reference) (Bragin et al., 2004; Lévesque et al., 2011). Again, as in method 1, the time lag between two consecutive cycles in the ripple frequency range had to be between 5 and 12.5 ms for ripples, and between 2 and 4 ms for fast ripples. Figure 2.2C shows a sample trace with the detected oscillations by method 3.

2.3.7. Statistical Analysis

2.3.7.1. Sensitivity

We first compared the sensitivity of all three methods. We thus calculated in each sample trace (n = 100) the number of “true positives”, defined as HFOs detected by each of the automated methods and one of the visual analyses . Thus, the sensitivity of each automated method was defined as:

$$\frac{Number\ of\ true\ positives}{Number\ of\ true\ positives + Number\ of\ false\ negatives} * 100$$

Since values were not normally distributed, the average sensitivity of the three methods was compared using non-parametric Friedman tests followed by post-hoc tests to which a Bonferroni correction for multiple comparisons was applied. The comparison of the average sensitivity during the pre-ictal, ictal and post-ictal periods was compared using non-parametric Kruskall-Wallis tests followed by Bonferroni post-hoc corrections for multiple comparisons. The level of significance was set at $p < 0.05$.

2.3.7.2. False detections

We then compared the number of “false detections” defined as HFOs detected by an automated method that was not detected by any of the reviewers. For each 1 s trace, the number of "false detections” was calculated and then divided by the total number of detected oscillations. The average number of “false detections” during the entire trace was compared using non-parametric Kruskall-Wallis tests followed by Bonferroni post-hoc tests for multiple comparisons.

2.4. Results

Method 1 detected 14 ripples and 25 fast ripples in the 100 sample traces. Method 2 detected 51 ripples and 80 fast ripples. Method 3 detected 156 ripples and 125 fast ripples. Reviewers that used the first visual analysis detected a total of 671 HFOs, 90 of which were detected by all 4 reviewers, 117 by 3 reviewers, 165 by 2 reviewers and 299 by only one reviewer. On the other hand, reviewers that used the second visual analysis detected a total of 1173 HFOs, among which 195 were detected by 4 reviewers, 202 by 3 reviewers, 279 by 2 reviewers and 503 by only one reviewer. Table1 shows a summary of the number of detected oscillations.

2.4.1. Comparison of the overall sensitivity between automated methods calculated with results obtained from the first visual analysis

As Mentioned earlier, the HFOs that were detected by both the automated method and the visual analysis were considered as "true" HFOs. A total of 11 true positives in the ripple frequency range and 21 true positives in the fast ripple frequency range were detected by method 1. Method 2 detected 37 true ripples and 60 true fast ripples. Method 3 detected 57 true ripples and 58 true fast ripples. Figure 2.3A shows the sensitivity of each method for ripples and fast ripples.

We observed a significant effect of method when comparing sensitivity levels (χ^2 = 44.7, df = 5, $p < 0.001$). As it can be seen in Figure 2.3, for ripples and fast ripples, post-hoc tests showed that the sensitivities of methods 2 and 3 were higher compared to the sensitivity of method 1 ($p < 0.05$). No significant differences were observed when comparing methods 2 and 3.

Overall, these results suggest that the sensitivity levels of methods 2 and 3 are similar to the first visual analysis for detecting both ripples and fast ripples. Method 1 that is normally used for the analysis of HFOs during the interictal periods performs poorly in terms of sensitivity compared to method 2 and 3.

2.4.2. Comparison between the sensitivities of the automated method and the first visual analysis for the pre-ictal, ictal and post-ictal periods

2.4.2.1. Pre-ictal period

During the pre-ictal period, method 1 detected 3 true ripples and 11 true fast ripples. Method 2 detected 16 true ripples and 22 true fast ripples. Method 3 detected true 18 ripples and 17 true fast ripples. There was a significant effect of method ($\chi^2 = 11.5$, df = 5, $p < 0.05$) but post-hoc comparisons revealed no significant differences between them (Fig 2.3B).

2.4.2.2. Ictal period

During the ictal period, method 1 detected 8 true ripples and 10 true fast ripples. Method 2 detected 17 true ripples and 31 true fast ripples. Method 3 detected 32 true ripples and 33 true fast ripples. There was a significant effect of method ($\chi^2 = 18.1$, df = 5, $p < 0.005$) and post-hoc comparisons showed that the sensitivity of method 3 for ripples is significantly higher compared to method 1 ($p < 0.05$) (Fig 2.3C). No significant differences were observed between methods for fast ripples.

2.4.2.3. Post-ictal period

No true ripples or true fast ripples were detected by method 1. Method 2 detected 4 true ripples and 7 true fast ripples. Method 3 detected 7 true ripples and 8 true fast ripples. We

observed no significant effect of methods. Overall, these results suggest that when using automated methods of HFO detection in different periods (pre-ictal, ictal and post-ictal), the sensitivity of method 3 is higher compared to method 1, but only during the ictal period and only for ripples. Method 2 does not perform better than method 1.

2.4.3. Comparison of sensitivity between automated methods calculated with results obtained from the second visual analysis

As in the previous section, we first compared the sensitivity of the automated methods by calculating their overall sensitivity, obtained by comparing detected HFOs with those obtained from the second visual analysis. Results showed that method 1 detected 13 true ripples and 21 true fast ripples. Method 2 detected 41 true ripples and 61 true fast ripples. Method 3 detected 97 true ripples and 85 true fast ripples. Statistical analyses showed a significant effect of method ($\chi^2 = 61.4$, $df = 5$, $p < 0.05$). Post-hoc comparisons showed that the sensitivities of method 2 and 3 were significantly higher compared to method 1 ($p < 0.05$) (Fig 2.4A).

Overall, these results suggest that methods 2 and 3 have higher sensitivity compared to method 1 in detecting both ripples and fast ripples, when the second method of visual analysis is used as the gold standard.

2.4.4. Comparison between the sensitivities of the automated methods and the second visual analysis for the pre-ictal, ictal and post-ictal periods

2.4.4.1. Pre-ictal period

Method 1, detected 4 true ripples and 12 true fast ripples. Method 2 detected 15 true ripples and 21 true fast ripples and method 3 detected 20 true ripples and 21 true fast

ripples. Although we observed a significant effect of methods (χ^2 = 11.7, df = 5, $p < 0.05$), there was no significant difference between them (Fig 2.4B).

2.4.4.2. Ictal period

Method 1 detected 9 true ripples and 9 true fast ripples. Method 2 detected 21 true ripples and 33 true fast ripples, and method 3 was able to detect 70 true ripples and 54 true fast ripples. Statistical analysis showed a significant effect of method (χ^2 = 37.5, df = 5, $p < 0.05$) and post-hoc tests showed a significant difference between the sensitivity of methods 1 and 3 ($p < 0.05$), for both ripples and fast ripples (Fig 2.4C).

2.4.4.3. Post-ictal period

No true ripples or true fast ripples were detected by method 1. Method 2 detected 5 true ripples and 7 true fast ripples, whereas method 3 detected 7 true ripples and 10 true fast ripples. No significant difference was observed between methods (Fig 2.4D).

These results suggest that when dividing seizures into the pre-ictal, ictal and post-ictal periods, we observed that method 3 has higher sensitivity compared to method 1, but only for the ictal period. No significant differences were observed between the sensitivities of the three automated methods for the pre- and post-ictal periods.

2.4.5. False detection of HFOs

2.4.5.1. Comparisons with the first visual analysis

When comparing results obtained with the automated methods to results obtained with the first visual analysis, method 1 detected 2 "false" ripples and 2 "false" fast ripples. Method 2 detected 3 "false" ripples and 4 "false" fast ripples. Method 3 detected 58 “false”

ripples and 38 “false” fast ripples. Statistical analysis showed a significant effect of methods (χ^2 = 35.8, df = 5, p < 0.001) and post-hoc tests showed that method 3 is detecting significantly more "false" ripples compared to methods 2 and 1, whereas no significant differences were observed between methods for fast ripples (Fig 2.5A). The high number of “false” ripples associated to method 3 was also higher during the ictal discharge (data not shown). This high number of false positives associated to method 3 could however be caused by the low number of detected events associated to the first method of visual analysis, since this difference is not observed when using the second method of visual analysis (see next section).

2.4.5.2. Comparisons with the second visual analysis

In contrast, when comparing results obtained with those obtained with the second visual analysis, method 1 detected no "false" ripple and 1 "false" fast ripple, method 2 detected 5 "false" ripples and 4 "false" fast ripples, and method 3 detected 17 "false" ripples and 4 "false" fast ripples. We observed a significant effect of methods (χ^2 = 35.8, df = 5, p < 0.001) but no significant differences between them for both ripples and fast ripples. Thus, when comparing “false” HFOs detected with those obtained with the second visual analysis, the number of false detections is similar between methods (Fig 2.5B).

2.5. Discussion

The main findings of our study can be summarized as follows: (1) when grouping all the periods (pre-ictal, ictal and post-ictal), method 3 shows higher sensitivity compared to method 1, when the first and second methods of visual analyses are used as gold standards

for the detection of HFOs; (2) when performing separate analyses for each period, method 3 shows higher sensitivity compared to method 1 during the ictal period; (3) the false detection rate of method 3 for ripples is significantly higher than methods 1 and 2 when the first visual analysis is used as the gold standard, but performs equally to the other two methods for fast ripples and when the second method of visual analysis is used as the gold standard. Therefore, we suggest that by using a reference period before seizure onset for signal normalization, as used in method 3, it produces results that are more similar to both methods of visual analysis when detecting HFOs during seizures.

One of the main advantages of using method 3 is that it can be easily implemented in any software, and parameters can be modified and adapted according to the type of signal that is analyzed. The time-consuming visual analysis that is usually performed on EEG traces would thus be greatly reduced since only a fast inspection of suspicious HFO events could be performed. For instance, HFOs caused by movement artifacts or those associated to sharp transients would have to be removed. However, by adding new parameters such as the wavelet transforms (Crépon et al., 2010) or by computing the time-frequency spectrum of each detected event (Bénar et al., 2010), one could identify events for which the energy of the oscillations spreads over the entire spectrum, and that are often caused by sharp transients.

Finally, it remains to be known whether this method can be applied to other types of signal, such as the cortical EEG or the depth recordings from epileptic patients. We have however shown recently that it can be applied to *in vitro* signals, since HFOs were detected during ictal events recorded in slices from the piriform cortex (Panuccio et al., 2012). Further studies should also investigate whether this method can be applied to HFO

detection during interictal periods. There would however be a need to select an artifact-free reference period between interictal spikes.

In conclusion, to our knowledge, this is the first method of HFO detection that can be applied to both the pre-, ictal and post-ictal periods. From a clinical perspective, analyzing HFOs during seizures could reveal the underlying mechanisms of seizures and help to develop targeted therapeutic interventions in epileptic patients.

Acknowledgements

This study was supported by the Canadian Institutes of Health Research (CIHR grants 8109, 74609 and 102710).

2.6. Tables

Table 2.1. Number of detected oscillation by each method

Total Number of oscillations detected by each method					
	Method 1	Method 2	Method 3	Visual 1	Visual 2
Ripples	14	51	156	94	205
F-Ripples	25	80	125	113	192
Total	39	131	281	207	397
Total Number of oscillations detected by each method during pre-ictal period					
Ripples	5	19	32	42	74
F-Ripples	14	32	23	33	62
Total	19	51	55	75	136
Total Number of oscillations detected by each method during ictal period					
Ripples	9	26	112	40	117
F-Ripples	10	40	76	66	106
Total	19	66	188	106	213
Total Number of oscillations detected by each method during post-ictal period					
Ripples	0	6	12	12	14
F-Ripples	1	8	26	14	24
Total	1	14	38	26	38

2.7. Figures

Figure 2.1

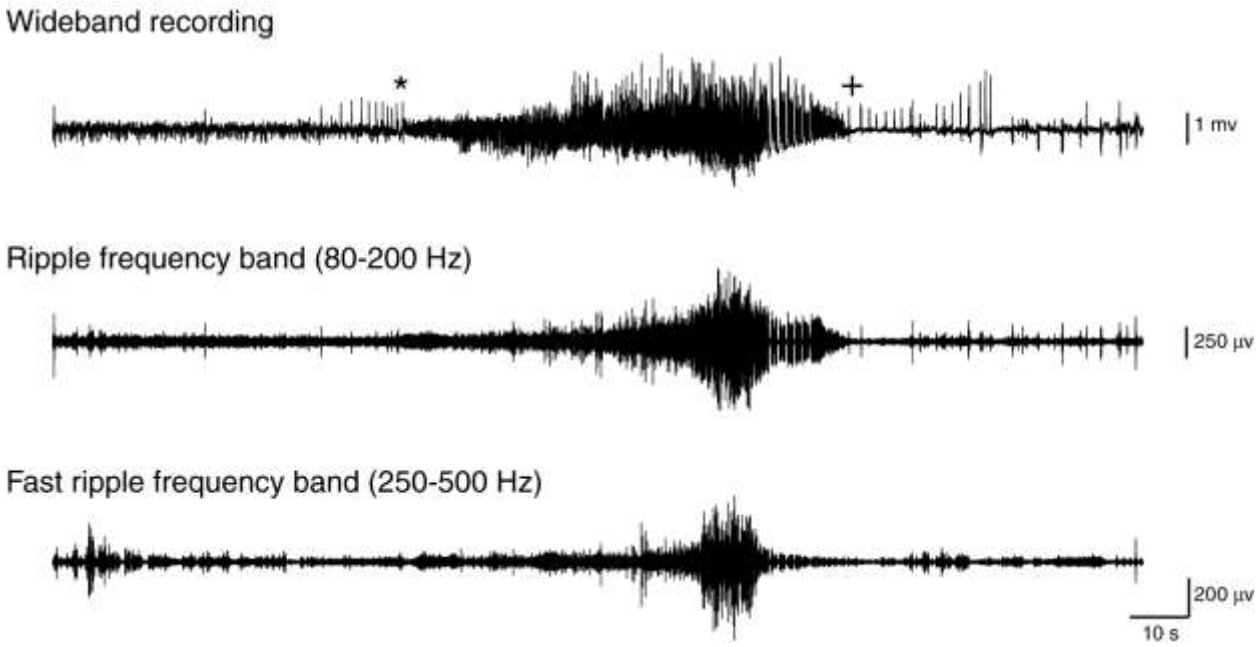

Figure 2.1. Representative local field potential recordings showing a seizure (* is indicating the onset and + is indicating the end of the seizure) from the CA3 region of hippocampus in a single rat. Filtered traces in the ripple (80-200Hz) and fast ripple frequency bands (250-500Hz) are shown.

Figure 2.2

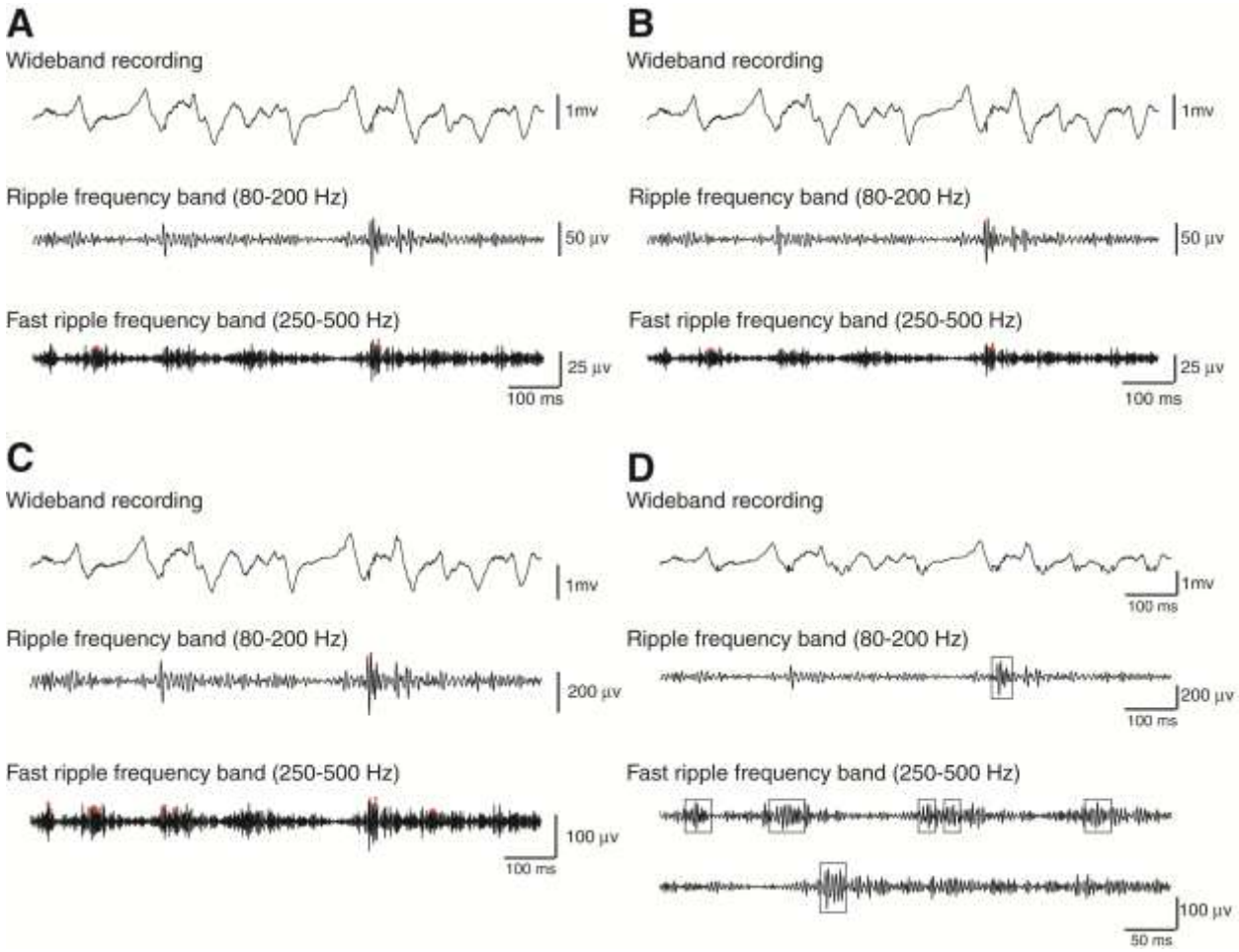

Figure 2.2. A sample trace from the seizure shown in Figure 2.1. Red asterisks indicate the detected ripples and fast ripples by three automated methods (Method 1 (**A**), Method 2 (**B**) and Method 3 (**C**)). **D.** Ripples and fast ripples (rectangles) detected with the visual analysis. The filtered trace in the fast ripple frequency range was split in half to facilitate the detection of oscillations.

Figure 2.3

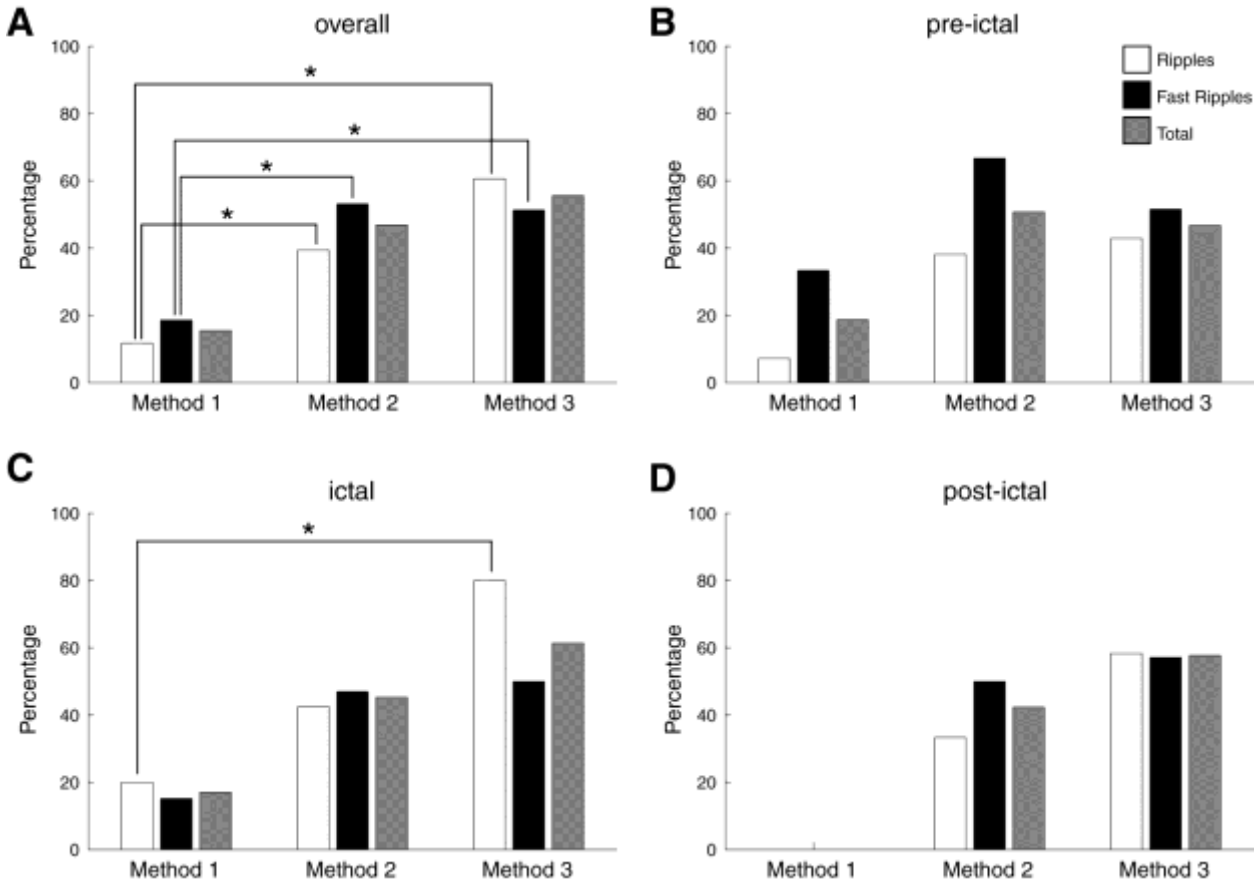

Figure 2.3. A. Overall sensitivity of the three automated methods according to the first visual analysis. The sensitivity ($\frac{Number\ of\ true\ positives}{Number\ of\ true\ positives + Number\ of\ false\ negatives} * 100$) of methods 2 and 3 were significantly higher compared to method 1 for both ripples and fast ripples. Sensitivity of the automated methods during the pre-ictal period (**B**), the ictal period (**C**) and the post-ictal period (**D**). The sensitivity of method 3 was significantly higher compared to method 1, but only for ripples (* $p < 0.05$).

Figure 2.4

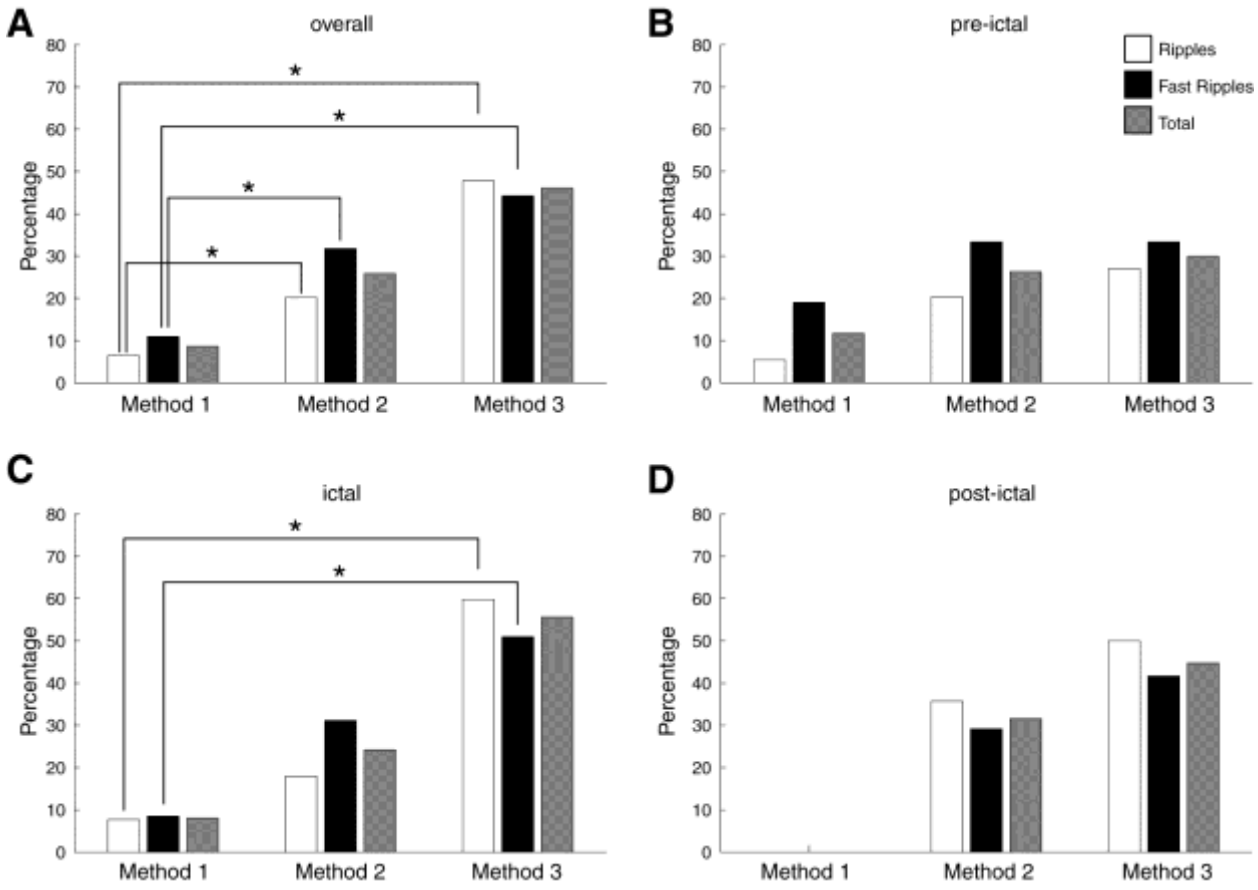

Figure 2.4. A. Overall sensitivity of each automated methods according to the second visual analysis. The sensitivity ($\frac{Number\ of\ true\ positives}{Number\ of\ true\ positives + Number\ of\ false\ negatives} * 100$) of methods 2 and 3 were significantly higher compared to method 1 for both ripples and fast ripples. Sensitivity of the automated methods during the pre-ictal period (**B**), the ictal period (**C**) and the post-ictal period (**D**). Method 3 showed higher sensitivity compared to method 1 for both ripples and fast ripples.

Figure 2.5

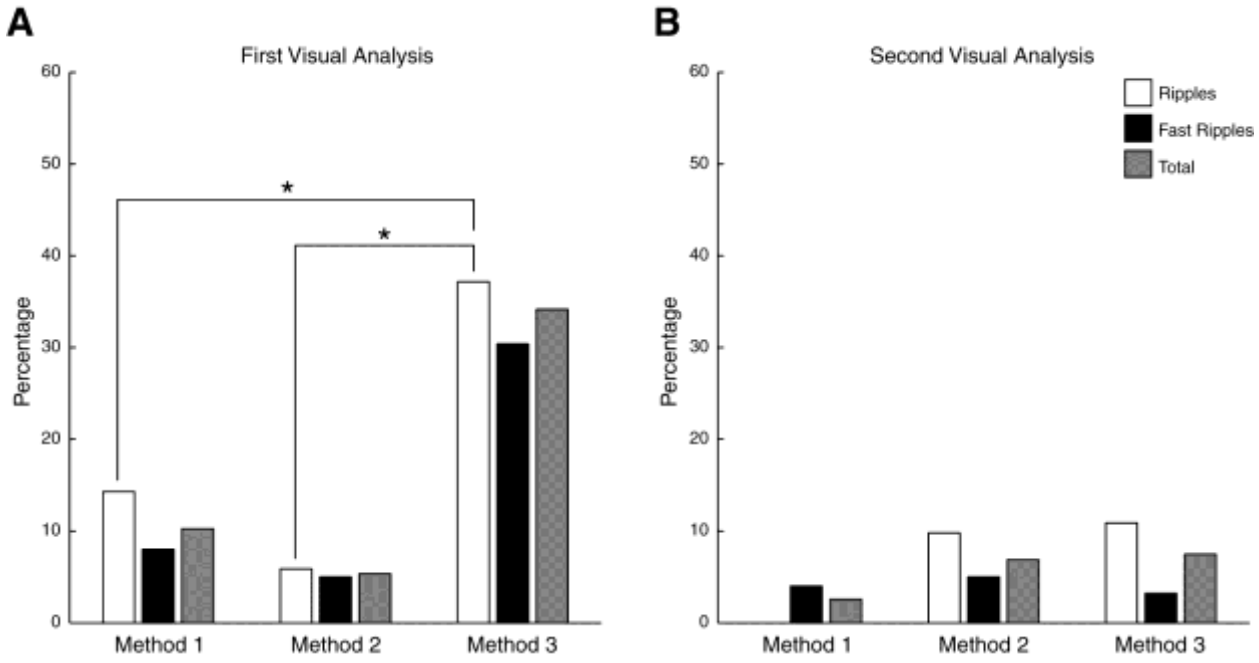

Figure 2.5. A. The percentage of false detections of each of the automated methods according to the first visual analysis. Method 3 showed higher false detection but only for ripples and when the first visual analysis was used as the gold standard. **B.** The percentage of false detections of each of the automated methods according to the second visual analysis. No significant differences between methods were observed.

3. Chapter 3

Two seizure-onset types reveal specific patterns of high-frequency oscillations in a model of temporal lobe epilepsy

Lévesque M, Salami P, Gotman J, Avoli M. *Journal of Neuroscience*, 2012 32(38): 13264-72.

Despite some studies addressing the role played by HFOs at the transition from pre-ictal to ictal period, the distribution of HFOs shortly before and during seizures remained undefined. Applying the most reliable method of HFO detection identified in the study reported in chapter 2, we analyzed in the study reported in chapter 3 the HFOs occurring during the pre-ictal and ictal periods of the seizures recorded in pilocarpine treated rats. Previous studies on HFOs reported an association between HFOs and seizure onset areas. Here, I identified an association between seizure onset patterns and the occurrence of HFOs in different frequency bands. The results of this chapter were published in 2012 in the *Journal of Neuroscience* in a manuscript entitled "Two seizure-onset types reveal specific patterns of high-frequency oscillations in a model of temporal lobe epilepsy".

3.1. Abstract

High-frequency oscillations (HFOs; 80-500Hz)are thought to mirror the pathophysiological changes occurring in epileptic brains. However, the distribution of HFOs during seizures remains undefined. Here, we recorded from the hippocampal CA3 subfield, subiculum, entorhinal cortex, and dentate gyrus to quantify the occurrence of ripples (80–200 Hz) and fast ripples (250–500 Hz) during low-voltage fast-onset (LVF) and hypersynchronous-onset (HYP) seizures in the rat pilocarpine model of temporal lobe epilepsy. We discovered in LVF seizures that (1) progression from pre-ictal to ictal activity was characterized in seizure-onset zones by an increase of ripple rates that were higher when compared with fast ripple rates and (2) ripple rates during the ictal period were higher compared with fast ripple rates in seizure-onset zones and later in regions of secondary spread. In contrast, we found in HYP seizures that (1) fast ripple rates increased during the pre-ictal period and were higher compared with ripple rates in both seizure-onset zones and in regions of secondary spread and (2) they were still higher compared with ripple rates in both seizure-onset zones and regions of secondary spread during the ictal period. Our findings demonstrate that ripples and fast ripples show distinct time- and region-specific patterns during LVF and HYP seizures, thus suggesting that they play specific roles in ictogenesis.

3.2. Introduction

High-frequency oscillations (HFOs; 80–500 Hz) are recorded in the EEG of temporal lobe epilepsy patients and in animal models mimicking this condition (Engel and da Silva, 2012; Jefferys et al., 2012b). HFOs occur in limbic structures such as the hippocampus and entorhinal cortex, as well as in the neocortex, and they are thought to reflect the activity of dysfunctional neural networks that underlie and sustain epileptogenesis (Bragin et al., 2004; Jacobs et al., 2009a, 2010; Ibarz et al., 2010; Jiruska et al., 2010a; Wu et al., 2010; Lévesque et al., 2011). HFOs are also better markers than interictal spikes to identify the seizure-onset zone, independently of the underlying pathology (Jacobs et al., 2008, 2009a; Crépon et al., 2010).

HFOs recorded from the hippocampal CA1 and CA3 subfields augment during the transition from preictal to ictal state in the *in vitro* low-Mg^{2+} model of epileptiform synchronization (Khosravani et al., 2005). Bragin et al. (2005) also found that HFOs increase in amplitude, duration, and frequency in the dentate gyrus at the onset of seizures occurring spontaneously *in vivo* in epileptic rats that have received a unilateral hippocampal injection of kainic acid. In keeping with these experimental data, Zijlmans et al. (2011) recently observed an increase in the percentage of time occupied by HFOs during the transition from preictal to ictal activity in epileptic patients, using time windows of 10 s before and 5 s after seizure onset; however, no significant increase in HFOs could be identified 1, 5, and 15 min before seizure onset in another clinical study (Jacobs et al., 2009a).

The temporal distribution of HFOs shortly before and during seizures is therefore undefined. In addition, we ignore whether ictal HFOs are differently expressed in seizure-

onset zones compared with other areas of the brain. Finally, the temporal and spatial distribution patterns of HFOs in different seizure-onset patterns remain unclear. Here, we addressed HFO dynamics across space and time during spontaneous seizures using chronic multichannel local field potential (LFP) recordings in the rat pilocarpine model of temporal lobe epilepsy. Specifically, we analyzed the occurrence of two different HFO categories [i.e., ripples (80 –200 Hz) and fast ripples (250 –500 Hz)] in low-voltage fast-onset (LVF) and hypersynchronous-onset (HYP) seizures (Velasco et al., 2000; Bragin et al., 2005, 2009a; Ogren et al., 2009b) during the preictal and ictal periods.

3.3. Materials and Methods

3.3.1. Animal preparation

Male Sprague Dawley rats (250–300 g) were obtained from Charles River and let habituate for 72 h after delivery before pilocarpine treatment. They were housed under controlled conditions, at 22°C (±2°C) and 12 h light/dark cycle (lights on from 7:00 A.M. to 7:00 P.M.) with food and water *ad libitum*. All procedures were approved by the Canadian Council of Animal Care, and all efforts were made to minimize suffering and the number of animals used.

Rats were given injections of scopolamine methylnitrate (1 mg/kg, i.p.; Sigma-Aldrich) and, 30 min later, a single dose of pilocarpine hydrochloride (380 mg/kg, i.p.; Sigma-Aldrich)(Bortel et al., 2010; Lévesque et al., 2011). Their behavior was scored according to the Racine scale (Racine, 1972), and *status epilepticus* was defined as continuous stage 5 seizures. *Status epilepticus* was terminated after 1 h by injection of

diazepam (5 mg/kg, i.p.; CDMV) and ketamine (50 mg/kg, i.p.; CDMV) (Martin and Kapur, 2008). The mortality rate was 13%. Surviving animals were allowed to recover for 72 h before surgery. They were then anesthetized with isoflurane (3%) in 100% O_2 and positioned in a stereotaxic frame so that lambda and bregma laid in the same horizontal plane. An incision was made in the skin to expose the skull plate. Four stainless steel screws (2.4 mm length) were fixed to the skull, and four small holes were drilled to allow the implantation of bipolar electrodes (20-30 kΩ; 30–50 mm length; distance between exposed tips, 500 μm) made by twisting and gluing two 0.006 inch resin-insulated copper wires. Contacts consisted of the cut edge of the wire (0.018 mm^2) (Châtillon et al., 2011). Electrodes were implanted in the CA3 subfield of the ventral hippocampus (AP, ±4.4; ML, ±4; DV, -8.8), medial entorhinal cortex (AP, ±6.6; ML, ±4; DV, -8.8), ventral subiculum (AP, ±6.8; ML, ±4; DV, -6) and dentate gyrus (AP, ±4.4; ML, ±2.4; DV, -3.4). Screws and electrode pins were connected with a pin connector and fastened to the skull with dental cement. A cortical screw placed in the frontal bone was used as reference, and a second screw, placed on the opposite side of the frontal region, was used as ground. After surgery, rats received topical chloramphenicol (Erfa) and lidocaine (5%; Odan) and were given subcutaneous injections of ketoprofen (5 mg/kg; Merail), buprenorphine (0.01– 0.05 mg/kg repeated every 12 h; CDMV) and 2 ml of 0.9% sterile saline.

3.3.2. Local field potential recordings and histological localization of depth electrodes

After surgery, rats were housed individually in custom-made Plexiglas boxes (30 x 30 x 40 cm) and let habituate to the environment for 24 h. The pin connector was then connected to a multichannel cable and electrical swivel (Slip ring T13EEG, Air Precision; or

Commutator SL 18C, HRS Scientific) and LFP-video monitoring (24 h per day) was performed. LFPs were amplified via an interface kit (Mobile 36chLTMProAmp; Stellate), low-pass filtered at 500 Hz, and sampled at 2 kHz per channel. Infrared cameras were used to record day/night video files that were time-stamped for integration with the electrophysiological data using monitoring software (Harmonie; Stellate). Throughout the recordings, animals were placed under controlled conditions (22 ± 2°C, 12 h light/dark schedule) and provided with food and water *ad libitum*. LFP-video recordings were performed up to 15 d after *status epilepticus*.

At the end of the recording, rats were deeply anesthetized with isoflurane, and electrode localization was aided by lesioning the surrounding tissue by passing current (500 μA, 120 s) through each recording electrode. Rats were maintained under deep anesthesia with isoflurane and decapitated. Brains were extracted and postfixed with formaldehyde (BioLynx) for at least 48hand later placed in a 30% sucrose–formalin solution for 48 h. They were then frozen in pulverized dry ice and sliced (30 μm thick) using a cryostat. Brain sections were mounted on gelatinized glass slides and stained using a cresyl violet solution. Location of the lesions was evaluated according to the atlas of (Paxinos and Watson, 1998) [see (Lévesque et al., 2011) for the histological localization of electrodes].

3.3.3. Detection of high-frequency oscillatory events

A multiparametric algorithm was used to identify oscillations in each frequency range, using routines based on standardized functions (Matlab Signal Processing Toolbox). For each seizure, raw LFP recordings were bandpass filtered in the 80–200 Hz and in the 250–

500 Hz frequency range using a finite impulse response filter; zero-phase digital filtering was used to avoid phase distortion. A 10 s artifact-free period (50–40 s before the seizure onset) was selected as a reference for signal normalization. LFPs from each region were normalized using their own reference period. To be considered as an HFO candidate, oscillatory events in each frequency band had to show at least four consecutive cycles having amplitude of 3 SD above the mean of the reference period. The time lag between two consecutive cycles had to be between 5 and 12.5 ms for ripples and between 2 and 4 ms for fast ripples. Furthermore, special care was taken to avoid the detection of false HFOs, since ripples were kept for analysis only if they were visible in the 80–200 Hz range, whereas fast ripples were kept only if they were visible in the 250–500 Hz range. Overlapping events, which may be caused by the filtering of sharp spikes (Bénar et al., 2010), were thus excluded from the analysis. Visual validation was also performed to eliminate the false positive created by movement artifacts. If a time period containing movement artifacts was observed on one channel, the same time period was removed on all channels. The final result was a list of "ripples" and "fast ripples," throughout the recording, for each region. Figure 3.1 shows examples of HFO events, whereas Figures 3.2*Ab*, *Bb*, *Cb*, and *Db* and 3*Ab*, *Bb*, *Cb*, and *Db* show HFOs during LVF and HYP seizures, respectively. Note that HFOs were visible on the wideband recordings and that there were no overlapping oscillatory events occurring simultaneously in the ripple and fast ripple frequency bands.

3.3.4. Detection of seizures and seizure-onset zones

Seizures were identified automatically with the ICTA-D seizure detector (Harmonie; Stellate). Validation of the results provided by the detector was performed by visual

inspection of LFPs and video. Termination of convulsive seizures was usually followed by wet-dog shakes. LFP recordings showed that seizures were characterized by paroxysmal discharges of increasing amplitude that involved multiple channels, for a duration of at least 5 s.

On average, the first seizure was observed 5.5 (±2.3) days after the pilocarpine induced *status epilepticus.* We considered the occurrence of the first seizure as the end of the latent period. All seizures used for analysis were thus extracted during the chronic period, up to 15 d after *status epilepticus.* Only seizures with good quality recordings on every channel were selected for analysis. Time periods containing the preictal and the ictal periods were exported for off-line analysis in Matlab 7.9.0 (Mathworks). To identify seizure-onset zones, the power spectral distribution of the LFPs from every region was computed, using a frequency range from 1 to 50 Hz. To enhance the detection of seizure onsets, a gamma correction with a factor 0.15 was applied to the spectrogram to improve the contrast to random noise.

Three reviewers blinded to electrode location were instructed to identify independently one or more seizure-onset zones, by looking at power spectral densities and LFPs. In addition, they were asked to point at the time of seizure onset in each brain structure. When seizure onset was preceded by focal interictal spikes (also termed preictal spikes; see (Huberfeld et al., 2011), the onset time was identified as the time of fast-activity onset (Figs. 3.2, 3.3, arrows). Whenever reviewers did not agree on the location of the seizure-onset zone or the time of onset, the recordings were further analyzed jointly until agreement was reached. Seizures could be categorized into four types: (1) seizures initiating in CA3 were labeled as “CA3”; (2) those originating from CA3 and another region

simultaneously were termed “CA3+”; (3) seizures initiating simultaneously in all regions were termed “widespread”; and (4) those that did not involve CA3 were labeled as “CA3-”.

Seizures were then transformed into a time scale from 1 (start of seizure) to 100 (end of seizure) to account for differences in seizure duration (range, 18 –135 s). The preictal period was also transformed into a time scale from 1 to 100. Values for the ripples and fast ripples were then averaged according to seizure type and region of onset. Distribution histograms of HFO occurrence were built for the preictal and ictal periods.

3.3.5. Classification of seizures

Seizures were classified in two groups according to their onset pattern (Velasco et al., 2000). LVFs were characterized by the occurrence of a positive- or negative-going spike that was followed by the appearance of low-amplitude, high-frequency activity (Fig. 3.2). HYPs were characterized at onset by a pattern of focal (preictal) spiking at a frequency of ~ 2 Hz (Fig. 3.3).

3.3.6. Statistical analysis

Rates and duration of each type of HFO (ripples, fast ripples) were computed for each region (CA3, entorhinal cortex, dentate gyrus, and subiculum) using the values that were obtained from all seizures. The preictal and ictal periods were divided in three equal parts, and rates of ripples and fast ripples in each part were compared using nonparametric Wilcoxon signed-rank tests followed by Bonferroni-Holm corrections for multiple comparisons. This allowed us to evaluate whether ripples or fast ripples predominated during each seizure type and at specific moments of the preictal and ictal periods, in seizure-onset zones and in regions of secondary spread. Nonparametric Kruskall-Wallis

tests were used to compare rates and duration of ripples and fast ripples between seizure types (i.e., LVF and HYP), regions (seizure-onset zones and regions of secondary spread), and time periods (preictal and ictal periods). We also evaluated whether ripple and fast ripple rates increased significantly during the preictal period by applying a linear regression between time and HFO rates. Statistical tests were performed in Matlab 7.9.0 (Mathworks) using the Statistics Toolbox. Results are expressed as mean ± SEM. The level of significance was set to $p < 0.05$.

3.4. Results

3.4.1. Seizure-onset zones

We analyzed a total of 42 seizures that were recorded in 6 epileptic animals. In one rat, all seizures were CA3; in two rats, they were CA3 in 53.9% and in 50% of cases, whereas the rest were CA3+. In the fourth rat, seizures were distributed as follows: CA3, 18.15%; CA3+, 36.4%; widespread, 27.3%; CA3-, 18.15%. In the fifth rat, 50% of seizures were widespread and 50% were CA3. In the sixth rat, seizures were always widespread.

3.4.2. Types of seizure onset

Representative examples of LVF and HYP seizures are shown in Figures 3.2 and 3.3, respectively. Fifty percent (21 of 42) of seizures were HYP, whereas 42.9% (18 of 42) were LVF. The remaining three seizures (7.1%) could not be classified as either HYP or LVF seizures and were excluded from the analysis. Three rats showed both types of seizures, one showed only LVF seizures, and two showed only HYP seizures. The duration of LVF

seizures [87.4 (±7.3) s] was significantly longer than the duration of HYP seizures [58.1 (±5.2) s] ($p < 0.05$) (Fig. 3.4*A*).

3.4.3. Relationship between seizure-onset zone and seizure-onset type

LVF seizures were characterized by a steady buildup of epileptic activity that started in the hippocampus (CA3) in 9 of 18 cases (50%), whereas the remaining seizures were widespread (22.2%), CA3+ (22.2%), or CA3- (5.6%) (Fig. 3.4*B*). On the other hand, 66.6% of HYP seizures (14 of 21) involved CA3 as the seizure-onset zone (CA3 or CA3+) (Fig. 3.4*B*). In six of seven CA3+ HYP seizures, the onset zones were in CA3 and the subiculum; in the remaining case, the onset zone was in CA3 and entorhinal cortex. The remaining seven HYP seizures were labeled as widespread. It should be noted that preictal spiking, characteristic of HYP seizures, only occurred in CA3 or in CA3 and another region simultaneously (CA3+) but never outside the hippocampus alone (e.g., the seizure shown in Fig. 3.3).

3.4.4. Duration of HFOs and relationship with the type of seizure onset

We recorded a total of 19,286 ripples and 19,868 fast ripples. Ripples lasted, on average, 47.9 (±0.2) ms, whereas fast ripples lasted, on average, 14.8 (±0.1) ms. When comparing the duration of ripples during the preictal and ictal periods of LVF and HYP seizures, we observed a significant effect of seizure type (LVF and HYP), region (seizure-onset zones and regions of secondary spread), and time periods (preictal and ictal) ($\chi^2 = 1002.2$; df = 7; $p < 0.001$). *Post hoc* comparisons revealed that during LVF seizures, (1) ripples lasted longer during the ictal period compared with the preictal period, both in seizure-onset zones and in regions of secondary spread; (2) ripples lasted longer in seizure-onset zones than in

regions of secondary spread ($p < 0.001$) (Fig. 3.5*A*, Ictal period), whereas (3) no significant differences were observed during the preictal period (Fig. 3.5, Pre-ictal period); and (4) ripples lasted longer during the ictal period of LVF seizures in both seizure-onset zones and regions of secondary spread, compared with those recorded during HYP seizures ($p < 0.001$) (Fig. 3.5*A*, Ictal period). The duration of fast ripples did not differ between seizure types, regions, or time periods (Fig. 3.5*B*).

3.4.5. Spatial and temporal distribution patterns of HFOs in temporal lobe regions

Figure 3.6 shows the temporal and spatial distribution of HFOs during LVF seizures in each region. Significantly higher ripple rates compared with fast ripple rates were observed in the preictal period in CA3, which was, in most cases (72.2%), the LVF seizure-onset zone (Fig. 3.6, CA3, Pre-ictal) ($p < 0.001$). During the ictal period, all regions showed significantly higher ripple rates compared with fast ripple rates ($p < 0.001$) (Fig. 3.6, Ictal).

Comparison of HFO rates during the preictal period of HYP seizures revealed significantly higher rates of fast ripples compared with ripples ($p < 0.001$) in all regions (Fig. 3.7, Pre-ictal). During the ictal period, higher fast ripple rates were still observed in all regions compared with ripple rates ($p < 0.001$) (Fig. 3.7, Ictal).

3.4.6. Spatial and temporal distribution patterns of HFOs in seizure-onset zones and regions of secondary spread

Comparing ripple and fast ripple rates that occurred during LVF seizures in onset zones and in regions of secondary spread revealed that during the preictal period, the formers increased significantly over time ($r^2 = 0.37$; $p < 0.0005$) and were higher than fast ripple rates ($p < 0.001$) in seizure-onset zones only (Fig. 3.8*A*, Pre-ictal period). In regions of

secondary spread, no significant difference between ripple and fast ripple rates were observed, and HFO rates did not increase significantly over time (Fig. 3.8*A*, Preictal period). During the ictal period, ripple rates continued to predominate over fast ripples in the seizure-onset zone ($p < 0.001$) (Fig. 3.8*A*, Ictal period) and became significantly higher compared with fast ripple rates during the last part of the seizure in regions of secondary spread ($p < 0.001$) (Fig. 3.8*A*, Ictal period). In addition, ripple rates were overall significantly higher in seizure-onset zones than in regions of secondary spread ($\chi^2 = 144.33$; df = 3; $p < 0.01$).

The comparison of HFO rates during HYP seizures revealed that during the preictal period, fast ripple rates had significant and linear increases in both seizure-onset zones ($r^2 = 0.37$; $p < 0.0005$) and regions of secondary spread ($r^2 = 0.62$; $p < 0.0001$) (Fig. 3.8*B*, Pre-ictal period). Fast ripple rates were also higher than ripple rates during the preictal period ($p < 0.001$, $p < 0.05$) in seizure-onset zones and in regions of secondary spread (Fig. 3.8*B*, Pre-ictal period). Throughout the ictal period, fast ripple rates were higher than ripple rates in seizure-onset zones and in regions of secondary spread ($p < 0.001$) (Fig. 3.8*B*, Ictal Period). No significant differences were observed when comparing rates of fast ripples in seizure-onset zones and in regions of secondary spread throughout the entire seizure.

3.5. Discussion

The main findings of our study can be summarized as follows: (1) spontaneous seizures observed after a pilocarpine-induced *status epilepticus* are characterized by either LVF or HYP onsets, the former seizures being longer in duration; (2) specific HFO patterns are

associated with these two types of seizures since ripples predominate during LVF seizures and fast ripples during HYP seizures; (3) ripple rates in LVF seizures increase over time before onset and are higher than fast ripple rates during both preictal and ictal periods; (4) ripples occurring during LVF seizures have longer duration and higher rates in seizure-onset zones than in regions of secondary spread; (5) ripple duration is longer in seizure-onset zones during the ictal period of LVF seizures compared with the preictal period and the duration of ripples occurring during HYP seizures; (6) HYP seizures are characterized by an increase over time of fast ripple rates before seizure onset that remains higher than ripple rates throughout the ictal period.

3.5.1. Seizure-onset patterns as a determinant of seizure duration

Spontaneous seizures occurring in pilocarpine-treated epileptic rats are characterized by either LVF or HYP onsets. These two types of seizure onset were originally identified in temporal lobe patients recorded with intracranial depth electrodes (Velasco et al., 2000) and later confirmed in rats made epileptic by intrahippocampal kainic acid injection (Bragin et al., 2005). The probability of occurrence of LVF and HYP seizures was indeed similar in our experiments, and both seizure types could be recorded in three rats. However, we discovered that LVF seizures lasted significantly longer than HYP seizures. The cellular and pharmacological mechanisms responsible for such difference remain to be established, but retrospective analysis of *in vitro* data obtained in the entorhinal cortex during application of the K^+ channel blocker 4-aminopyridine suggests a role for $GABA_A$ receptor signaling because (1) ictal events characterized by an LVF-like onset pattern (Lopantsev and Avoli, 1998b) last longer than those preceded by continuous interictal spiking (Lopantsev and Avoli, 1998a) and (2) blocking ionotropic glutamatergic

transmission in these experiments reveals the presence of synchronous GABA receptor-mediated potentials only in brain slices that generate LVF-like onset discharges (Lopantsev and Avoli, 1998a, 1998b).

3.5.2. Fast ripples and ripples characterize different seizure-onset patterns

We have also found in this model of temporal lobe epilepsy that the pattern of HFO occurrence is related to seizure-onset type. It has been reported in epileptic patients that the occurrence of HYP seizures may be related to hippocampal atrophy and gliosis since patients presenting with LVF seizures show more diffuse neuronal loss (Park et al., 1996; Velasco et al., 2000; Staba et al., 2007; Ogren et al., 2009b). However, our results do not favor the hypothesis that neuronal loss defines the type of seizure onset (i.e., HYP and LVF) because three of six rats showed both types of seizures. Hence, our findings indicate that HFOs reflect dynamic processes that may rest on the functional organization of neuronal clusters during the ictal period rather than the level of neuronal damage, which in our experimental model was induced by the initial pilocarpine-induced *status epilepticus.*

The occurrence of distinct types of HFOs during HYP and LVF seizures could also depend on the location of the seizure-onset zone. Previous studies have shown that HYP seizures are rather restricted in origin and often start in the hippocampus, whereas LVF seizures initiate from widespread regions often involving extrahippocampal areas (Velasco et al., 2000; Bragin et al., 2005). This evidence would explain the high rates of fast ripples recorded during HYP seizures and their relative absence during LVF seizures, assuming that fast ripples occur in areas that are located in or near the epileptic generator (Bragin et al., 1999c; Staba et al., 2002; Jirsch et al., 2006; Jiruska et al., 2010b). However, we have

observed that ripples could also act as markers of seizure-onset zones when the type of seizure onset is considered since ripples increased over time before the initiation of LVF seizures; in addition, ripples occurred at higher rates compared with fast ripple rates both during the preictal and ictal periods in LVF seizure-onset zones. In contrast, fast ripples mainly characterized HYP seizures. Therefore, in temporal lobe regions, before and during ictal events, both ripples and fast ripples would be pathological events, as they would reflect the activity of distinct neural networks that eventually give rise to the different seizure-onset patterns observed on the EEG in the clinical context.

3.5.3. Fast ripples and ripples reflect neural network dynamics during seizures

Our results support the hypothesis that HFOs may trigger seizures (Traub et al., 2001), since ripple rates increased during the preictal period of LVF seizures and fast ripple rates increased a few seconds before HYP seizure onset. Although the exact mechanisms underlying the generation of ripples and fast ripples are not well defined, previous work has suggested that the generation of HFOs characterized by different frequencies rests on specific neuronal mechanisms. Ripples at frequencies up to 200 Hz, which can also be recorded in conditions of physiological excitability, have been proposed to represent IPSP populations generated by principal neurons entrained by network of synchronously active interneurons (Buzsáki et al., 1992; Ylinen et al., 1995). In contrast, fast ripples (at 250–500 Hz) do not depend on inhibitory transmission since they are recorded during $GABA_A$ receptor blockade and are believed to reflect the synchronous firing of principal (glutamatergic) neurons (Dzhala and Staley, 2004; Engel et al., 2009; Bragin et al., 2011). In addition, it has been proposed that fast ripples may result from the loss of synchronization during jittery, out-of-phase burst firing of principal cells in the epileptic hippocampus

(Foffani et al., 2007; Ibarz et al., 2010). Hence, the preferential association of ripples or fast ripples with LVF and HYP seizures in the pilocarpine model of temporal lobe epilepsy strongly suggest that specific mechanisms underlying network synchronization are linked to each seizure type.

As mentioned above, LVF seizures recorded in our study shared similar morphological features with a type of ictal-like discharge that is induced *in vitro* by application of 4-aminopyridine. These ictal-like discharges, which initiate with a long-lasting depolarization of principal neurons followed by fast activity, are thought to be related to an inhibitory process with enhancement of interneuronal activity, mediated by GABAergic signaling at seizure onset (Avoli and de Curtis, 2011). Thus, ripples recorded during these *in vitro* seizure-like discharges could reflect summated IPSPs generated by pyramidal cells in response to inhibitory interneuron firing. In line with this hypothesis, we have recently reported high rates of ripples along with the virtual absence of fast ripples during ictal-like events generated by piriform cortex networks after the administration of 4-aminopyridine (Panuccio et al., 2012). Therefore, evidence obtained *in vitro* support the hypothesis that LVF seizures rely on interneuronal activation and GABAergic synchronization.

3.6. Conclusions

From a clinical perspective, our study emphasizes the need to distinguish seizure-onset patterns in the analysis of HFOs during the preictal and ictal periods. Our findings also put further emphasis on the existence of different types of seizure onset that can co-occur in

the same animal over time and that presumably results from different underlying pathophysiological mechanisms of seizure onset. Additional studies should investigate whether fast ripples and ripples show distinct patterns of occurrence during interictal periods depending on the occurrence over time of different seizure types and whether HFOs recorded during interictal events reflect the same mechanisms as HFOs recorded during ictal events. Studies should also investigate the cellular mechanisms and relate single-cell activity to HFOs and seizure-onset patterns. Combining these information together could help to delineate better therapeutical targets in the treatment of temporal lobe epilepsy.

3.7. Figures

Figure 3.1

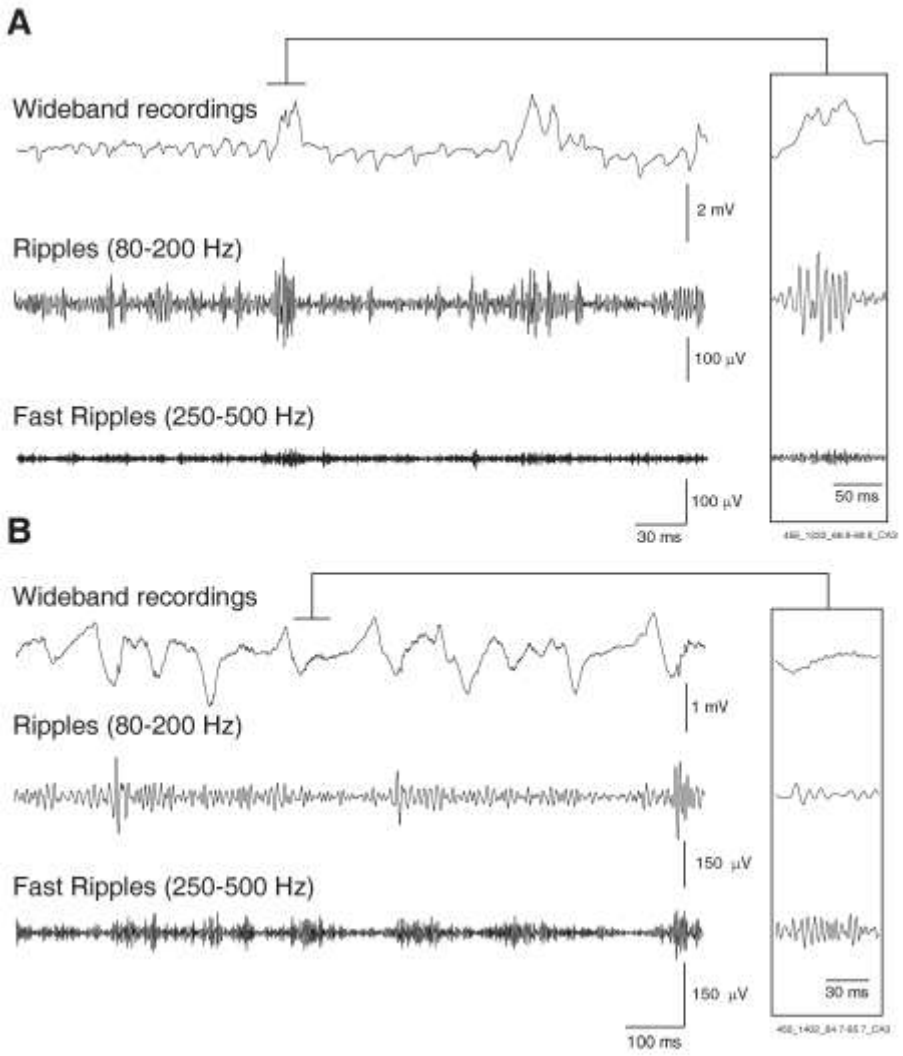

Figure 3.1. A. Representative local field potentials recorded from the CA3 region during an HYP seizure, 6.8 s after seizure onset showing the occurrence of a ripple (80 –200 Hz) (inset). **B**. Representative local field potentials from the CA3 region during another HYP seizure in the same rat, showing the occurrence of a fast ripple (250 –500 Hz) (inset) 24.7 s after seizure onset.

Figure 3.2

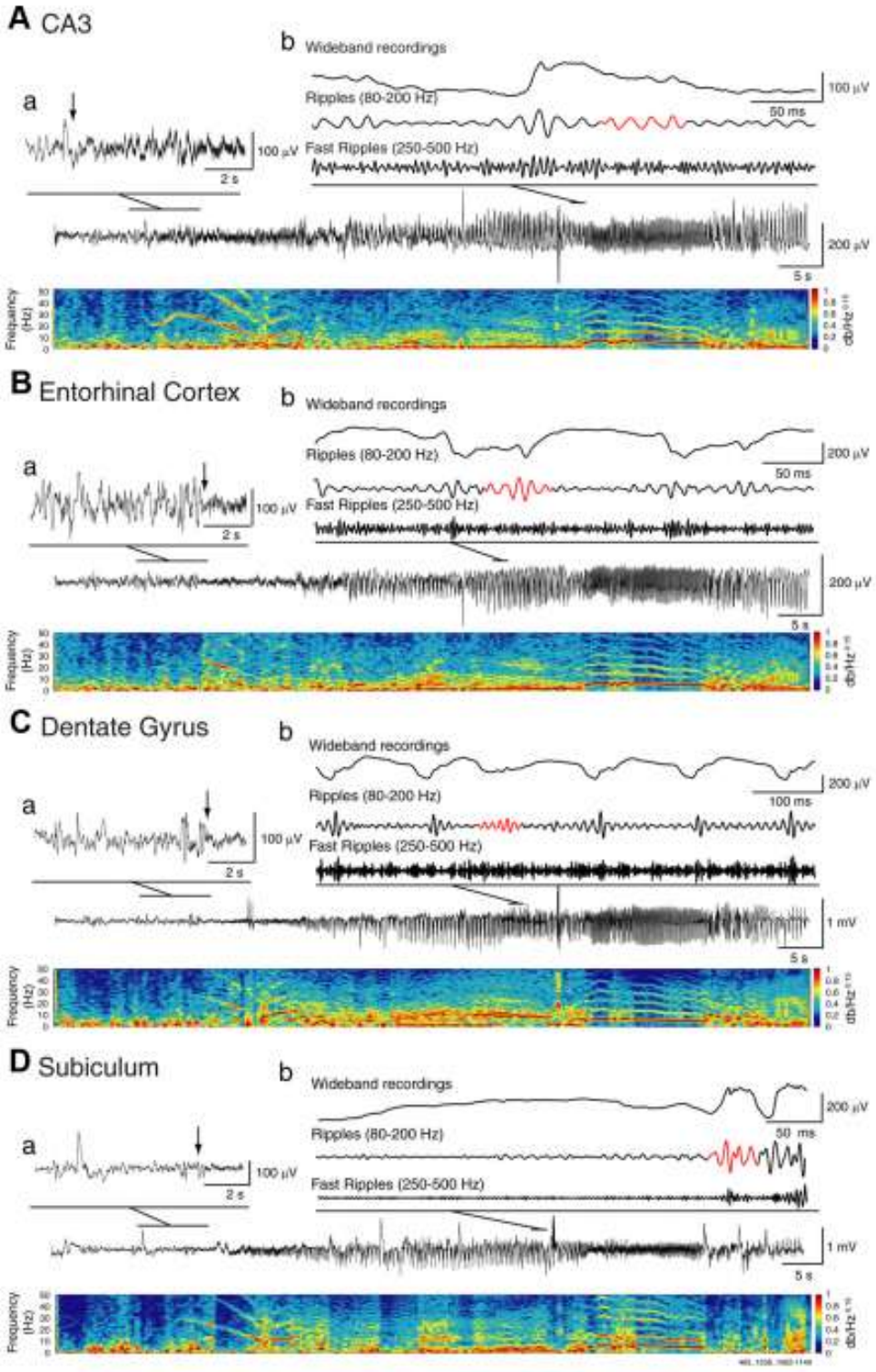
A CA3
b Wideband recordings
Ripples (80-200 Hz)
100 µV
50 ms
a
100 µV
Fast Ripples (250-500 Hz)
2 s
200 µV
5 s
Frequency (Hz)
B Entorhinal Cortex
b Wideband recordings
Ripples (80-200 Hz)
200 µV
50 ms
a
100 µV
Fast Ripples (250-500 Hz)
2 s
200 µV
5 s
Frequency (Hz)
C Dentate Gyrus
b Wideband recordings
Ripples (80-200 Hz)
200 µV
100 ms
a
100 µV
Fast Ripples (250-500 Hz)
2 s
1 mV
5 s
Frequency (Hz)
D Subiculum
b Wideband recordings
200 µV
Ripples (80-200 Hz)
50 ms
a
100 µV
Fast Ripples (250-500 Hz)
2 s
1 mV
5 s
Frequency (Hz)

Figure 3.2. Representative LVF seizure recorded simultaneously from the CA3 region **(A)**, the entorhinal cortex **(B)**, the dentate gyrus **(C)**, and the subiculum **(D)** with corresponding spectrograms. Note in the spectrogram of CA3 that highly rhythmic activity in the 10 –20 Hz frequency range characterizes the onset of ictal activity; this change was used by the reviewers to identify the seizure-onset time and zone. Note also that the initial phase of the seizure is shown in **a** on an expanded time scale; arrows indicate the onset of fast activity in CA3 and in the areas of propagation. Wideband and filtered signals in the ripple (80 –200 Hz) and fast ripple (250 –500 Hz) frequency ranges are also shown, with detected HFOs highlighted in red (**b**). Note that HFOs are visible on the wideband unfiltered signal and that they do not always occur on the spike component.

Figure 3.3

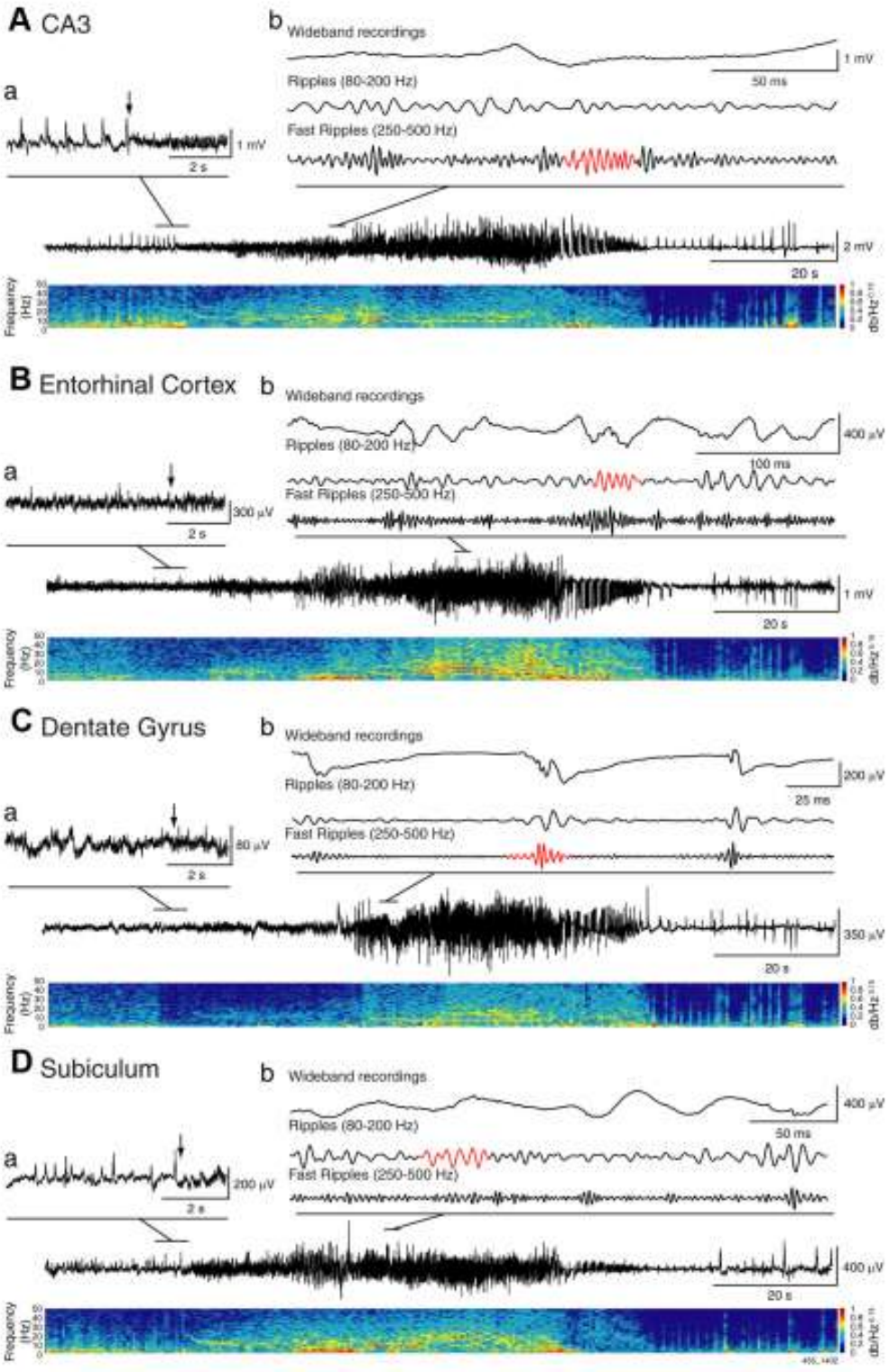
A CA3
a
b Wideband recordings
Ripples (80-200 Hz)
Fast Ripples (250-500 Hz)
1 mV
50 ms
2 s
2 mV
20 s
Frequency (Hz)
db/Hz
B Entorhinal Cortex
400 µV
100 ms
300 µV
1 mV
C Dentate Gyrus
200 µV
25 ms
80 µV
350 µV
D Subiculum
50 ms
200 µV
400 µV

Figure 3.3. Representative HYP seizure recorded simultaneously from the CA3 region (**A**), the entorhinal cortex (**B**), the dentate gyrus (**C**), and the subiculum (**D**). The initial phase of the seizure on an expanded time scale is shown in **a;** arrows indicate the onset of fast activity in CA3 and in the areas of propagation. Note that preictal spikes typical of HYP seizures occurred, in most cases, in CA3 and subiculum. Wideband and filtered signals in the ripple (80 –200 Hz) and fast ripple (250 –500 Hz) frequency range are shown in **b**, with HFOs highlighted in red.

Figure 3.4

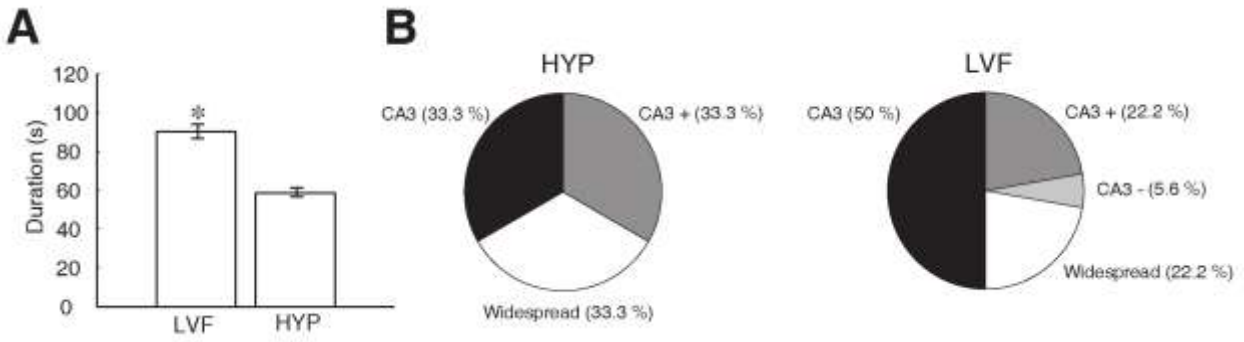

Figure 3.4. A. Bar graph showing the average duration of LVF and HYP seizures. HYP seizures were significantly shorter compared with LVF seizures (*$p < 0.05$), **B.** Pie charts showing the percentage of seizures labeled as CA3, CA3+, CA3-, and widespread for LVF and HYP seizures. Note that, in most cases, the CA3 was involved as a seizure-onset zone (66.6% of HYP seizures and 72.2% of LVF seizures).

Figure 3.5

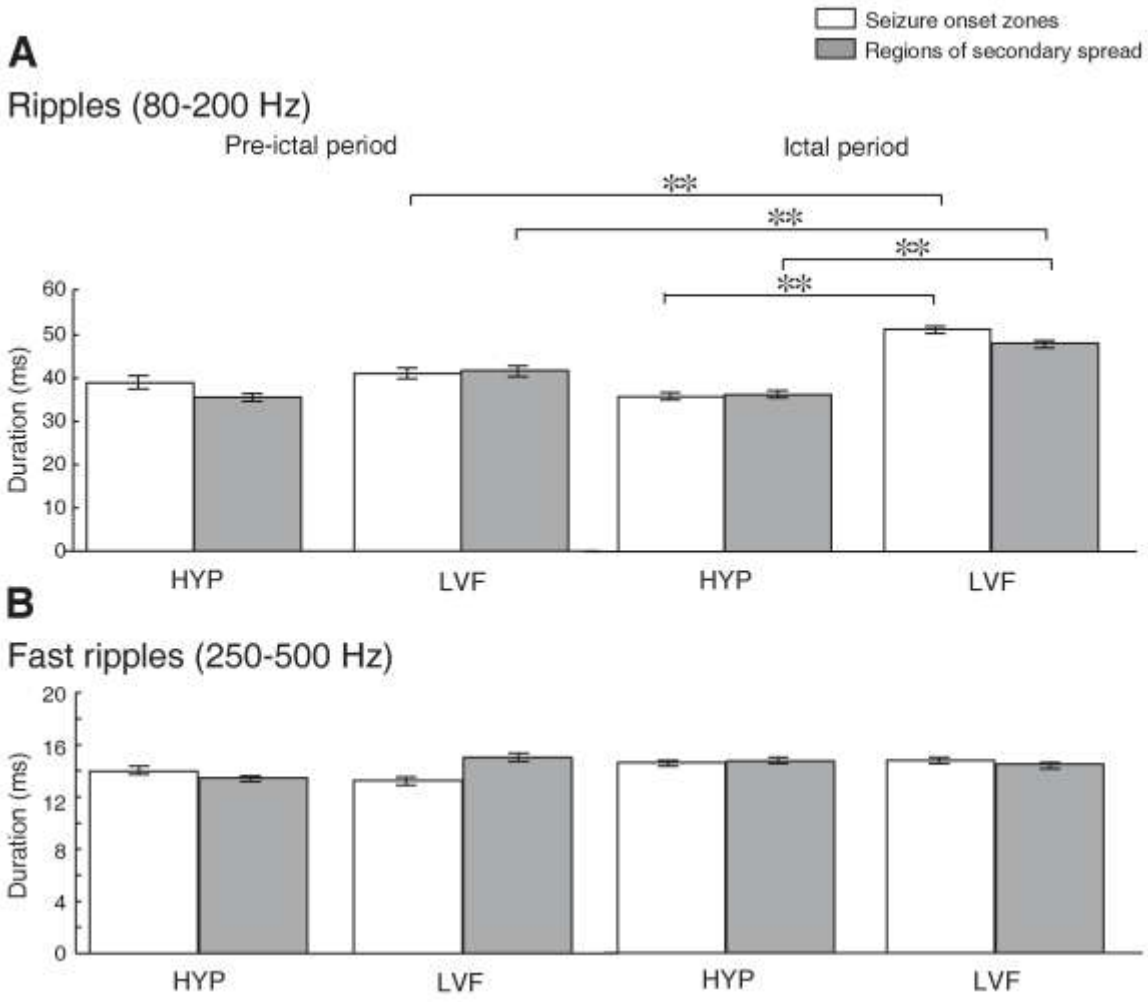

Figure 3.5. Bar graph showing the duration of ripples (***A***) and fast ripples (***B***) during the preictal and ictal periods for HYP and LVF seizures, in seizure-onset zone and in regions of secondary spread. Note that the duration of ripples was significantly longer during LVF seizures in seizure-onset zones and in regions of secondary spread, compared with HYP seizures. Ripples also lasted longer in seizure-onset zones of LVF seizures compared with regions of secondary spread. During LVF seizures, the duration of ripples was also longer during the ictal period compared with the preictal period (**$p < 0.001$).

Figure 3.6

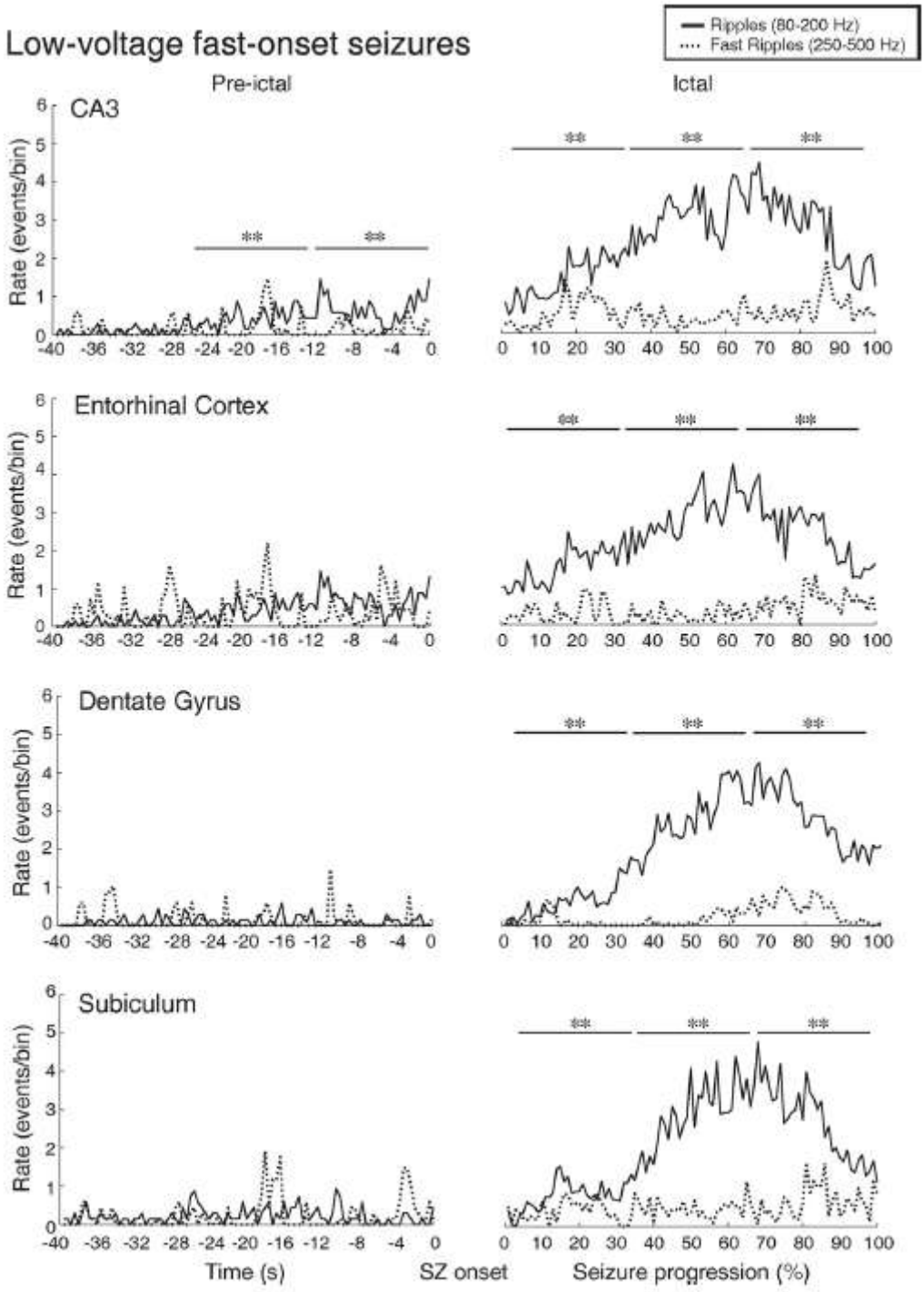
Low-voltage fast-onset seizures
Ripples (80-200 Hz)
Fast Ripples (250-500 Hz)
Pre-ictal
Ictal
CA3
Entorhinal Cortex
Dentate Gyrus
Subiculum
Rate (events/bin)
Time (s)
SZ onset
Seizure progression (%)

Figure 3.6. Spatial and temporal distribution patterns of HFOs during LVF seizures in CA3, entorhinal cortex, dentate gyrus, and subiculum. Ripple rates were higher compared with fast ripples rates during the preictal period of LVF seizures, in CA3, which was, in most cases, the seizure-onset zone. During the ictal period, all regions showed high rates of ripple compared with fast ripple rates (**$p < 0.001$).

Figure 3.7

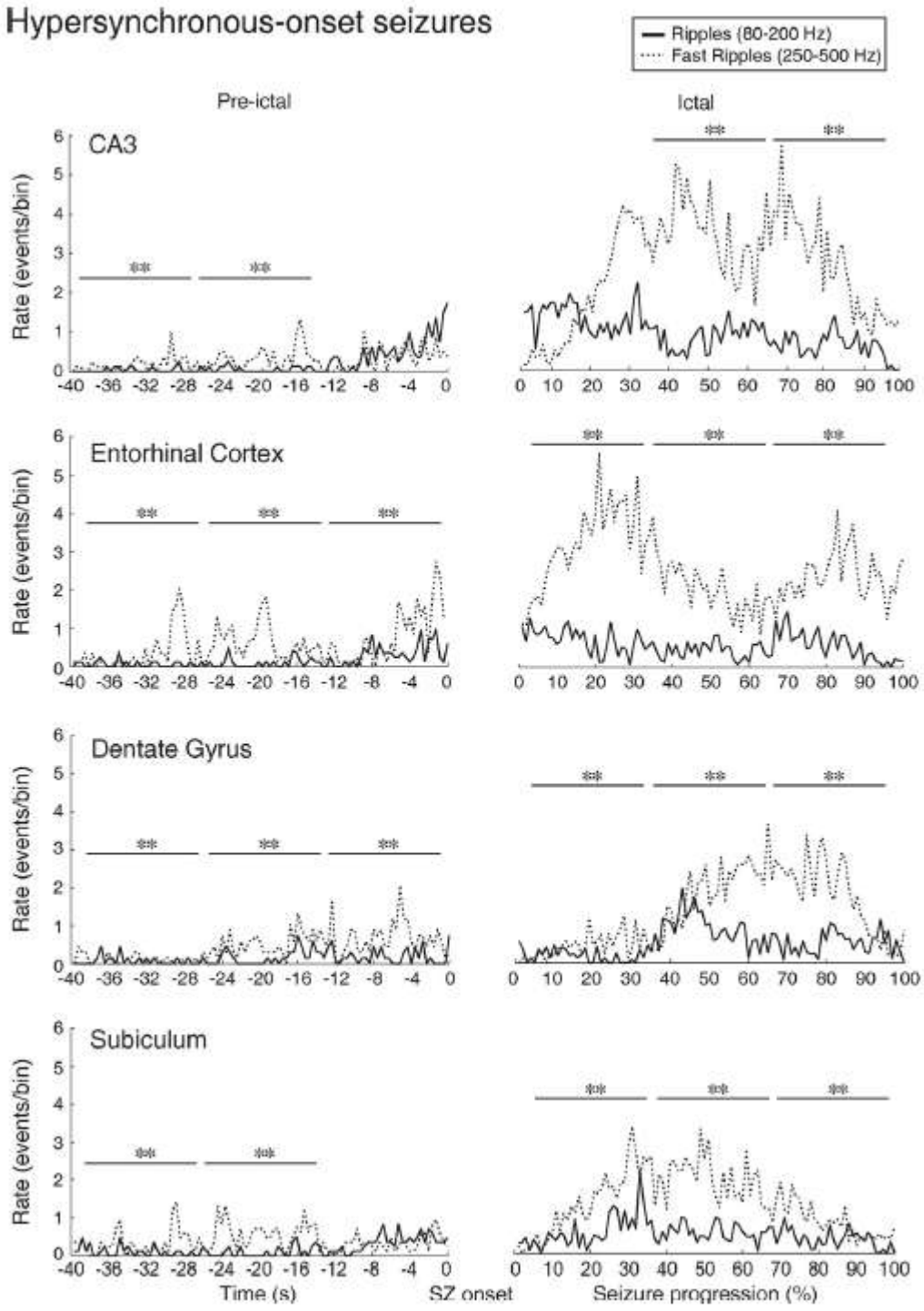
Hypersynchronous-onset seizures
Ripples (80-200 Hz)
Fast Ripples (250-500 Hz)
Pre-ictal
Ictal
CA3
Entorhinal Cortex
Dentate Gyrus
Subiculum
Rate (events/bin)
Time (s)
SZ onset
Seizure progression (%)

Figure 3.7. Spatial and temporal distribution patterns of HFOs during an HYP seizure in CA3, entorhinal cortex, dentate gyrus, and subiculum. Fast ripple rates were higher compared with ripple rates in all regions during the preictal and ictal periods (**$p < 0.001$).

Figure 3.8

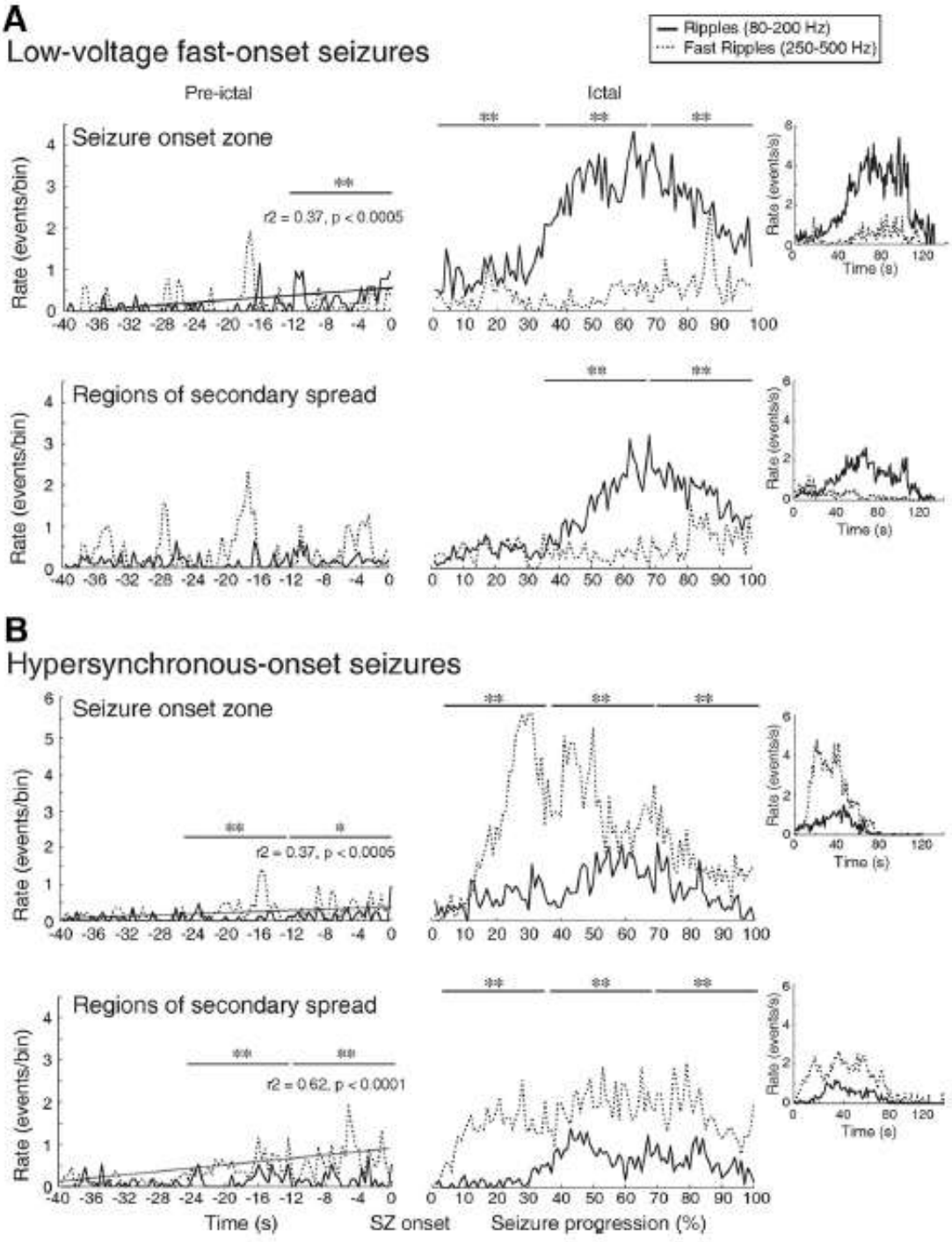
A
Low-voltage fast-onset seizures
Ripples (80-200 Hz)
Fast Ripples (250-500 Hz)
Pre-ictal
Ictal
Seizure onset zone
r2 = 0.37, p < 0.0005
Regions of secondary spread
Rate (events/bin)
Rate (events/s)
Time (s)
B
Hypersynchronous-onset seizures
Seizure onset zone
r2 = 0.37, p < 0.0005
Regions of secondary spread
r2 = 0.62, p < 0.0001
Time (s)
SZ onset
Seizure progression (%)

Figure 3.8. Spatial and temporal distribution patterns of HFOs during LVF (***A***) and HYP (***B***) seizures in seizure-onset zones and in regions of secondary spread. **A**. During the preictal period of LVF seizures, in seizure-onset zones, significantly higher rates of ripples were observed compared with fast ripple rates. Moreover, we observed a significant increase of ripple rates over time. During the ictal period, in the seizure-onset zone, the same pattern was observed, as ripple rates were higher compared with fast ripple rates. In regions of secondary spread, ripple rates were higher compared with fast ripple rates, but this occurred later during the seizure. **B**. During the preictal period of HYP seizures, fast ripple rates were higher compared with ripple rates in the seizure onset zone and in regions of secondary spread, and a significant increase of fast ripple rates was observed over time. During the ictal period, the same pattern was observed, as fast ripples were predominant compared with ripples. Insets show rates of HFOs occurring over seconds occurring throughout all seizures recorded (*$p < 0.05$; **$p < 0.001$).

4. Chapter 4

Temporal lobe epileptiform activity following systemic administration of 4-aminopyridine in rats

Lévesque M, Salami P, Behr C, Avoli M. *Epilepsia,* 2013 54(4) 596-604.

In chapter 3, I discovered the occurrence of two main seizure onset patterns, low-voltage fast (LVF) and hypersynchronous (HYP), in pilocarpine-treated rats. It was proposed that different mechanisms might be involved in the generation of these two distinct patterns since they were associated with different high frequency oscillations, namely ripples and fast ripples.

Previously, in our laboratory, we found that the administration of 4-aminopyridine (4AP) *in vitro* leads to the ictal-like events characterized mainly by LVF onset patterns. In this chapter, I investigated the EEG and clinical features of seizures induced by the systemic injection of 4AP *in vivo*. The results of this study were published in *Epilepsia* in 2013 as a manuscript entitled "Temporal lobe epileptiform activity following systemic administration of 4-aminopyridine in rats".

4.1. Abstract

Purpose: The K^+ channel blocker 4-aminopyridine (4AP) induces epileptiform synchronization in brain slices maintained *in vitro* without interfering with γ-aminobutyric acid $(GABA)_A$ receptor–mediated inhibition and, actually, even enhancing it. The hypothesis that similar electrographic epileptiform patterns occur *in vivo* following systemic 4AP injection was tested here.

Methods: Sprague-Dawley rats (n = 13) were implanted with bipolar electrodes aimed at the hippocampal CA3 region, entorhinal cortex, subiculum, dentate gyrus, and amygdala. They were then injected with a single dose of 4AP (4–5 mg/kg, i.p.), and video-monitoring/electroencephalography (EEG) recordings were performed.

Key Findings: 4AP induced convulsive or nonconvulsive seizures in 12 of 13 rats, along with generalized fascicular twitching, wet-dog shakes, and myoclonic jerks. On EEG, we observed in 7 (58.3%) of 12 animals long-lasting interictal spikes from the subiculum before the occurrence of the first seizure. Once seizures had started, interictal spikes occurred in all areas with no fixed site of origin. Most seizures (41/60, 68.3%) were characterized by a low-voltage fast-activity onset pattern and were convulsive (48/60, 80%). 4AP also induced highly rhythmic theta (6–11 Hz) oscillations in CA3 and entorhinal cortex before seizure occurrence.

Significance: Our study shows that systemic 4AP administration *in vivo* can enhance theta oscillations and induce slow interictal spikes and low-voltage fast-onset seizures similar to those reported in brain slices. We propose that these effects may reflect, at least in part, enhanced GABAA receptor–mediated inhibition as reported in *in vitro* studies.

4.2. Introduction

Knowledge of the fundamental mechanisms leading to epileptiform synchronization has greatly advanced during the last three decades thanks to the use of the *in vitro* brain slice preparation. Early studies - which were often carried out in ‘‘isolated’’ hippocampus slices - provided detailed information on the cellular and pharmacologic correlates of short-lasting (interictal-like) discharges induced by γ-aminobutyric acid $(GABA)_A$-receptor antagonists (see for review, (Avoli and de Curtis, 2011). Later, in vitro experiments conducted in extended brain slices including parahippocampal areas have shown that both interictal-like and long-lasting (ictal- or seizure-like) discharges occur following experimental procedures that do not fully block $GABA_A$ receptor– mediated inhibition (e.g., increased $[K^+]$ or removal of Mg^{2+} in the bathing medium) and even enhance it (e.g., bath application of the K^+ channel blocker 4-aminopyridine (4AP); see for review, (Avoli and de Curtis, 2011)).

Aminopyridines can induce seizures in humans as reported following accidental overdose (Schwam, 2011). Moreover, local application of 3AP to the somatosensory cortex elicits tonic seizures (Szente and Pongrácz, 1979), whereas intraperitoneal administration of 4AP in rodents causes generalized tremors and tonic–clonic seizures (Mihály et al., 1990). Depth electrode recordings in rats treated with systemic 4AP have also shown generalized tonic seizures that were associated with epileptiform discharges occurring in hippocampus, amygdala, and neocortex (Fragoso-Veloz et al., 1990). In contrast, local application of 4AP to the hippocampus or entorhinal cortex (EC) induced local hypersynchronous activity but not convulsive seizures (Fragoso-Veloz et al., 1990; Martín and Pozo, 2003; Medina-Ceja et al., 2008; Medina-Ceja and Ventura-Mejía, 2010).

Despite these *in vivo* findings, it remains unclear how interictal and ictal epileptiform discharges induced by systemic 4AP interrelate in multiple depth structures of the temporal lobe as well as whether and how these electrographic events correlate with specific behavioral symptoms. Therefore, we obtained depth electroencephalography (EEG) recordings from the hippocampal CA3 region, EC, subiculum, dentate gyrus, and amygdala along with video monitoring to study in Sprague-Dawley rats the effects induced by systemic 4AP injection. We report here that intraperitoneal administration of 4AP induces highly rhythmic theta (6–11 Hz) oscillations, a specific type of slow interictal discharge in the subiculum, and seizure activity that is often characterized by low-voltage fast-onset pattern (LVF).

4.3. Materials and Methods

4.3.1. Ethical approval

All procedures were approved by the Canadian Council of Animal Care, and all efforts were made to minimize the number of animals used and their suffering.

4.3.2. Animal preparation

Sprague-Dawley rats (250–300 g), obtained from Charles River Laboratories (St-Constant, QC, Canada), were housed under controlled environmental conditions (22 (±2) ˚C and 12 h light/12 h dark cycle) with food and water *ad libitum*. On the day of surgery, animals were anesthetized with isoflurane (3%) in 100% O2. They were then positioned in a stereotaxic frame so that lambda and bregma were in the same horizontal plane. An incision was made in the skin to expose the skull plate. Four stainless steel screws (2.4 mm length) were fixed

to the skull and used as anchors. Up to five small holes were drilled in order to implant bipolar electrodes (20–30 kΩ, 30–50 mm length, distance between exposed tips: 500 μm) made by gluing two insulated copper wires. Electrodes were implanted in temporal lobe regions, that is, the CA3 region of the ventral hippocampus (anteroposterior (AP): -4.4, mediolateral (ML): ±4.6, dorsoventral (DV): -7.6), medial EC (AP: -6.7, ML: ±4.6, DV: -8.4), ventral subiculum (AP: -6, ML: ±4.4, DV: -8.6), dentate gyrus (AP: -4.4, ML: ±2.4, DV: -3.5), and amygdala (AP: -2, ML: ±4.5, DV: -9). In order to rule out a cortical origin of seizures, we implanted additional animals (n = 2) with electrodes in temporal lobe regions and in the neocortex (AP: -1, ML: ±1.1, DV: -1.5). Screws and electrode pins were connected with a connector and fastened to the skull with dental cement. A cortical screw placed in the frontal bone was used as the reference, and a second screw, placed on the opposite side of the frontal region, was used as ground. After surgery, animals received topic application of chloramphenicol (Erfa, Montreal, QC, Canada) and lidocaine (5%; Odan, Pointe-Claire, QC, Canada) and were injected with carprofen (5 mg/kg, s.c.; Merail, Montreal, QC, Canada), buprenorphine (0.01–0.05 mg/kg, s.c., repeated every 12 h if necessary; CDMV, Saint-Hyacinthe, QC, Canada), and 2 ml of 0.9% sterile saline (s.c.).

4.3.3. EEG recordings and systemic injection of 4AP

Following surgery, rats were housed individually in custom-made acrylic glass boxes (30 x 30 x 40 cm) and allowed to habituate to the environment for 24 h. Animals were placed in controlled conditions (22 (±2) °C and 12 h light/ dark schedule) and provided with food and water *ad libitum*. On the day before 4AP injection, the pin connector was connected to multichannel cables and electrical swivels (Slip ring T13EEG; Air Precision, Le Plessis Robinson, France; or Commutator SL 18C; HRS Scientific, Montreal, QC, Canada), and EEG-

video monitoring was performed. EEG signals were amplified with an interface kit (Mobile 36ch LTM ProAmp; Stellate, Montreal, QC, Canada), and sampled at 2 kHz per channel. Infrared cameras were used to record video files that were time-stamped for integration with the electrophysiologic data using monitoring software (Harmonie; Stellate, Montreal, QC, Canada). On the day of 4AP (4–5 mg/kg, i.p.) injection, EEG-video recordings were obtained up to 4 h after injection.

4.3.4. Detection of seizures and seizure-onset zones

EEG signals were extracted from the Stellate Harmonie software and exported to Matlab for offline analysis. Seizure-onset zones were identified by visually analyzing EEG traces and spectrograms. The occurrence of activity between 5 and 20 Hz was considered as the onset of an ictal event (Fig. 4.3). Seizure-onset zones could be localized in one region or in two regions simultaneously. If the seizure started in more than three regions simultaneously, it was termed as ‘‘widespread.’’ Seizures were also classified as nonconvulsive (stage 0–2 of the Racine’s scale) or convulsive (stage 3–5; (Racine, 1972).

4.3.5. Detection of theta (6–11 Hz) oscillations

EEG recordings were analyzed using the spectrogram method, and calculated using the discrete short-time Fourier transform. Data sampled at 2 kHz were decimated by a factor of 15 after being low-pass filtered by a 100th order finite impulse response filter. The spectrogram was then elaborated from the data set and separated into 1-s intervals (134 points) to which a Hamming window was applied. The discrete Fourier transforms were evaluated over 1,024 points with zero padding.

The EEG was analyzed to identify time periods of strong theta oscillations. To enhance the detection of significant oscillations, a gamma correction with a factor of 0.15 was applied to the spectrogram to improve their contrast to random noise. A multiparametric algorithm was then used to identify oscillations in the 6–11 Hz band of the spectrogram. For each time slot, the algorithm identified the peak frequency in the band of interest and calculated the energy within a 1-Hz band centered on this peak. The energy within the peak must have been at least 40% of the largest peak within a 1-s window (time domain criterion), and contain at least 60% of the band energy at that time (frequency domain criterion) to be considered a valid candidate. An oscillation event was then identified by a succession of peaks with a specific track in time and frequency. Moreover, the relative peak intensities must not have varied in time by >100% per second, successive peak frequencies must not have varied by more than 7.5 Hz per second, and there must have been a continuous track of candidate peaks at least 5 s long.

4.3.6. Statistical tests

Because values were not normally distributed, nonparametric tests were used and are mentioned in the text when applied. The level of significance was set at $p < 0.05$. Statistical analyses were performed in Matlab 7.9.0 (Mathworks, Natick, MA, U.S.A.) using the Statistics Toolbox. Values are expressed as medians (95% confidence intervals) when compared with nonparametric tests; otherwise they are expressed as means (±standard error of mean).

4.4. Results

4.4.1. Preictal and interictal behavior

Increased exploratory behavior, widespread fasciculation with wet-dog shakes, as well as myoclonic jerks of the rear and forelimbs or of the entire body were observed in all animals 4.6 (±0.8) min after 4AP injection. The frequency of these behavioral symptoms increased progressively over time before reaching a peak approximately 20 min following 4AP injection. Moreover, we observed a high occurrence of wet-dog shakes shortly after 4AP administration and increases in their occurrence between seizures (Fig. 4.1A,B). In contrast, myoclonic jerks increased in occurrence later compared to wet-dog shakes (Fig. 4.1C). Two rats died 30 min after injection and one died 2.5 h after injection during strong convulsive seizures, giving a mortality rate of 16.7%.

4.4.2. 4AP-induced epileptiform activities on EEG

Interictal spikes were the first EEG abnormality to occur 11.4 (±8.5) min after 4AP injection. In 7 (58.3%) of 12 rats, this initial interictal activity was observed in the subiculum and consisted of long-lasting events (duration = 3.26 ± 0.12 s, n = 5 animals; Fig. 4.2A,B). The initial EEG change seen in the remaining animals after 4AP injection consisted of interictal spikes occurring in any region (not illustrated). Following the first seizure occurrence, interictal spikes were recorded from all regions (Fig. 4.2C). In addition to having shorter duration (0.74 ± 0.45 s) than those initially recorded in subiculum, these interictal spikes had no fixed site of origin.

Systemic injection of 4AP was effective in inducing seizures in 12 of 13 rats (n = 60 seizures). The remaining rat showed only subicular long-lasting interictal spikes that were

later followed by the appearance of short interictal spikes in all regions, with no fixed site of origin. Most seizures (41/60, 68.3%) were characterized by an LVF pattern, that is, they started with a negative or a positive spike followed by oscillatory activity in the 5–20 Hz frequency range and, later on, by high-amplitude low-frequency spikes (Fig. 4.3A). The remaining seizures were hypersynchronous-onset seizures (HYP; 16/60, 26.7%), since they were characterized at onset by a pattern of focal (preictal) spiking at a frequency of approximately 2 Hz (not illustrated). The remaining seizures could not be classified (3/60, 5%). Most seizures (48/60, 80%) were convulsive (stage 3–5 on the Racine scale); they were first characterized by behavioral arrest, followed by a short and discrete tonic phase, characterized by a mild extension of the head, with an axial twist of both head and neck and/or a tonic elevation of the tail. This was followed by a clonic phase, characterized by myoclonic activity of rear and forelimbs, which could evolve to rearing, running, and loss of balance (Racine stage 5). Seizure termination was characterized by immobility, during which the animal laid on his side.

Nonconvulsive seizures were characterized by automatisms (chewing, sniffing, swallowing) and an increase of occurrence of exploratory behaviors, followed by discrete tonic (head and trunk extension) symptoms. Wet-dog shakes were observed following both convulsive and nonconvulsive seizures. Fifty percent of the animals showed only convulsive seizures, whereas one rat showed only nonconvulsive seizures. The remaining rats showed both types of seizures, but convulsive seizures were more frequently observed, as they represented on average 72.1 (±12.1)% of seizures in these animals (n = 5).

The latency between 4AP injection and the occurrence of the first seizure was 23.6 (±19.8) min (n = 59 seizures observed in 12 animals), and successive seizures occurred on average every 28 (±24.5) min, giving a rate of 1.3 (±1.02) seizures per hour. The average duration of seizures was 123.9 (±48.7) s. Seizure rates were highest during the first hour and decreased progressively over time (Fig. 4.3B). Moreover, during the first hour after 4AP, rates of convulsive seizures were significantly higher compared to rates of nonconvulsive seizures (Wilcoxon signed-rank test, $p < 0.05$; Fig. 4.3C); this difference was not present from the second to the fourth hours after 4AP, and the occurrence of both seizure types decreased progressively over time. Convulsive seizures lasted longer than nonconvulsive seizures (Wilcoxon rank-sum test, $p < 0.05$; Fig. 4.3D).

On the EEG, convulsive and nonconvulsive seizures showed similar patterns of activity (Fig. 4.4). However, careful analysis of nonconvulsive seizures showed that mild behavioral symptoms (automatisms, increased exploratory behaviors) could co-occur with the onset of local epileptiform activity in the seizure-onset zone. For instance, Fig. 4.4A shows a nonconvulsive seizure characterized by initial symptoms such as automatisms and sustained exploratory behaviors, with the onset of fast activity (5–20 Hz) in the EC. Head and trunk extension then occurred when epileptiform activity spread outside of the seizure-onset zone. During convulsive seizures, as shown in Fig. 4.4B, the tonic and clonic phases were associated with widespread and high-amplitude epileptiform activity across the seizure-onset zone and ipsilateral regions.

Seizures induced by 4AP were initiated from mesial temporal lobe regions. A propagation of ictal activity to the cortex occurred late after seizure onset, and was associated with the convulsive phase of the seizure (Fig. 4.S1). In temporal lobe regions,

seizures most often started from the EC (20/60, 33.3%), whereas the remaining seizures started from the CA3 area, (9/60, 15%), the subiculum (7/60, 11.7%), or the amygdala (2/60, 3.3%). In 13.3% of seizures (8/60), the onset zone was located in CA3 and in another structure, simultaneously. Finally, 22% (13/60) of seizures were labeled as ‘‘widespread,’’ since they started on all channels simultaneously.

Although theta oscillations (6–11 Hz) were observed in all regions following 4AP administration, we analyzed oscillatory activity in the CA3 region and EC, since (1) it was more prominent in these regions than in other areas, and (2) these areas were mostly involved as seizure-onset zones. We identified a total of 919 runs of theta oscillations (n = 514 and 405 in EC and CA3, respectively). Compared to the baseline period (before 4AP), theta oscillations became highly sustained following 4AP (Fig. 4.5). They did not appear, however, to be related to any behavioral symptoms. The duration of theta oscillations in CA3 (median 18, 95% confidence interval [CI] 2.8 s) was not significantly different from the duration of theta oscillations in EC (median 18, 95% CI2.6 s), although they were significantly longer than periods of theta oscillations recorded before 4AP (CA3: median 7, 95% CI 3 s, EC: median 11, 95% CI 6.4 s, Wilcoxon rank sum test, $p < 0.01$, n = 3 animals).

4.5. Discussion

The main findings of our study can be summarized as follows: (1) systemic injection of 4AP induces initially behavioral symptoms such as widespread fasciculations, wet-dog shakes, and myoclonic jerks; (2) long-lasting interictal spikes appear in the subiculum before the occurrence of the first seizure, whereas shorter interictal spikes with no fixed site of origin

recur once seizures appear; (3) most seizures are characterized by an LVF onset pattern, are convulsive, and initiate from the EC or the CA3 region of the hippocampus; and (4) highly rhythmic activities in the theta (6–11 Hz) frequency band are disclosed by 4AP injection.

4.5.1. Initial 4AP-induced behavioral symptoms

As previously reported (Fragoso-Veloz and Tapia, 1992; Világi et al., 2009), we have found here that systemic 4AP administration induces wet-dog shakes, myoclonic jerks, fascicular twitching, forepaw tremor, chewing, myoclonus, and tonic–clonic seizures. The detailed mechanisms underlying such variety of symptoms remain unknown, although generalized fascicular twitching should presumably reflect enhanced neurotransmission at the neuromuscular junction (cf., Fastier and McDowall, 1958), as also suggested by the use of 4AP in the treatment of myasthenia gravis (Miller, 1979) and botulism (Ball et al., 1979). On the other hand, other symptoms may be linked to central effects induced by 4AP. For instance, wet-dog shakes that occurred early after injection could reflect an effect of 4AP on the limbic system, since these symptoms can be reproduced by electrical or pharmacologic stimulation of the hippocampus (Lerner-Natoli et al., 1984; Leung and Shen, 2006), the lateral septum, or the amygdala (Le Gal La Salle and Cavalheiro, 1981). Wet-dog shakes are also thought to be dependent on GABAergic processes (Tuff et al., 1983; Leung and Shen, 2006), making this behavior another GABAergic correlate of 4AP action. However, serotoninergic processes in limbic structures and dopaminergic processes in mesodiencephalic structures have also been linked to wet-dog shakes (Wang et al., 2005; Leung and Shen, 2006).

4.5.2. Occurrence of long interictal spikes in the subiculum before first seizure occurrence

The subiculum, which represents the major output of the hippocampus, plays a central role in modulating neuronal activity from the hippocampus to the EC and to other cortical and subcortical regions (Menendez de la Prida et al., 2006). Several studies have shown that subiculum generates interictal spikes and may thus serve as a generator of epileptiform activity or as a gate for the propagation of epileptic activity to other limbic and extralimbic areas (Benini and Avoli, 2005; Menendez de la Prida et al., 2006). In addition, Cohen et al. (2002) have reported that interictal spikes can occur in the human subiculum in an *in vitro* brain slice preparation without any epileptiform activity in the CA1–CA3 regions of the hippocampus. These interictal spikes were shown to rely on depolarizing $GABA_A$-receptor signaling contributed by the synchronous activation of interneurons. Similar findings have been obtained in human neocortical temporal lobe tissue (Köhling et al., 1998). The local generation of subicular interictal spikes that occurred following 4AP in our study is thus compatible with these previous *in vitro* findings.

4.5.3. Theta oscillations induced by 4AP in CA3 and entorhinal cortex

We have also observed that 4AP induces sustained and highly rhythmic runs of theta oscillations. These effects were more pronounced in EC and CA3, the two regions that were involved as seizure-onset zones in our experiments. These results–which are consistent with those obtained *in vivo* (Fragoso-Veloz et al., 1990) and *in vitro* (Henderson et al., 2010), following 4AP administration as well as during kindling stimulation of the perforant path (Popova et al., 2008; Kitchigina and Butuzova, 2009) - suggest that theta oscillations may have a role in ictogenesis (Butuzova and Kitchigina, 2008). Of interest, theta

oscillations are believed to result from the interaction between pyramidal cells and interneurons, and more specifically on GABAergic inputs to pyramidal cells (Klausberger, 2009). In line with this view (Buzsáki, 2002) has reported that theta oscillations are abolished by the $GABA_A$-receptor antagonist picrotoxin. Therefore, we are inclined to propose that the occurrence of high amplitude and highly rhythmic theta oscillations following 4AP rests on the ability of this drug to increase GABAergic transmission (Avoli and de Curtis, 2011).

4.5.4. 4AP-induced ictal events and seizure-onset zones

As in early *in vitro* 4AP studies (Avoli et al., 1996; Benini et al., 2003), we have found that seizures recorded *in vivo* frequently initiated in the EC. This finding is also in line with what was reported in experiments performed in combined hippocampus-EC slices bathed in Mg2+-free medium (Jones and Lambert, 1990; Dreier and Heinemann, 1991) and with evidence obtained *in vivo* by stimulating the hippocampus (Stringer and Lothman, 1992). In addition, dysfunctional EC has been identified in patients with temporal lobe epilepsy (Rutecki et al., 1989; Deutch et al., 1991; Spencer and Spencer, 1994). However, we also identified that some seizures initiated in CA3 or in CA3 and another region simultaneously. This evidence is in keeping with what has been reported *in vivo* in chronic models of temporal lobe epilepsy (Ben-Ari and Cossart, 2000; Bortel et al., 2010; Lévesque et al., 2011).

Systemic administration of 4AP induced seizure-onset patterns that could be classified as HYP or LVF. Similar findings have been recently obtained in animal models of temporal lobe epilepsy (Bragin et al., 2005; Lévesque et al., 2012) and in patients with

epilepsy (Velasco et al., 2000; Ogren et al., 2009b). However, 4AP could induce a higher proportion of LVF compared to HYP seizures (68.3% and 26.7%, respectively). Of interest, similar LVF ictal-like discharges have been identified in most of the *in vitro* experiments performed with 4AP, as well as that intracellular recordings from principal neurons have shown that these ictal events are shortly preceded (and thus presumably initiated) by a long-lasting GABAergic potential that reflects the synchronous activity of interneurons (cf., (Avoli and de Curtis, 2011). Furthermore, we have recently reported that *in vivo* and *in vitro*, LVF seizures are associated with an increased occurrence of ripples (80–200 Hz; (Lévesque et al., 2012; Panuccio et al., 2012), which are thought to reflect summated inhibitory postsynaptic potentials (IPSPs) generated by principal cells in response to inhibitory interneuron firing (Jefferys et al., 2012b). Therefore, the *in vivo* prevalence of LVF seizures indicates that also in this type of preparation 4AP may enhance GABAergic mechanisms.

It is also well established that 4AP blocks Kv1 channels (Yao and Tseng, 1994; Coetzee et al., 1999; Gutman et al., 2005), thus increasing action potential duration in nerve cells including interneurons (Zhang and McBain, 1995). In line with this mechanism of action, Smart et al. (1998) have found that spontaneous seizures and signs of peripheral neuronal hyperexcitability are observed in the Kv1.1 null mice model. This evidence, along with the results reported here, points at the role of K^+ channels in epilepsy and at their relevance as targets for antiepileptic drugs (Wickenden, 2002).

Acknowledgements

This study was supported by the Canadian Institutes of Health Research (CIHR grants 8109 and 74609). ML was recipient of a postdoctoral fellowship from the Savoy Foundation.

4.6. Figures

Figure 4.1

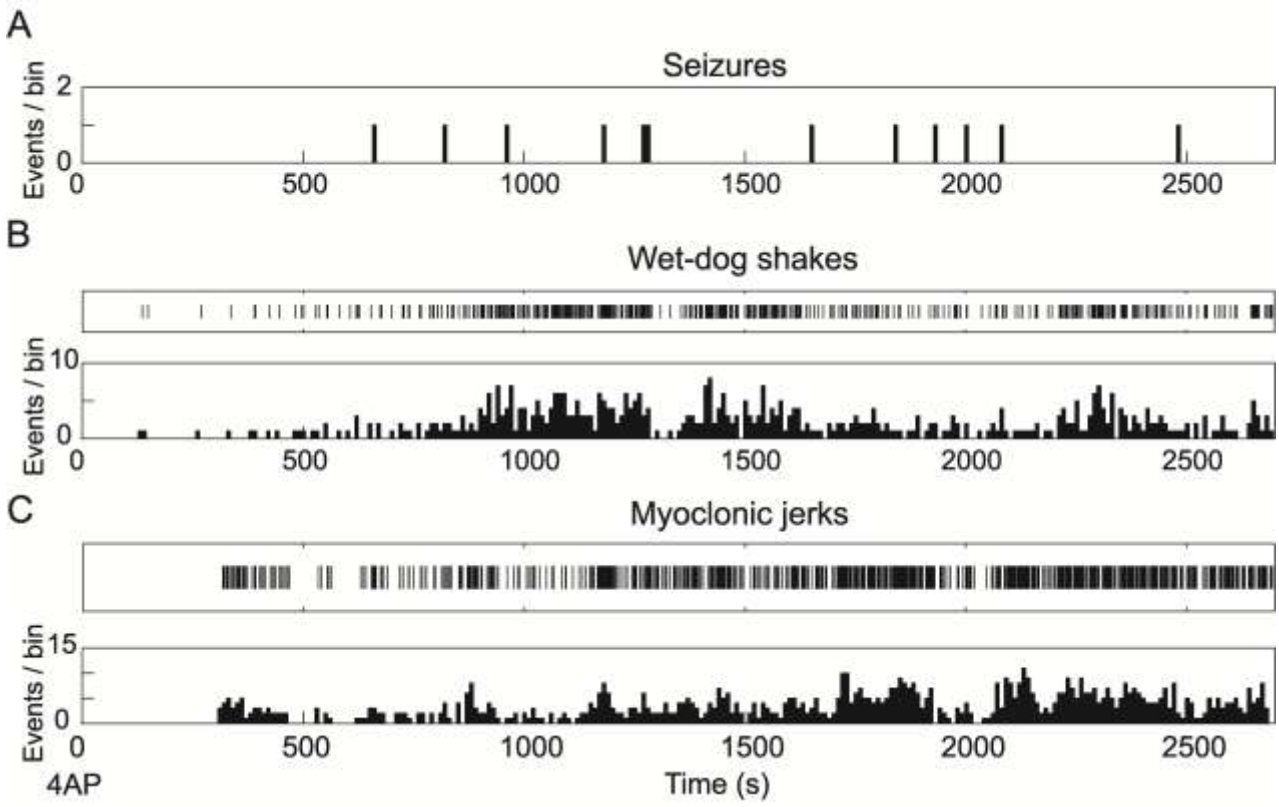

Figure 4.1. Development of seizures, wet-dog shakes, and myoclonic jerks following administration of 4AP in four rats. A. Occurrence of seizures over time after 4AP administration. **B, C.** Raster plots and corresponding frequency distribution histograms showing the occurrence of behavioral symptoms over time. Note that occurrence of wet-dog shakes **(B)** is higher after 4AP administration compared to myoclonic jerks that increased in occurrence later after 4AP administration **(C).**

Figure 4.2

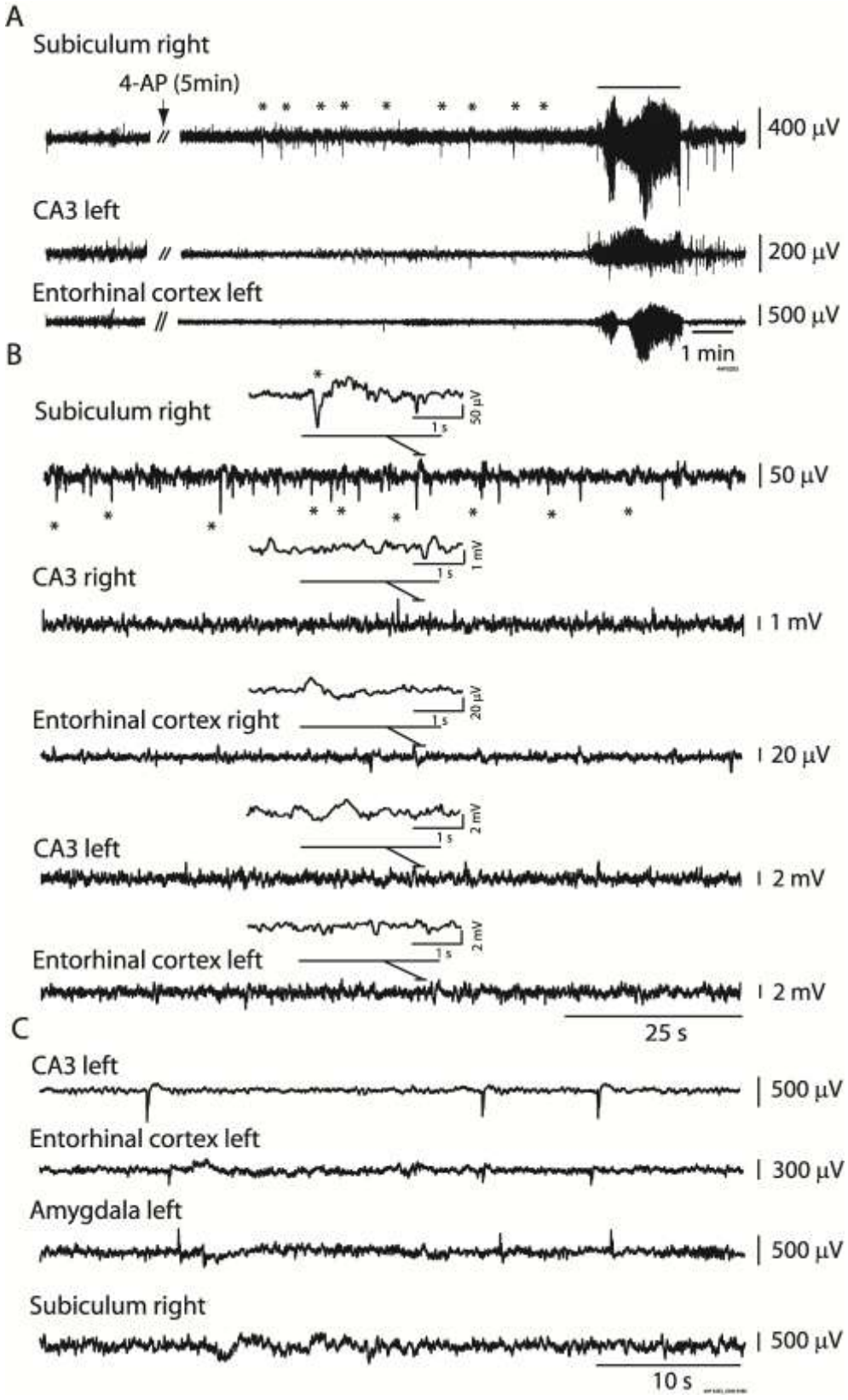
A
Subiculum right
4-AP (5min)
400 µV
CA3 left
200 µV
Entorhinal cortex left
500 µV
1 min
B
Subiculum right
50 µV
1 s
50 µV
CA3 right
1 mV
1 mV
Entorhinal cortex right
20 µV
20 µV
CA3 left
2 mV
2 mV
Entorhinal cortex left
2 mV
2 mV
25 s
C
CA3 left
500 µV
Entorhinal cortex left
300 µV
Amygdala left
500 µV
Subiculum right
500 µV
10 s

Figure 4.2. Interictal activity induced by systemic 4AP administration. A. EEG recordings obtained from an animal before and after the systemic administration of 4AP (arrow); note the early appearance of interictal spikes in the subiculum (asterisks) that precede the occurrence of the first seizure 12 min after injection. **B.** EEG recordings from a different rat after the administration of 4AP demonstrate at low speed the occurrence of interictal spikes only in the subiculum before the occurrence of the first seizure. Insets show simultaneous recordings (4 s) in all regions during an interictal spike occurring in the subiculum (asterisk). **C.** Representative recordings showing interictal spikes occurring in all regions once seizures started to occur. These interictal spikes had no fixed site of origin.

Figure 4.3

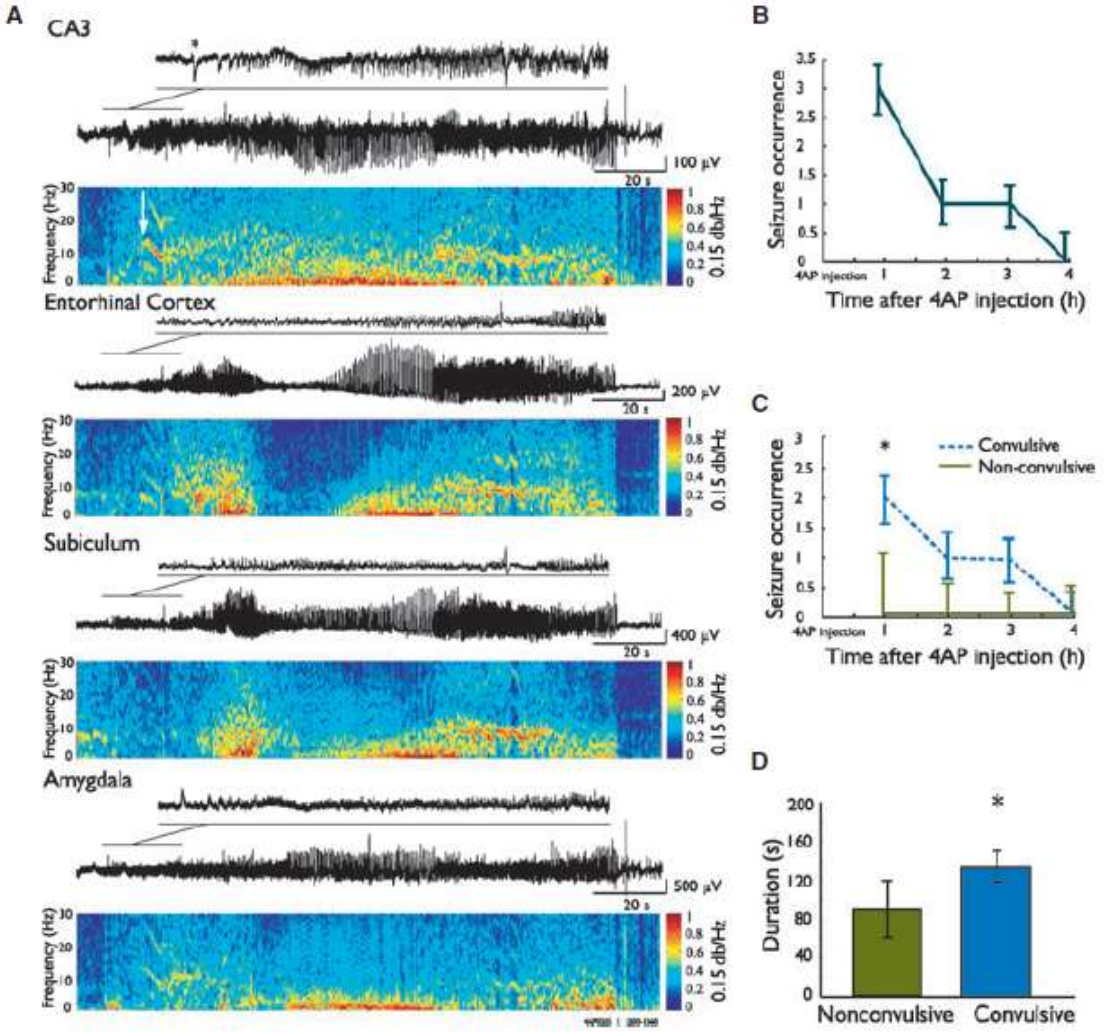
A
CA3
100 µV
20 s
Frequency (Hz)
0.15 db/Hz
Entorhinal Cortex
200 µV
Subiculum
400 µV
Amygdala
500 µV
B
Seizure occurrence
4AP injection
Time after 4AP injection (h)
C
Convulsive
Non-convulsive
Seizure occurrence
Time after 4AP injection (h)
D
Duration (s)
Nonconvulsive
Convulsive

Figure 4.3. Ictal activity induced by systemic 4AP administration. A. Representative seizure recorded after 4AP systemic administration from four structures simultaneously. Note at seizure onset the occurrence of a negative spike (asterisk) in the CA3 region of the hippocampus, followed by the occurrence of fast activity in the 5–20 Hz range; this spike is mirrored by a positive-going spike in the amygdala. The white arrow in the power spectrogram indicates seizure onset time, based on the first occurrence of fast activity. During this seizure, fast activity first occurred in CA3, which was considered as the seizure-onset zone. **B.** Rate of seizures per hour recorded after 4AP in 12 animals. **C.** Duration of convulsive and nonconvulsive seizures over time after 4AP in these 12 rats. Note that the occurrence of convulsive seizures was higher during the first hour after 4AP. **D.** Bar graph showing the duration of convulsive and nonconvulsive seizures recorded from these 12 animals; note that convulsive seizures lasted significantly longer compared to nonconvulsive seizures. Medians and 95% confidence intervals are shown (*$p < 0.005$).

Figure 4.4

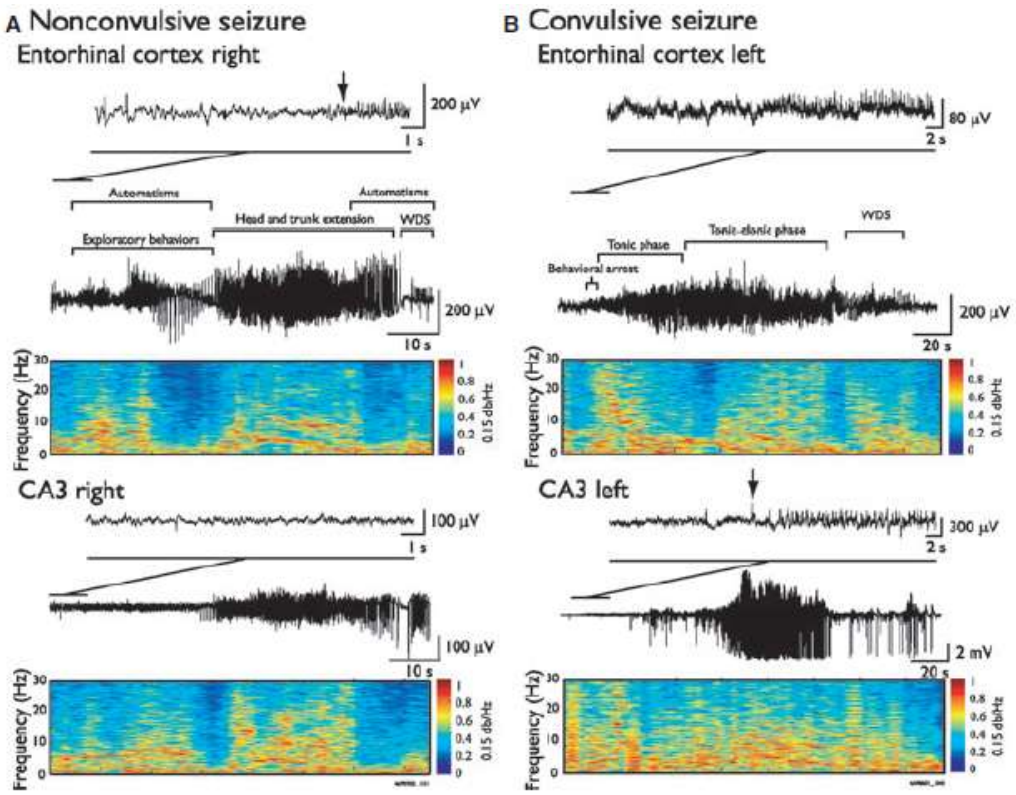

Figure 4.4. EEG-behavioral correlates of ictal events induced by systemic 4AP administration. Representative EEG recordings of a nonconvulsive **(A)** and a convulsive seizure **(B)** in the ipsilateral CA3 and EC, with corresponding behavioral symptoms. Arrows indicate seizure-onset time. In **(A)**, automatisms and an increase of exploratory behaviors occurred during the nonconvulsive seizure after onset in EC, whereas head and trunk extension occurred when the epileptiform activity was also observed in the ipsilateral CA3. Panel **(B)** shows a convulsive seizure with a tonic phase, characterized by head and trunk extension, followed by a tonic–clonic phase, characterized by a head and trunk extension associated with rearing and falling. Both the tonic and the tonic–clonic phase were associated to epileptiform activity in both CA3 and EC. Both seizure types were followed by wet-dog shakes (WDS).

Figure 4.5

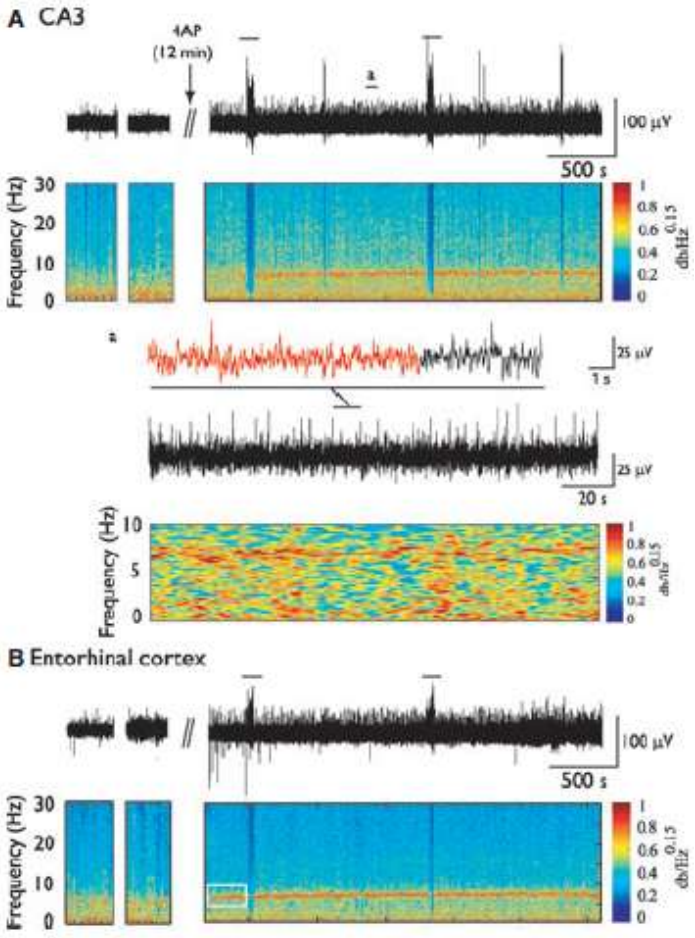

Figure 4.5. Theta oscillations are potentiated by systemic injection of 4AP. EEG recordings and corresponding spectrograms obtained from CA3 **(A)** and the EC **(B)** before and after 4AP injection (arrow). Solid lines indicate seizures. EEG samples obtained before 4AP correspond to periods when the rat was immobile. Note the highly rhythmic and sustained activity in the theta frequency range (6–11 Hz) after 4AP compared to before injection. Note that in that case, especially in EC, highly rhythmic theta oscillations occurred before first seizure occurrence (white rectangle). Inset **(a)** shows an example of theta oscillations from CA3 on a shorter time scale, with the corresponding spectrogram. Theta oscillations were not associated with any behavioral symptoms.

Figure 4.S1

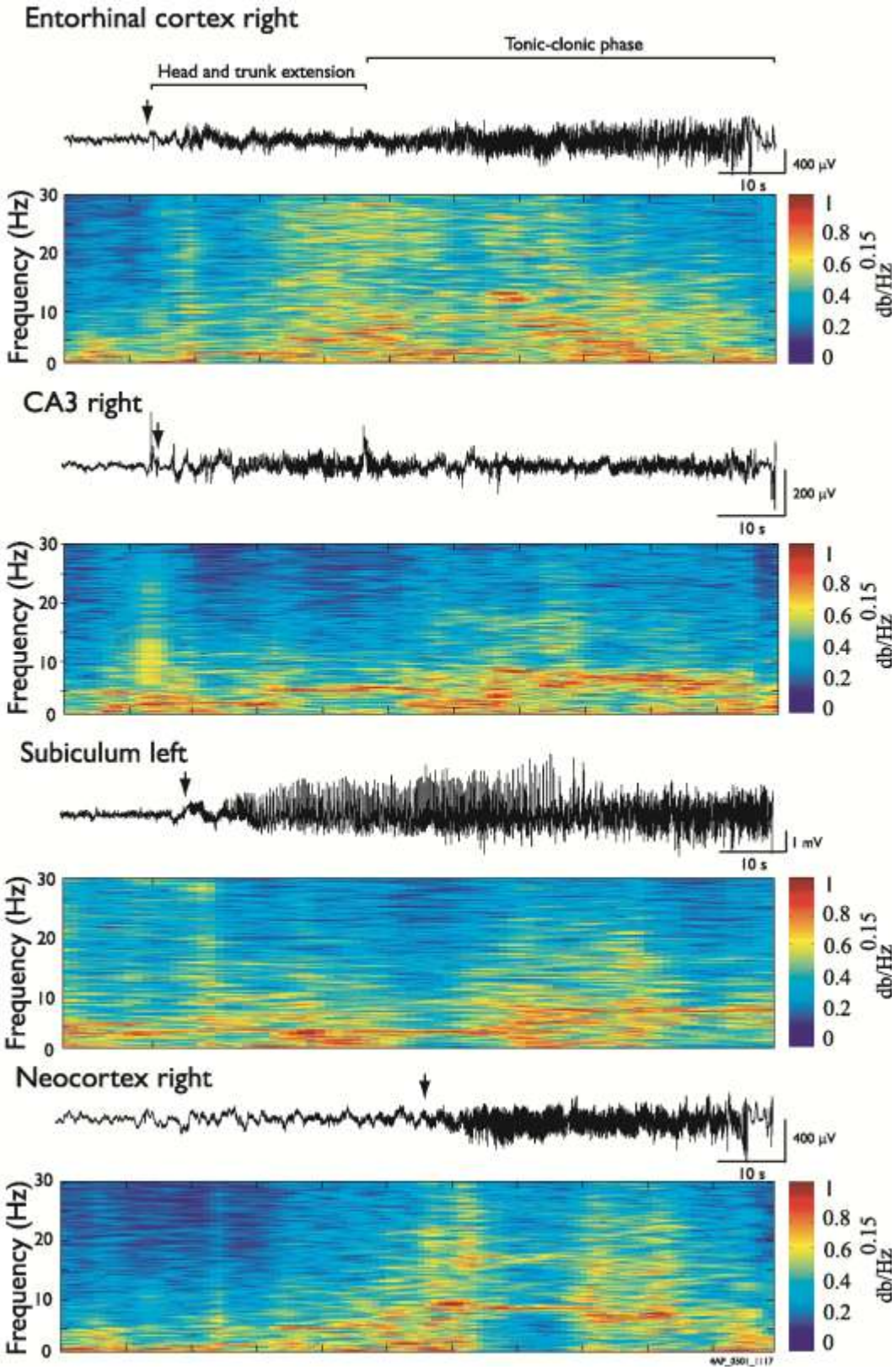
Entorhinal cortex right
Tonic-clonic phase
Head and trunk extension
400 µV
10 s
Frequency (Hz)
30
20
10
0
1
0.8
0.6
0.4
0.2
0
0.15
db/Hz
CA3 right
200 µV
10 s
Subiculum left
1 mV
10 s
Neocortex right
400 µV
10 s

Figure 4.S1 – Ictal activity induced by 4AP in mesial temporal lobe and neocortical regions. Representative seizure recorded from mesial temporal lobe regions and the neocortex simultaneously in a single rat. Note the onset of the seizure (arrows) in the right entorhinal cortex and right CA3 region of the hippocampus followed by a propagation of ictal activity to the left subiculum and later the right neocortex. Behavioral symptoms such as head and trunk extension occurred during ictal activity in temporal lobe regions whereas the tonic-clonic phase of the seizure occurred when ictal activity propagated to the neocortex.

5. Chapter 5

Distinct EEG seizure patterns reflect different seizure generation mechanisms

Salami P, Lévesque M, Gotman J, Avoli M. *Journal of Neurophysiology*, 2015 *doi: 10.1152/jn.00031.2015*

In chapter 4, I showed that the administration of 4-aminopyridine (4AP) induces seizures that display predominantly low-voltage fast (LVF) characteristics.

In the following chapter, I specifically analyzed high-frequency oscillations (HFOs) following the administration of 4AP, and compared these findings to those induced by picrotoxin. The original manuscript of this chapter was published in 2015 in the *Journal of Neurophysiology* with the title "Distinct EEG seizure patterns reflect different seizure generation mechanisms".

5.1. Abstract

Low-voltage fast- (LVF) and hypersynchronous- (HYP) seizure onset patterns can be recognized in the EEG of epileptic animals and patients with temporal lobe epilepsy. Ripples (80-200 Hz) and fast ripples (250-500 Hz) have been linked to each pattern, with ripples predominating during LVF seizures and fast ripples predominating during HYP seizures in the rat pilocarpine model. This evidence led us to hypothesize that these two seizure-onset patterns reflect the contribution of neural networks with distinct transmitter signaling characteristics. Here, we tested this hypothesis by analyzing the seizure activity induced with the K^+ channel blocker 4-aminopyridine (4AP, 4-5 mg/kg, i.p.) - which enhances both glutamatergic and GABAergic transmission - or the $GABA_A$ receptor antagonist picrotoxin (3-5 mg/kg, i.p.); rats were implanted with electrodes in the hippocampus, the entorhinal cortex and the subiculum. We found that LVF-onset occurred in 82% of 4AP-induced seizures while seizures following picrotoxin were always HYP. In addition, HFO analysis revealed that 4AP-induced LVF seizures were associated to higher ripple rates compared to fast ripples ($p<0.05$), whereas picrotoxin-induced seizures contained higher rates of fast ripples compared to ripples ($p<0.05$). These results support the hypothesis that two distinct patterns of seizure onset result from different pathophysiological mechanisms.

5.2. Introduction

Recent studies on ictogenesis in animals and humans have revealed the existence of two main patterns of seizure onset that were termed low-voltage fast (LVF) and hypersynchronous (HYP) onset patterns (Velasco et al., 2000; Bragin et al., 2005; Lévesque et al., 2012; Perucca et al., 2014). LVF seizures start with a positive or negative going spike followed by low-amplitude, high frequency activity whereas HYP seizures are characterized at onset by the occurrence of focal periodic spiking. Imaging studies have suggested that these two seizure onset patterns are linked to distinct underlying pathologies; patients with HYP seizures are indeed more likely to show focal onset and greater neuronal loss in the hippocampus than those showing LVF seizures that are often associated to more diffuse lesions (Velasco et al., 2000; Ogren et al., 2009a).

We have recently discovered in the pilocarpine model of temporal lobe epilepsy (TLE) that these two patterns of seizure onset are associated to distinct patterns of occurrence of high-frequency oscillations (HFOs) (Lévesque et al., 2012). Specifically, LVF seizures show high rates of ripples (80-200 Hz) compared to fast ripples (250-500 Hz) whereas HYP seizures are associated to high rates of fast ripples compared to ripples (Lévesque et al., 2012). This evidence led us to speculate that HFOs may mirror different functional properties of neural networks during ictogenesis. Ripples are thought to reflect summated IPSPs generated by pyramidal cells in response to inhibitory interneuron firing whereas fast ripples should mirror the hypersynchronous bursting of principal (glutamatergic) cells (Bragin et al., 1999a; Dzhala and Staley, 2004; Foffani et al., 2007; Jefferys et al., 2012b). Since 4-aminopyridine (4AP) is known to enhance interneuron

excitability and to induce GABAergic synchronization *in vitro* (Avoli and de Curtis, 2011), we used in this study systemic injections of 4AP (Lévesque et al., 2013) or of the $GABA_A$ receptor antagonist picrotoxin to test the hypothesis that LVF seizures are mainly caused by GABAergic-mediated synchronization whereas glutamatergic interactions, enhanced by the blockade of $GABA_A$ receptor signaling, predominate during HYP seizures. We also postulated that 4AP-induced LVF seizures would be associated to higher rates of ripples compared to fast ripples in temporal lobe regions shortly before and after the onset of ictal activity, while picrotoxin would induce HYP seizures associated to the occurrence of higher rates of fast ripples compared to ripples.

5.3. Materials and Methods

5.3.1. Animal housing

Male Sprague-Dawley rats (250-300 g) were obtained from Charles River (St-Constant, Qc, Canada), and let habituate for 72 h after delivery before the implantation of electrodes. They were housed in controlled conditions, at 22 (± 2) ˚C and under a 12 h light/12 h dark cycle (lights on from 7:00 a.m. to 7:00 p.m.) with food and water *ad libitum*. All procedures were approved by the Canadian Council of Animal Care and all efforts were made to minimize suffering and the number of animals used.

5.3.2. Surgery for the implantation of electrodes

A total of nine animals underwent surgery for the implantation of electrodes before 4AP or picrotoxin treatment. Before surgery, rats received topical Lidocain (5%; Odan, Canada). An incision was then made in the skin to expose the skull plate, from bregma to lambda.

Four stainless steel screws (2.4 mm length) were fixed to the skull as anchor screws and in addition 4 small holes were drilled to allow the implantation of bipolar electrodes (20-30 kΩ; 5-10 mm length; distance between exposed tips: 500 µm) (MS303/2-B/spc, Plastics One, VA, USA). Electrodes were implanted in the CA3 region of the right hippocampus (AP: -4.3, ML:±4, DV:-7.8), the right entorhinal cortex (EC) (AP: -8.6, ML: ±5.2, DV : -6.8), and the left subiculum (AP: -6.0, ML: ±4.3, DV: -8.3) (Paxinos and Watson, 1998). A fourth bipolar electrode was placed under the frontal bone, after the removal of insulating material, and used as reference. During surgery, animals received a preventive antibiotherapy (Enrofloxacine, 10 mg/kg, s.c.). After surgery, rats were injected with Ketoprofen (5 mg/kg, s.c. Merail, Canada), Buprenorphine (0.01-0.05 mg/kg, s.c., repeated every 12 h; CDMV, Canada) and 2 ml of 0.9% sterile saline (s.c.) repeated every 12 hours if necessary.

5.3.3. EEG recording

Two days after surgery, rats were placed in custom-made Plexiglas boxes (30*20*40 cm) and provided with food and water *ad libitum.* Electrodes were then connected to multichannel cables and swivels. EEGs were amplified using an interface kit (Mobile 36 chlTMPro Amp, Stellate) and low-pass filtered at 500 Hz and sampled at 2kHz per channel. On the day of injection, animals were given either 4AP (4-5 mg/kg, i.p.) or picrotoxin (3-5 mg/kg, i.p.) in order to induce acute seizures (Pitkänen et al., 2005). EEG-video monitoring was performed using the Stellate system for 4 h following the injection (Lévesque et al., 2013).

5.3.4. Seizure detection and classification

Seizures were detected visually and only seizures with good quality recordings were selected. They were then exported to Matlab 7.11.0 (R2010b) (Mathworks, Natick, MA, USA) and analyzed offline using custom-built routines. In the 4AP-treated group, 11 seizures were selected for analysis whereas 12 seizures were selected in the picrotoxin-treated group. All seizures were visually analyzed by four reviewers and the seizure-onset time was marked. The reviewers were blind to the treatments. At least three of the four reviewers agreed on the onset time for all seizures. Selected seizures in the 4AP- and picrotoxin-treated group were then classified based on their onset pattern; i.e. low-voltage fast-onset (LVF) and hypersynchronous-onset (HYP) seizures (Velasco et al., 2000; Lévesque et al., 2012) (see Fig. 5.1 for examples). The seizures that could not classify in any of the groups were excluded from the study.

5.3.5. High-frequency oscillation analysis

HFOs were analyzed from 60 s before the onset of the seizure up to 60 s after. Raw EEG recordings were first band-pass filtered in the 80-200 Hz and in the 250-500 Hz frequency range using a finite impulse response filter; zero-phase digital filtering was used to avoid phase distortion. Filtered EEGs from each region were then normalized using a 10 s reference period selected from 70 s to 60 s before the onset of the seizure. To be considered as an HFO candidate, oscillatory events in each frequency band had to show at least four consecutive cycles having amplitude of 3 SD above the mean of the reference period. The time lag between two consecutive cycles had to be between 5 and 12.5 ms for ripples and between 2 and 4 ms for fast ripples. Ripples and fast ripples occurring at the

same time (overlapping events) were removed from analysis to avoid the effect of sharp events (Bénar et al., 2010; Lévesque et al., 2012; Salami et al., 2012)

5.3.6. Statistical analysis

To compare the rates of occurrence of ripples and fast ripples in each region during pre-ictal and ictal periods, we divided each period in three equal parts of 20 s. Wilcoxon signed-rank tests were used for multiple comparisons followed by Bonferroni-Holm corrections. Kruskall-Wallis tests were used to compare the duration of ripples and fast ripples in between regions and during preictal and ictal periods. The level of significance was set to $p<0.05$.

5.4. Results

5.4.1. Seizure-onset patterns

Seizures were recorded from five rats treated with 4AP. Eleven seizures were recorded in these experiments, from which 82% (9/11) were categorized as LVF seizures and 18% (2/11) were categorized as unclassified. LVF seizures had an average duration of 134 (± 16) s, whereas unclassified seizures lasted 131 (± 42) s. Figure 5.1A shows an example of an LVF seizure recorded from a 4AP-treated animal. In the picrotoxin-treated group, twelve seizures were recorded from four animals. All seizures in the picrotoxin-treated group were classified as HYP (Fig 5.1B). The average duration of HYP seizures was 77 (± 9) s. The number of injected animals in each group was balanced to have a comparable number of seizures in the two groups.

5.4.2. Rates of occurrence over time of high-frequency oscillations during seizures

During both 4AP- and picrotoxin-induced seizures, HFOs could be detected in all recorded regions. Representative examples of HFOs detected during an HYP seizure following picrotoxin injection recorded in subiculum are shown in Fig 5.2A. The average duration of ripples during 4AP-induced seizures was 44.77 ms and the average duration of ripples during picrotoxin-induced seizures was 37.12 ms. The average duration of fast ripples during 4AP-induced seizures was 17.37 ms and the average duration of fast ripples during picrotoxin-induced seizures was 15.79 ms. Kruskal-Wallis tests were used to compare the duration of ripples or fast ripples during the seizures. The statistical analysis revealed no significant differences between the duration of ripples or fast ripples during the seizures after the injection of 4AP or picrotoxin.

In order to study the temporal evolution of HFOs over time, the number of HFOs per second was calculated for each seizure and then averaged. The average rate of HFO occurrence was calculated from 60 s before the seizure onset up to 60 s after the start of the seizure. This analysis revealed that 20 s before the onset of LVF seizures induces with 4AP, ripples occurred at higher rates compared to fast ripples in all recorded regions ($p<0.05$) (Fig. 5.2B). This difference was maintained over time during the ictal period, as ripples occurred at higher rates compared to fast ripples from the onset of the seizure up to 60 s later ($p<0.05$) (Fig. 5.2B).

Figure 5.2C shows the temporal changes of HFOs during picrotoxin-induced HYP seizures. Ripples and fast ripples occurred at similar rates during the pre-ictal period in the CA3 region and in the subiculum. However, a significantly higher rate of fast ripples compared to ripples was observed in both of these regions during seizures ($p<0.05$) (Fig.

5.2C). No significant differences were observed between the rate of ripples and fast ripples in the EC during the ictal period; however, in this limbic structure, ripple rate was higher than that of fast ripples during the preictal period in HYP recorded seizures after the injection of picrotoxin (Fig. 5.2C).

5.5. Discussion

The main findings of our study can be summarized as follows. First, 4AP mostly induced LVF seizures whereas picrotoxin always induced HYP seizures; second, LVF seizures induced with 4AP were mostly associated to ripples, and their rate of occurrence increased 20 s before the onset of the seizure; third, seizures induced with picrotoxin were mostly associated to fast ripples.

5.5.1. Seizure-onset patterns and GABA-receptor mediated activity

With the systemic administration of drugs that either block or enhance GABA-receptor mediated transmission, we were able to reproduce the two main patterns of seizure-onset observed in clinical studies and in animal models of TLE (Velasco et al., 2000; Bragin et al., 2005; Lévesque et al., 2012). Seizures following the administration of the K^+ channel blocker, 4AP, were mostly characterised by an LVF onset pattern, suggesting that $GABA_A$ receptor signaling may be involved in the initiation of this pattern of seizure onset. On the other hand, all seizures following the administration of the $GABA_A$ antagonist picrotoxin had the characteristics of HYP onset patterns, indicating that excitatory signaling could result in the initiation of this seizure-onset pattern.

Our results thus support the hypothesis that the activity of distinct neuronal networks may underlie different seizure onset types (Bragin et al., 2009a). Indeed, *in vitro* studies have suggested that LVF ictal-like activity induced by 4AP in brain slices results from synchronous GABA receptor-mediated potentials, since they are abolished by $GABA_A$ receptor antagonists (Avoli and de Curtis, 2011). Contrary to what was observed with 4AP, picrotoxin only induced HYP seizures. These results are in line with studies performed in human tissue maintained *in vitro*, in which it was shown that these periodic spikes at the onset of ictal activity reflect pyramidal cell firing and depend on glutamatergic mechanisms (Huberfeld et al., 2011).

5.5.2. High-frequency oscillations associated to seizures induced with 4AP and picrotoxin

We have also found that the two seizure-onset patterns were characterized by two distinct patterns of HFO occurrence. Following the injection of 4AP, LVF seizures were associated to higher rates of ripples compared to fast ripples shortly before seizure onset as well as during the ictal discharge. On the contrary, the rate of occurrence of fast ripples was higher than that of ripples during HYP seizures recorded in the CA3 region and subiculum after the administration of picrotoxin. Since HFOs are believed to reflect neuronal network activity in epileptic regions, these findings indicate that different mechanisms should underlie the two seizure-onset patterns. Surprisingly, in the EC of picrotoxin-treated rats we observed a higher rate of ripple occurrence during the pre-ictal period and we did not observe any significant difference between ripple and fast ripple rates of occurrence during the ictal period. This finding is unexpected since high rates of fast ripples compared to ripples occur in the EC during HYP spontaneous seizures in pilocarpine-treated animals

(Lévesque et al., 2012). This difference may result from the fact that picrotoxin-induced seizures were acutely induced in control animals whereas spontaneous seizures in pilocarpine-treated epileptic rats occur after a latent period that is associated to cellular and molecular changes. In spite of this difference, our findings support the view that ripples should reflect population IPSPs generated by principal cells entrained by synchronously active interneuron networks whereas fast ripples are thought to reflect the hypersynchronous firing of principal (glutamatergic) neurons (Jefferys et al., 2012b; Staba et al., 2014); in fact, higher rates of ripples, compared to fast ripples, were associated to LVF seizures induced by 4AP (which enhance both inhibitory and excitatory currents) while higher rates of fast ripples, compared to ripples occurred during HYP seizures induced by picrotoxin (which is known to antagonize $GABA_A$ receptor mediated inhibition). Although, more analysis along with single cell recording could be helpful to identify the mechanisms underlying the ripples or fast ripples in both seizure onset patterns. Recent studies showed that there might be different mechanisms underlying the oscillations in the same frequency band (Alvarado-Rojas et al., 2015). More specifically, the mechanisms responsible for the ripple frequency band during interictal ripples differ from the mechanisms responsible for the same frequency band during the preictal period. It would be interesting to see if the ripples and fast ripples recorded in the LVF and HYP onset patterns share the same mechanisms or they have different characteristics.

Distinct patterns of HFOs occur during the two seizure-onset patterns in the pilocarpine model of TLE (Lévesque et al., 2012). In line with what we have previously reported, we propose here a possible diagnostic role for both types of HFOs depending on the pattern of seizure onset. More specifically, in patients with LVF-onset pattern seizures,

ripples could be more significant compared to fast ripples, whereas in patients with HYP-onset pattern seizures, the occurrence of fast ripples could be more useful in identifying the seizure onset zone. Therefore, the two types of HFOs could be used differently to help localize the seizure onset zone. However, the validity of this hypothesis remains to be supported based on the identification of the mechanisms underlying the different frequency bands.

This study could improve our understanding of the basic mechanisms underlying ictogenesis and as a result our findings can have an important role in identifying therapeutic targets to treat epilepsy since the two seizure-onset patterns reported here were almost specific to the pharmacological treatment. It has been previously shown that both of these seizure-onset patterns can be recorded in humans and in animal models of TLE (Velasco et al., 2000; Bragin et al., 2005; Lévesque et al., 2012; Perucca et al., 2014). Our findings thus suggest that patients with apparently the same pathology (mesial temporal sclerosis) but with different seizure-onset patterns could benefit from different pharmacological treatments.

Acknowledgements

This study was supported by the Canadian Institutes of Health Research (8109 and 74609). PS received a student scholarship from the Savoy Foundation for Epilepsy.

5.6. Figures

Figure 5.1

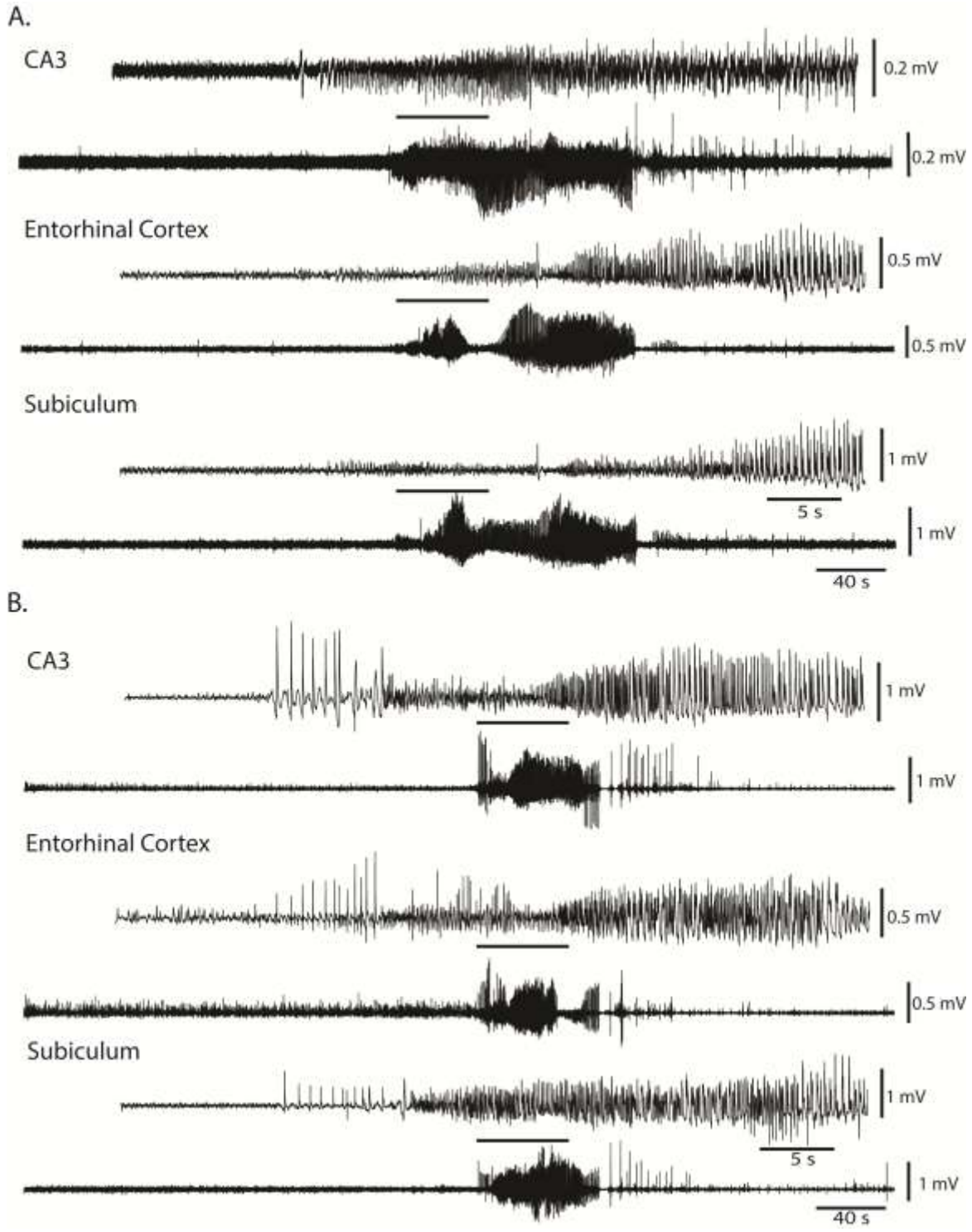

Figure 5.1. Representative seizures induced by 4AP or picrotoxin. A. LVF seizure recorded simultaneously from the CA3 region of hippocampus, the entorhinal cortex, and the subiculum in a rat 12 min following 4AP treatment. The insets show the onset of the seizure that is characterized by the occurrence of a spike followed by a low-voltage fast activity. **B.** HYP seizure recorded simultaneously from the CA3 region of hippocampus, the entorhinal cortex, and the subiculum 30 min following picrotoxin treatment. The insets indicate the onset of the seizure and the expanded time scale of the periodic focal spikes at its onset. The bold lines on top of the traces are indicating the expanded time of the seizure.

Figure 5.2

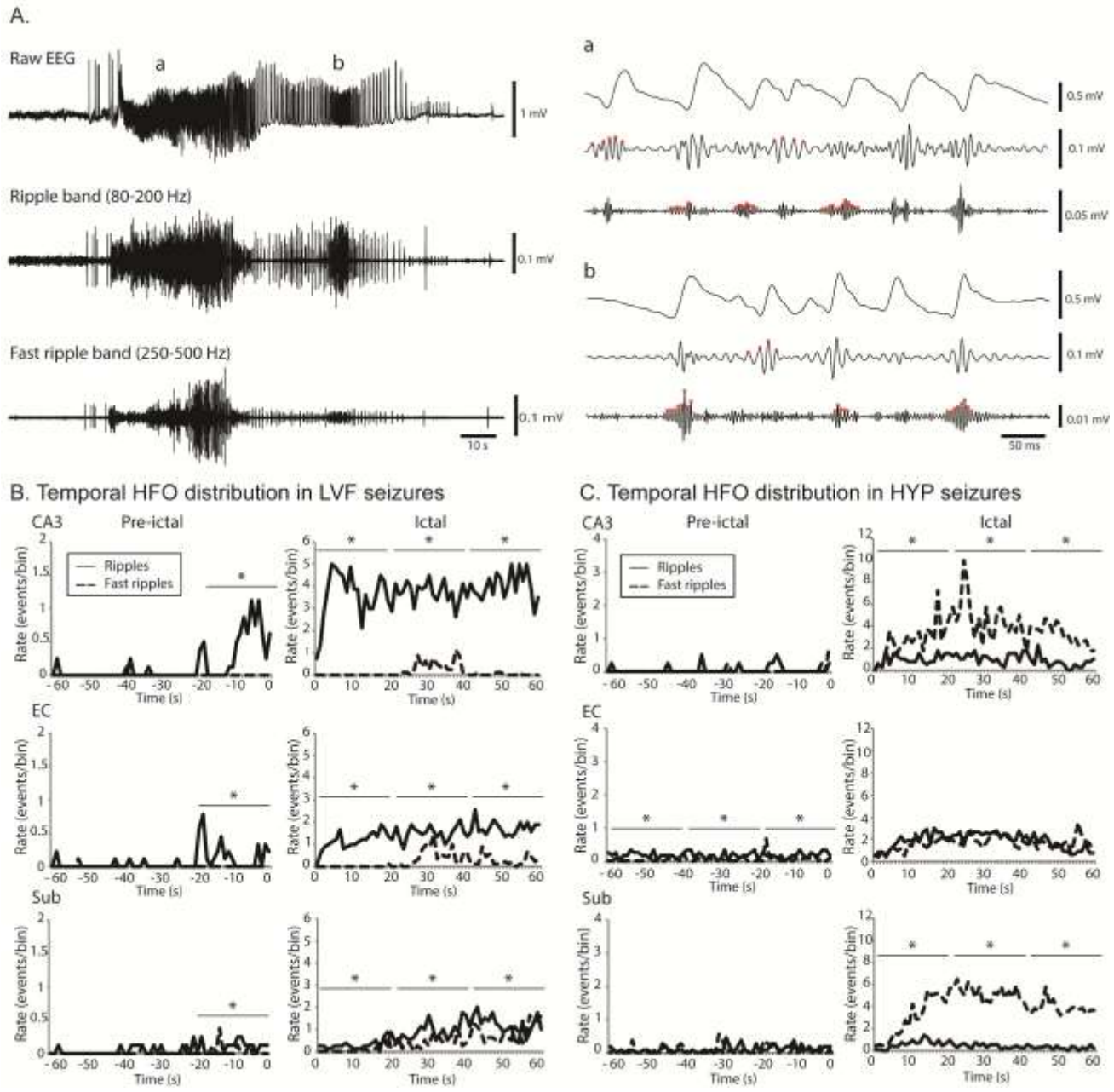
A.
Raw EEG
a
b
1 mV
Ripple band (80-200 Hz)
0.1 mV
Fast ripple band (250-500 Hz)
0.1 mV
10 s
a
0.5 mV
0.1 mV
0.05 mV
b
0.5 mV
0.1 mV
0.01 mV
50 ms
B. Temporal HFO distribution in LVF seizures
C. Temporal HFO distribution in HYP seizures
CA3
Pre-ictal
Ictal
Ripples
Fast ripples
EC
Sub
Rate (events/bin)
Time (s)

Figure 5.2. HFOs during seizures following the injection of 4AP and picrotoxin. A. Raw EEG recordings of a HYP seizure recorded from the subiculum in a picrotoxin-treated rat, as well as filtered traces in the ripple frequency band (80-200 Hz) and fast ripple frequency band (250-500 Hz). Expanded time scale of the selected part (**a** and **b**) of raw EEG recording, ripple frequency band, and the fast ripple frequency band of the seizure shown in **(A). B.** Temporal distribution of HFOs in all LVF recorded seizures from 4AP-treated animals in the hippocampal CA3 region, the entorhinal cortex and the subiculum. Left panels show the temporal evolution of HFOs 60 s before the seizure onset whereas right panels show the distribution from the onset to 60 s after. Note that all regions show higher rates of ripples compared to fast ripples in the 20 s time-period that preceded the onset of the seizure and during the seizure (* $p<0.05$). **C.** Temporal distribution of HFOs in all HYP recorded seizures from picrotoxin-treated rats in the CA3, the entorhinal cortex and the subiculum. Note that the CA3 region and subiculum show higher rates of fast ripples compared to ripples during the 60 s time-period that followed seizure onset (* $p<0.05$) as well as that there was no significant difference during the ictal period between the rate of occurrence of ripples and fast ripples in the entorhinal cortex. Note the difference in the scale of pre-ictal and ictal period.

6. Chapter 6

Dynamics of interictal spikes and high-frequency oscillations during epileptogenesis in temporal lobe epilepsy

Salami P, Lévesque M, Benini R, Behr C, Gotman J, Avoli M. *Neurobiology of Disease*, 2014 67:97-106.

In the previous chapters, I addressed the participation of high-frequency oscillations (HFOs) to ictogenesis. The main goal of the following chapter is to identify the changes in HFOs that occur when the silent periods ends and the first seizure occurs. Therefore, I have attempted to analyze the changes in HFOs and interictal spikes during the last stage of the epileptogenetic process.

The differences in the characteristics of interictal spikes between the latent and the chronic periods have been previously reported in different studies. However, the relation between them and HFOs during epileptogenesis has not been identified, yet.

The results presented in this chapter were published in 2014 in the *Neurobiology of Disease* in a manuscript entitled "Dynamics of interictal spikes and high-frequency oscillations during epileptogenesis in temporal lobe epilepsy".

For purposes of clarity, in this chapter, the latent and chronic periods are termed latent phase and chronic phase, respectively.

6.1. ABSTRACT

Mesial temporal lobe epilepsy (MTLE) is characterized in humans and in animal models by a seizure-free latent phase that follows an initial brain insult; this period is presumably associated to plastic changes in temporal lobe excitability and connectivity. Here, we analyzed the occurrence of interictal spikes and high frequency oscillations (HFOs; ripples: 80-200 Hz and fast ripples: 250-500 Hz) from 48 hours before to 96 hours after the first seizure in the rat pilocarpine model of MTLE. Interictal spikes recorded with depth EEG electrodes from the hippocampus CA3 area and entorhinal cortex (EC) were classified as type 1 (characterized by a *spike* followed by a *wave*) or type 2 (characterized by a *spike* with no *wave*). We found that: (i) there was a switch in the distribution of both types of interictal spikes before and after the occurrence of the first seizure; during the latent phase both types of interictal spikes predominated in the EC whereas during the chronic phase both types of spikes predominated in CA3; (ii) type 2 spike duration decreased in both regions from latent to chronic phase; (iii) type 2 spikes associated to fast ripples occurred at higher rates in EC compared to CA3 during the latent phase while they occurred at similar rates in both regions in the chronic phase; and (iv) rates of fast ripples outside of spikes were higher in EC compared to CA3 during the latent phase. Our findings demonstrate that the transition from latent to chronic phase is paralleled by dynamic changes in interictal spike and HFO expression in EC and CA3. We propose that these changes may represent biomarkers of epileptogenicity in MTLE.

6.2. Introduction

Mesial temporal lobe epilepsy (MTLE), one of the most common forms of partial epilepsy, is characterized by recurrent seizures that originate from the hippocampus, amygdala or entorhinal cortex (EC), and that often occur after a latent phase of many years following an initial brain insult such as febrile seizures, encephalitis, or *status epilepticus* (Salanova et al., 1994; Engel, 1996; Gloor, 1997). This latent phase is presumably characterized by reorganization of neural networks and by changes in cellular excitability (Dudek and Staley, 2012). Interictal spikes, and more recently high-frequency oscillations (HFOs, 80-500 Hz), recorded from patients with MTLE and in animal models mimicking this disorder have been considered markers of abnormal neural network activity (Jefferys et al., 2012a, 2012b). However, the relation between interictal spikes, HFOs and epileptogenesis remains unclear.

A few years ago, we found that interictal spikes recorded from the hippocampus CA3 area, EC, and amygdala in pilocarpine-treated epileptic rats change in duration and rate of occurrence following the first seizure (Bortel et al., 2010). More recently, Chauvière et al. (2012) have reported in the hippocampus CA1 area the occurrence of two types of interictal discharges following pilocarpine- or kainic acid-induced *status epilepticus*: type 1 consisted of a *spike* followed by a *wave* whereas type 2 was characterized by a *spike* without *wave*. They also found changes over time in the rate of occurrence of these two types of interictal discharge; the rate of occurrence of type 1 spikes decreased from the latent to the chronic phase whereas the rate of occurrence of type 2 spikes increased. Therefore, both studies suggested that interictal spikes may represent a biomarker of

epileptogenicity (i.e., the electrophysiological signature of the changes in brain excitability leading to the chronic epileptic condition).

To date, no study has addressed the relation between interictal spikes and HFOs during epileptogenesis. HFOs, categorized as ripples (80-200 Hz) and fast ripples (250-500 Hz), occur in the EEG of epileptic patients and animals in coincidence with interictal spikes but also in their absence, and they are thought to reflect the activity of dysfunctional neural networks (Zijlmans et al., 2009a; Jacobs et al., 2012; Jefferys et al., 2012a, 2012b). In addition, both clinical and experimental studies support the view that HFOs are better markers than interictal spikes to identify seizure onset zones (Urrestarazu et al., 2007; Jacobs et al., 2008, 2012; Jiruska et al., 2010a, 2010c; Jefferys et al., 2012a, 2012b). Finally, it has been reported in pilocarpine-treated animals that during the chronic phase there is a high correlation between interictal spikes associated with HFOs and seizure onset zones (Lévesque et al., 2011). Therefore, in this study, we used the pilocarpine model of MTLE to analyze the evolution of interictal spikes and the occurrence of HFOs at the transition from latent to chronic phase. We recorded the hippocampus CA3 area and EC, as they are in most cases the seizure onset zones in this model of MTLE (Bortel et al., 2010; Lévesque et al., 2011, 2012).

6.3. Materials and Methods

6.3.1. Pilocarpine treatment

Male Sprague-Dawley rats (250-300 g; n=9) were acquired from Charles River Laboratories (St-Constant, Qc, Canada) and let habituate to the environment for 72 hours

before pilocarpine treatment. On the day of injection, they were administered scopolamine methylnitrate (1 mg/kg i.p.; Sigma-Aldrich, Canada) and 30 min later a single dose of pilocarpine hydrochloride (380 mg/kg, i.p.; Sigma-Aldrich, Canada) (Curia et al., 2008; Bortel et al., 2010; Lévesque et al., 2011, 2012). Their behavior was scored according to the Racine scale (Racine, 1972), and *status epilepticus* was defined as continuous stage 5 seizures. *Status epilepticus* was terminated after 1 h by injection of diazepam (5 mg/kg, s.c.; CDMV, Canada) and ketamine (50 mg/kg, s.c.; CDMV, Canada) (Martin and Kapur, 2008).

6.3.2. Implantation of bipolar depth electrodes

Two days after *status epilepticus*, rats were anaesthetized with isoflurane (3%) in 100% O_2. Bipolar electrodes (20-30 kΩ; 5-10 mm in length; distance between exposed tips: 500 µm) were implanted in the CA3 area of the ventral hippocampus (AP: -4.3, ML: ±4, DV: -7.8) and EC (AP: -8.6, ML: ±5.2, DV: -6.8). Screws placed in the frontal bone were used as reference and ground (*cf.*, Bortel et al., 2010; Lévesque et al., 2011). All procedures were approved by the Canadian Council of Animal Care and all efforts were made to minimize the number of animals used and their suffering.

6.3.3. Local field potential recordings

After surgery, rats were housed individually in custom-made Plexiglas boxes (30 x 30 x 40 cm) and let habituate to the environment for 24 h. Electrodes were then connected to a multichannel cable and electrical swivel (Slip ring T13EEG, Air Precision, France; or Commutator SL 18C, HRS Scientific, Canada) and EEG-video monitoring (24 h per day) was performed. EEGs were amplified via an interface kit (Mobile 36ch LTM ProAmp, Stellate, Montreal, QC, Canada), low-pass filtered at 500 Hz and sampled at 2 kHz per channel.

Infrared cameras were used to record day/night video files that were time-stamped for integration with the electrophysiological data using monitoring software (Harmonie, Stellate). Throughout the recordings, animals were placed under controlled conditions (22 ± 2 ˚C, 12 h light/dark schedule) and provided with food and water *ad libitum.* EEG-video recordings were performed up to 15 days after *status epilepticus*.

6.3.4. Selection of epochs

Spontaneous seizures started 6.1 (± 0.7) days after *status epilepticus*. EEG recordings were extracted at 5 time points before the occurrence of the first seizure (defined as time 0): -48 h, -36 h, -24 h, -12 h, and -2 h. Six time points after the first seizure were also selected for analysis: +2 h, +12 h, +24 h, +48 h, + 72 h, +96 h. For each time points, 10 min epochs were selected in each rat. Only epochs of slow-wave sleep were used for analysis, because of the low rates of movement artifacts and since HFOs are more prominent during this sleep state (Staba et al., 2004; Bagshaw et al., 2009). Slow-wave sleep epochs were selected based on the occurrence of EEG activity in the 1-6 Hz range. During these periods, rats were immobile and in a curled body position. In order to minimize the effects of seizure occurrence during the chronic phase, the 10 min epochs were selected from periods at least 1 h before or after seizures. Overall, epochs of slow-wave sleep were extracted in a range of ± 2h from the time point (e.g., for the epoch at -48 h, it was selected from -46 to -50 h before first seizure occurrence). EEGs were then exported to Matlab 8.1 (R2013a) (Mathworks, Natick, MA, USA) and analyzed off-line using custom-built routines. The original epochs were reviewed and all sections with artifacts were removed from the analysis.

6.3.5. Classification and analysis of interictal spikes

Interictal spikes were detected based on threshold crossings (mean and standard deviation), calculated over the entire period for the 10 min epoch. The reviewer blind to the phase (latent or chronic) to which each epoch belonged, adapted the threshold visually to account for differences in detection performance (range: 2.7-3.5 standard deviations). Every event that crossed the threshold was then analyzed visually and only interictal spikes were kept for analysis. Interictal spikes were then classified visually into two types as in Chauvière et al. (2012). Type 1 spikes were characterized by a *spike* followed by a *wave* that was clearly distinguishable from the background, whereas type 2 spikes were characterized by a *spike* without a *wave* (see Figures 6.1, 6.2 and 6.3). The duration of the *spike* component was calculated from the first deflection from baseline to the return to baseline. The duration of the *wave* in type 1 spikes was calculated from the end of the *spike* component to the return to baseline after the *wave*.

6.3.6. Analysis of high-frequency oscillations

The same epochs used for analyzing interictal spikes were used for HFO analysis. A multi-parametric algorithm was employed to identify oscillations in each frequency range (80-200 Hz and 250-500 Hz), using routines based on standardized functions (Matlab Signal Processing Toolbox). Raw EEG recordings were bandpass filtered in the 80–200 Hz and in the 250–500 Hz frequency range using a finite impulse response filter; zero-phase digital filtering was used to avoid phase distortion. Filtered EEGs from each region were then normalized using their own average RMS value calculated over the 10-min epoch. To be considered as an HFO candidate, oscillatory events in each frequency band had to show at least four consecutive cycles having amplitude of 3 SD above the mean. The time lag

between two consecutive cycles had to be between 5 and 12.5 ms for ripples and between 2 and 4 ms for fast ripples (Lévesque et al., 2011, 2012; Salami et al., 2012). HFOs were considered as co-occurring with a spike if they occurred within a time window of ± 500 ms from the peak of an interictal spike. Furthermore, special care was taken to avoid the detection of false HFOs: ripples were kept for analysis if they were only detected in the 80–200 Hz range, whereas fast ripples were kept if they were detected only in the 250–500 Hz range. Overlapping events, which could be caused by filtering spikes (Bénar et al., 2010) were thus excluded from the analysis. The ratio of interictal spikes occurring with HFOs to the total number of interictal spikes was calculated and changes over time were analyzed. The rates of occurrence of ripples and fast ripples on both types of spikes were calculated by dividing the number of ripples or fast ripples on spikes by the total number of the corresponding spike type. HFOs occurring outside of spikes were analyzed separately.

6.3.7. Statistical analysis

In order to study the evolution of rates of interictal spikes over time, values corresponding to the latent phase (48 h, 36 h, 24 h, 12 h and 2 h before the first seizure) were averaged together and were compared to values corresponding to the average value of the chronic phase time points (2 h, 12 h, 24 h, 48 h, 72 h and 96 h after the first seizure). Since values were not normally distributed, we used the non-parametric Kruskall-Wallis and Mann-Whitney-Wilcoxon tests. The level of significance was set at $p < 0.05$.

6.4. Results

6.4.1. Rates of occurrence of type 1 and type 2 spikes during the latent and chronic phases

We analyzed a total of 9,328 spikes from CA3 and EC; 294 type 1 spikes and 4,150 type 2 spikes were detected in CA3 while 288 type 1 spikes and 4596 type 2 spikes were detected in EC. Type 1 and type 2 spikes were seen during both latent and chronic phases. Examples of type 1 and type 2 spikes occurring in the CA3 area during the latent and chronic phases are shown in Figure 6.1A and C, respectively, and the first seizure seen in this animal is illustrated in Figure 6.1B. Examples of type 1 and type 2 spikes recorded from the EC during latent (panel A) and chronic (panel C) phases, along with the first spontaneous seizure (panel B), in another rat are illustrated in Figure 6.2. The first spontaneous seizure recorded from these 9 pilocarpine-treated rats was characterized by CA3 (n= 3) or EC (n= 2) onset while in 4 animals no clear seizure onset zone could be defined (i.e., seizures appear to start at the same time in CA3 and EC). Seizure onset for 68 seizures recorded during the first 96 hours of the chronic phase in these 9 animals was defined as follows: (i) CA3 in 18 seizures (27% of total); (ii) EC in 9 seizures (13% of total) and (iii) simultaneous onset in 41 seizures (60 % of total). Consistent with the results reported by Toyoda et al. (2013), seizures started in the hippocampus in most of the recorded animals. Figure 6.3 shows superimposed waveform shapes of type 1 and type 2 interictal spikes in CA3 and EC from a single animal and highlights the consistency in waveform shape across different interictal events.

We then analyzed the rates of occurrence of type 1 and type 2 spikes. As illustrated in Figure 6.4A, the rate of occurrence of type 1 (panel a) and type 2 (panel b) spikes was

characterized in both CA3 and in EC by dynamic changes during the time period analyzed our experiments. To better compare these modifications, we subtracted the rate average for each time point in CA3 from the equivalent time-point in EC, and then we plotted the values over time (Figure 6.4B). By doing so, we found that the occurrence of both type 1 and type 2 spikes was higher in EC compared to CA3 during the latent phase. This difference gradually decreased until the first spontaneous seizure occurred; this dynamic progression marked the start of the chronic phase, after which both types of interictal spikes occurred at higher rates in the CA3 area compared to EC (Figure 6.4B). Statistical analysis confirmed that there were more type 1 spikes in EC compared to CA3 during the latent phase but more type 1 spikes in CA3 compared to EC during the chronic phase ($p<0.05$; asterisk in Fig. 6.4Ba). Similar to type 1 spikes, type 2 spikes also occurred at higher rates in EC compared to CA3 during the latent phase, but their rate was higher in CA3 compared to EC during the chronic phase ($p<0.05$; asterisk in Figure 6.4Bb).

Finally, in order to test for any individual variability of our results, we analyzed in each animal the changes in occurrence of type 1 and type 2 spikes in CA3 and EC. We found that 67 % of animals showed an increase in occurrence of type 1 and type 2 spikes in CA3 from the latent to the chronic phase. In the EC, type 1 spikes decreased in occurrence from the latent to chronic phase in 71 % of animals while in 86 % of them type 2 spikes decreased in occurrence from the latent to the chronic phase. Figure 6.4C summarizes the average duration of the *spike* and *wave* components of type 1 spikes and the average duration of type 2 spikes in CA3 and EC during the latent and chronic phases. We found that there was no difference in the duration of the *spike* or of the *wave* component of type 1 spikes between the latent and chronic phases in CA3 or EC. In contrast, the duration of type

2 spikes decreased significantly in CA3 and EC from the latent to the chronic phase ($p<0.05$).

6.4.2. Type 1 and type 2 spikes co-occurring with high-frequency oscillations

It has been reported in epileptic patients that HFOs can co-occur with interictal spikes or independently of interictal spikes (Jacobs et al., 2008; Zijlmans et al., 2009a). We first performed an analysis of the whole recordings, independently of the time of seizure occurrence. As illustrated in Figure 6.5, we found that in pilocarpine-treated epileptic rats both ripples and fast ripples occurred during both type 1 and type 2 spikes (panels A and B) as well as outside of interictal spikes (panel C). Analysis of the duration of ripples and fast ripples co-occurring with spikes or occurring outside of spikes revealed no significant differences between them in CA3 (Figure 6.5D). There was also no significant difference in duration of ripples co-occurring with spikes and occurring outside of spikes in EC (Figure 6.5D). However, fast ripples occurring outside of spikes were significantly shorter compared to fast ripples co-occurring with spikes in EC ($p<0.05$; asterisk in Figure 6.5D).

Next, we analyzed the rates of occurrence of type 1 and type 2 spikes that were associated with ripples and fast ripples in CA3 and EC between 48 h before and 96 h after the first seizure (Figure 6.6). No significant differences between the latent and chronic phases were found when the rates of type 1 spikes with either ripples or fast ripples were analyzed in EC and CA3 (Figure 6.6Aa). The difference of the occurrence of type 1 interictal spikes between EC and CA3 did not show any significant difference between latent and chronic phases (Figure 6.6Ab). In addition, the average occurrence of type 1 spikes with ripples (Figure 6.6 Ac) or fast ripples (Figure 6.6 Ad) did not differ significantly between

latent and chronic phases for both regions. In contrast, as illustrated in figure 6.6Bb, the difference between rates of type 2 spikes with fast ripples in EC and CA3 was higher during the latent phase compared to the chronic phase ($p < 0.05$) (absolute values in 6.6Ba). It was also found that this difference reached its maximum 2 h before the first seizure (Figure 6.6Ba). Overall, the average rate of occurrence of type 2 spikes with ripples was higher in CA3 than in EC during the chronic phase ($p<0.05$; asterisk in Figure 6.6Bc) while the average rate of occurrence of type 2 spikes with fast ripples was higher in EC compared to CA3 during the latent phase ($p<0.05$; asterisk in Figure 6.6Bd).

6.4.3. High-frequency oscillations occurring outside of interictal spikes

Finally, we analyzed the rate of ripples and fast ripples occurring outside of interictal spikes during the latent and chronic phases. Statistical analyses revealed that during the latent phase ripples outside of spikes occurred at similar rates in CA3 and EC (Figure 6.7A) while fast ripples outside of spikes had significantly higher rates in EC than in CA3 ($p<0.05$; asterisk in Figure 6.6B). In contrast, during the chronic phase the rate of fast ripples outside of spikes was higher in CA3 compared to EC (but marginally significant, $p=0.06$; Figure 6.7B). Rates of ripples or fast ripples outside of spikes did not show any specific pattern at the transition between the latent and the chronic phase (data not shown).

6.5. Discussion

The main findings of our study can be summarized as follows. First, there was a switch in the distribution of both types of interictal spikes before and after the occurrence of the first seizure: during the latent period they prevailed in EC while during the chronic period they

predominated in CA3. Second, the duration of type 2 spikes decreased significantly in both regions from the latent to the chronic phase. Third, type 2 spikes associated to fast ripples occurred at higher rate in EC than CA3 during the latent phase whereas they occurred at similar rate in the chronic phase. Finally, rates of fast ripples outside of interictal spikes were higher in EC compared to CA3 during the latent phase.

6.5.1. Structure-specific expression of interictal spikes during the latent and chronic phases

We have found that interictal spike rates in EC and CA3 change over time following pilocarpine-induced *status epilepticus*. Specifically, we identified a shift from higher interictal spike occurrence in EC to higher interictal spike occurrence in CA3 at the transition from the latent to the chronic phase. These results suggest that modifications in interictal spike expression in these two limbic structures may reflect the dynamics of dysfunctional network activity and interactions that should occur during epileptogenesis. According to our findings, the distribution of interictal spikes switches at the transition between the latent to the chronic phase. Interictal spikes predominate in the hippocampus CA3 subfield as compared to EC during the chronic phase suggesting that more robust changes in excitability and connectivity may occur shortly after *status epilepticus* (and thus earlier) in the former structure. This view is in line with a previous study in which the EC was found to be hyperexcitable and more vulnerable to neuronal damage shortly after *status epilepticus* induced by lithium-pilocarpine (André et al., 2007); these investigators found that entorhinal and piriform cortices were the initial structures to exhibit signal changes on MRI scans, as early as 6 h after *status epilepticus*. Moreover, they reported that the extent of EC damage correlated with the length of the latent phase (which was longer

when EC damage was minimal). Finally, according to these experiments, neuronal damage in the hippocampus was delayed (André et al., 2007).

More recently, Bragin et al. (2009b) have obtained evidence supporting the involvement of the EC during the early stages of the latent phase and thus, presumably, during epileptogenesis. In this study, which was performed in brain slices obtained from lithium-pilocarpine-treated rats, a high percentage of neurons in the EC layer 5 responded to weak stimulation with polysynaptic burst discharges during the latent phase. These findings were attributed to a depolarizing shift of the IPSP reversal potential consequent to intracellular accumulation of Cl^- due to upregulation of the inward transporter NKCC1 and downregulation of the outward transporter KCC2. Therefore, according to these investigators MTLE primarily develops in the EC, and only over time it would involve other limbic areas including the hippocampus (Bragin et al., 2009b). The predominance of occurrence of interictal spikes in the hippocampus CA3 area compared to the EC observed after the first spontaneous seizure is also in line with the hypothesis that parahippocampal and hippocampal structures are involved at different time points following the initial insult (André et al., 2007; Bragin et al., 2009b). Interestingly, (El-Hassar et al., 2007) have reported that synaptic current properties in the CA1 area of pilocarpine-treated rats are remarkably different during the early and late parts of the latent phase as well as when compared to those seen during the chronic phase.

6.5.2. Changes in duration of type 2 interictal spikes during epileptogenesis

Contrary to what was reported by (Chauvière et al., 2012), type 1 interictal spikes in our study did not decrease in duration when analyzed during the latent phase and, after the

first seizure, during the chronic phase. This discrepancy may be explained by the fact that we did not record from the same hippocampal regions (i.e., the CA1 area). In addition, the decrease in duration of type 1 spikes in the study by (Chauvière et al., 2012) was observed over a timescale ranging from 8 days before until the day of first seizure occurrence whereas in our study we restricted our analysis to interictal spikes occurring during the 48 h that preceded the first spontaneous seizure. We have however observed a significant decrease in duration of type 2 spikes from the latent to the chronic phase, in both CA3 and EC. Although the cellular and pharmacological mechanisms underlying type 2 spikes remain undefined, it has been proposed that they arise from the synchronous activity of local networks of excitatory cells (Chauvière et al., 2012; Demont-Guignard et al., 2012). This view is supported by evidence obtained from several *in vitro* experiments in which short-lasting interictal discharges similar to type 2 spikes were shown to result from enhancement of synaptic excitation due to weakening of inhibition, and to rest on recurrent excitation and regenerative Ca^{2+} currents leading to the synchronous firing of a large number of principal cells (Dingledine and Gjerstad, 1980; Schwartzkroin and Prince, 1980; Traub and Wong, 1982). A primary role of glutamatergic mechanisms along with synchronous firing has also been documented for the short-lasting interictal spikes recorded from the CA3 area of brain slices superfused with the K^+ channel blocker 4-aminopyridine, a pharmacological procedure that enhances both GABAergic and glutamatergic neurotransmission (Avoli and de Curtis, 2011). Therefore, the decreased duration of type 2 spikes from the latent to the chronic phase in both CA3 and EC could reflect progressive changes in neural network synchrony mainly supported by glutamatergic mechanisms.

6.5.3. Type 2 spikes with HFOs may mirror epileptogenesis

The breakdown of type 1 and type 2 interictal spikes into subcategories comprising spikes with ripples or fast ripples has revealed that their rates of occurrence vary over time in both regions. Type 1 spikes with either ripples or fast ripples did not change between latent and chronic phase. In contrast, type 2 spikes with fast ripples occurred more frequently during the latent phase in the EC compared to CA3. These data indicate that type 2 spikes with fast ripples could be a better marker of epileptogenesis than type 1 spikes with HFOs or type 2 spikes with ripples.

The mechanisms underlying pathologic HFOs are still under study but evidence suggests that pathologic HFOs in the ripple band represent population IPSPs generated by principal neurons entrained by synchronously active interneuron networks while fast ripples mirror the synchronous firing of abnormally active principal cells reflecting glutamatergic conductances and being independent of inhibitory neurotransmission (Bragin et al., 1999a, 1999b; Dzhala and Staley, 2004; Foffani et al., 2007). According to this view the high rates of type 2 spikes with fast ripples in EC during the latent phase may reflect a dynamic increase in excitatory activity that will eventually lead to the onset of spontaneous seizures; such conditions would be then shifted to the CA3 area once chronic seizures start to occur.

6.5.4. High-frequency oscillations occurring outside of interictal spikes

Fast ripples occurring outside of spikes had higher rates in EC than in CA3 during the latent phase while the opposite occurred during the chronic epileptic phase (although large, this latter difference was not statistically significant). However, the analysis of their rates of

occurrence over time did not show any specific shift at the transition between the latent and chronic phases. These findings suggest that HFOs outside of spikes may be less reliable markers of epileptogenicity compared to HFOs co-occurring with spikes. This is in accordance with clinical studies showing that the co-occurrence of HFOs with interictal spikes is a better marker of seizure onset zones in epileptic patients than HFOs occurring alone (Wang et al., 2013).

6.6. Conclusions

Our results demonstrate that progressive structure-dependent changes in limbic excitability follow pilocarpine-induced *status epilepticus*; specifically, we found that type 2 interictal spikes, type 2 interictal spikes associated to fast ripples, and fast ripples outside of spikes predominate in EC during the latent phase and predominate in CA3 during the chronic phase. More specifically the increase in the rate of occurrence of spikes co-occurring with fast ripples in CA3 during the chronic phase seems to be a better pathological marker than other interictal spikes. We propose that these changes reflect the progressive pathological reorganization of limbic neuronal networks leading to the occurrence of spontaneous seizures. Future studies with single-cell recordings are needed to establish the participation of principal cells and interneurons to these interictal events. Moreover, these findings should be validated by careful studies of the interictal patterns (including spikes and HFOs) recorded with depth electrodes from MTLE patients. Although it is impossible to implement this approach during the latent phase in humans, our

experimental results may help understanding the progression of epileptogenicity in cases with a relatively high risk of developing epilepsy such as after a traumatic brain injury.

Acknowledgements

This study was supported by the Canadian Institutes of Health Research (CIHR grants 8109, 74609 and 102710).

6.7. Figures

Figure 6.1

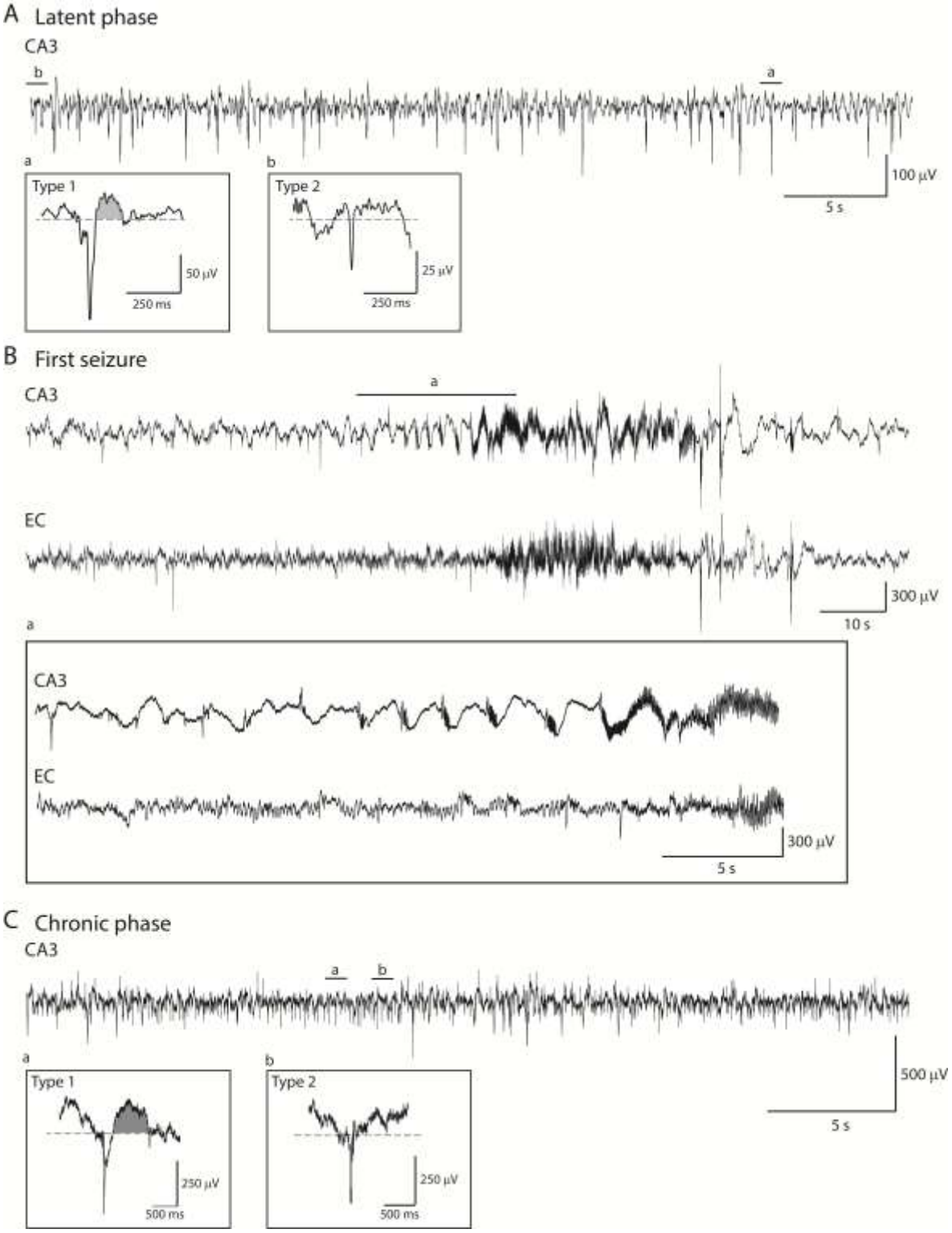

Figure 6.1. Representative examples of type 1 and type 2 interictal spikes recorded from the CA3 region in a pilocarpine-treated rat. A. EEG recordings obtained during the latent phase showing type 1 (**a**) and type 2 (**b**) spikes. **B.** First spontaneous seizure recorded from this animal. Note the hypersynchronous-onset pattern (pre-ictal spikes at a frequency of 0.4-0.7 Hz) that occurs in CA3, which also represents the seizure onset area. **C.** EEG recordings obtained during the chronic phase showing type 1 (**a**) and type 2 (**b**) spikes. Shaded areas in **Aa** and **Ca** highlight the *wave* component of type 1 spikes. Abbreviations in this and the following figures are: CA3: hippocampus CA3 subfield; EC: entorhinal cortex.

Figure 6.2

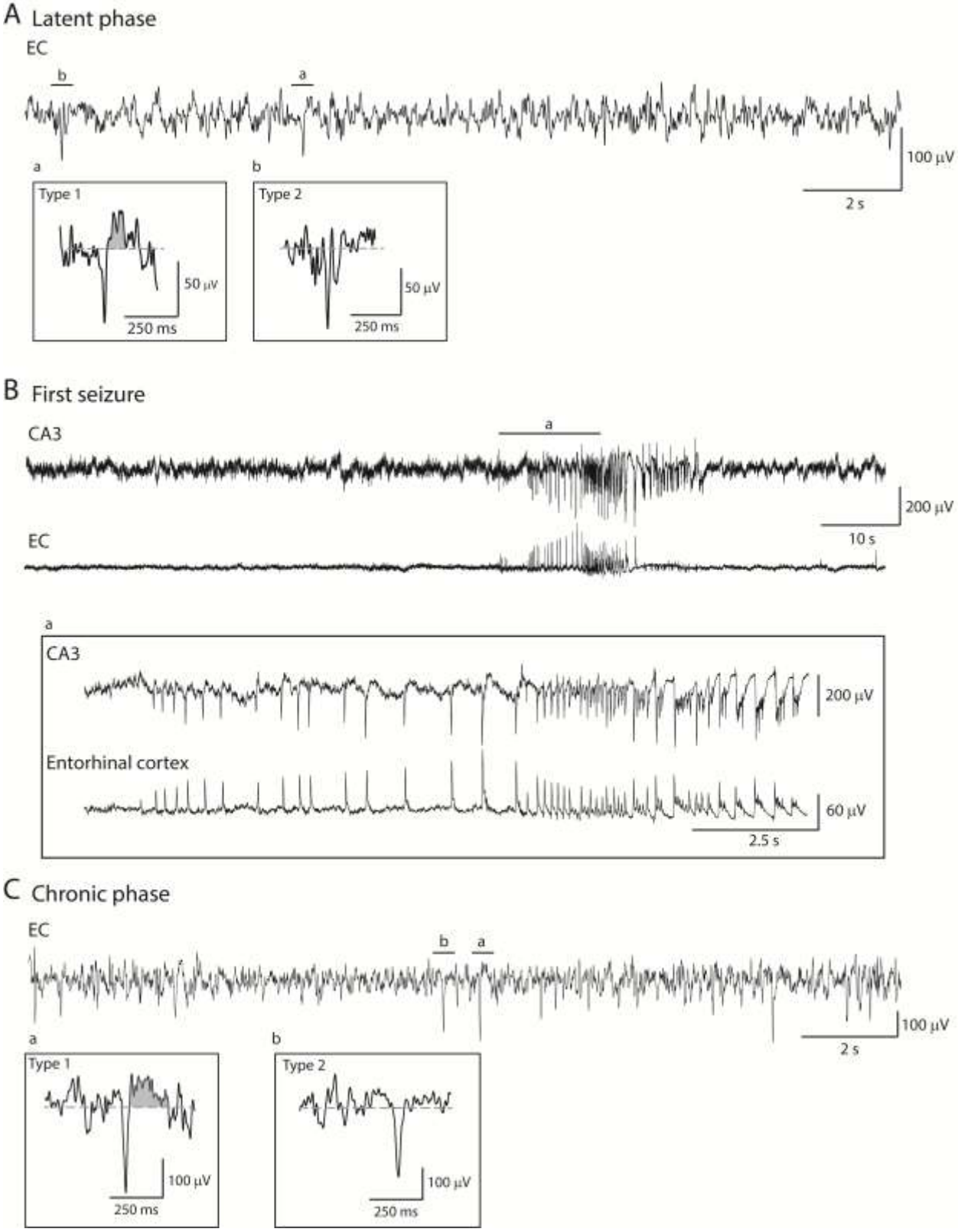
A Latent phase
EC
b
a
100 µV
2 s
a
Type 1
50 µV
250 ms
b
Type 2
50 µV
250 ms
B First seizure
CA3
a
200 µV
10 s
EC
a
CA3
200 µV
Entorhinal cortex
60 µV
2.5 s
C Chronic phase
EC
b
a
100 µV
2 s
a
Type 1
100 µV
250 ms
b
Type 2
100 µV
250 ms

Figure 6.2. Representative examples of type 1 and type 2 interictal spikes recorded from the EC in a pilocarpine-treated rat. A. EEG recordings obtained during the latent phase showing type 1 (**a**) and type 2 (**b**) spikes. **B.** First spontaneous seizure recorded from this animal. Note also in this case that the seizure onset is characterized by a hypersynchronous pattern with pre-ictal spikes at a frequency of ranging from 1.6 to 2.3 Hz that occurs in both CA3 and EC but appears to start in the EC. **C.** EEG recordings obtained during the chronic phase showing type 1 (**a**) and type 2 (**b**) spikes.

Figure 6.3

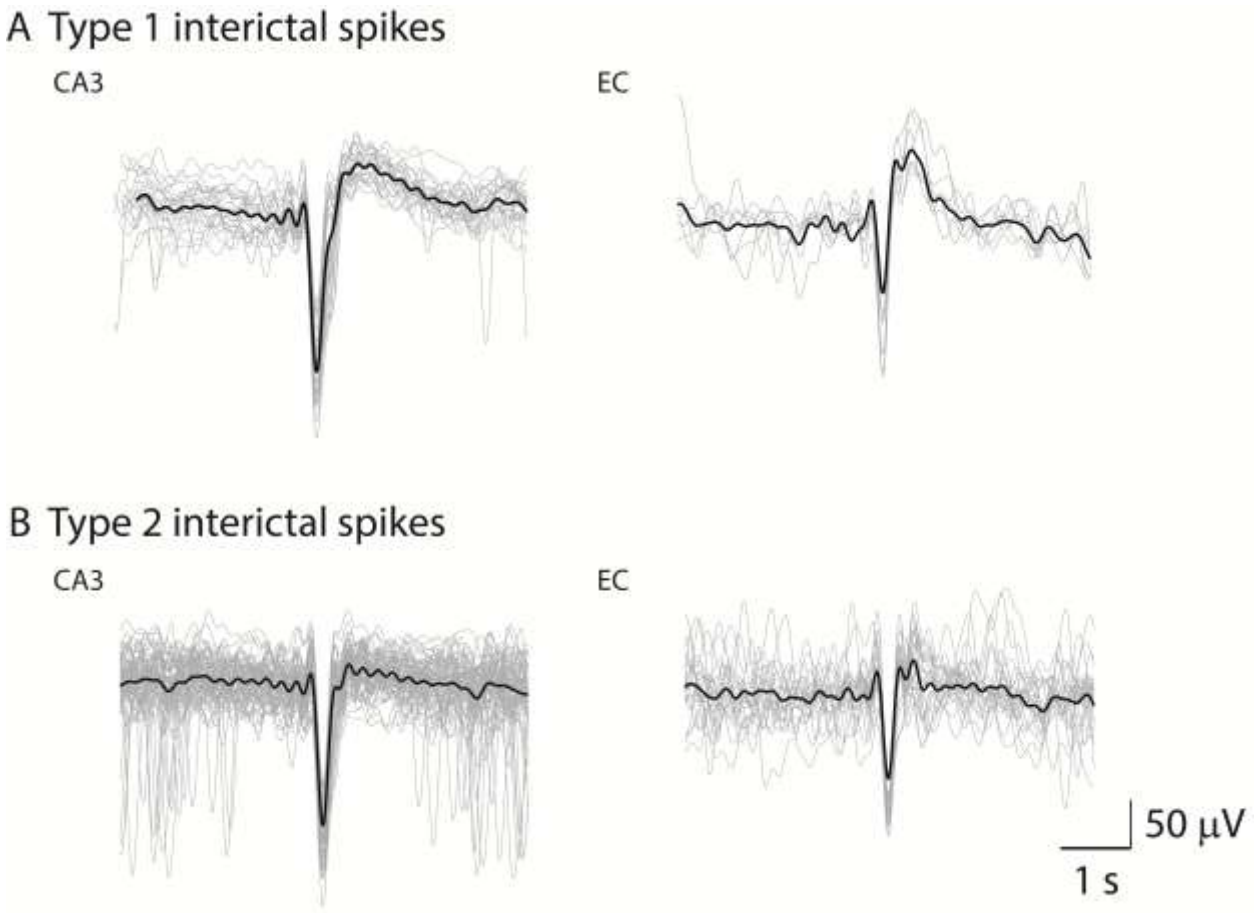

Figure 6.3. Superimposed spike waveform shapes for type 1 and type 2 interictal spikes in CA3 and EC. A. Type 1 spikes recorded in one rat from the CA3 and EC during the chronic period. **B.** Type 2 spikes recorded during the same time points in the CA3 and EC of the same animal. The solid lines represent the mean.

Figure 6.4

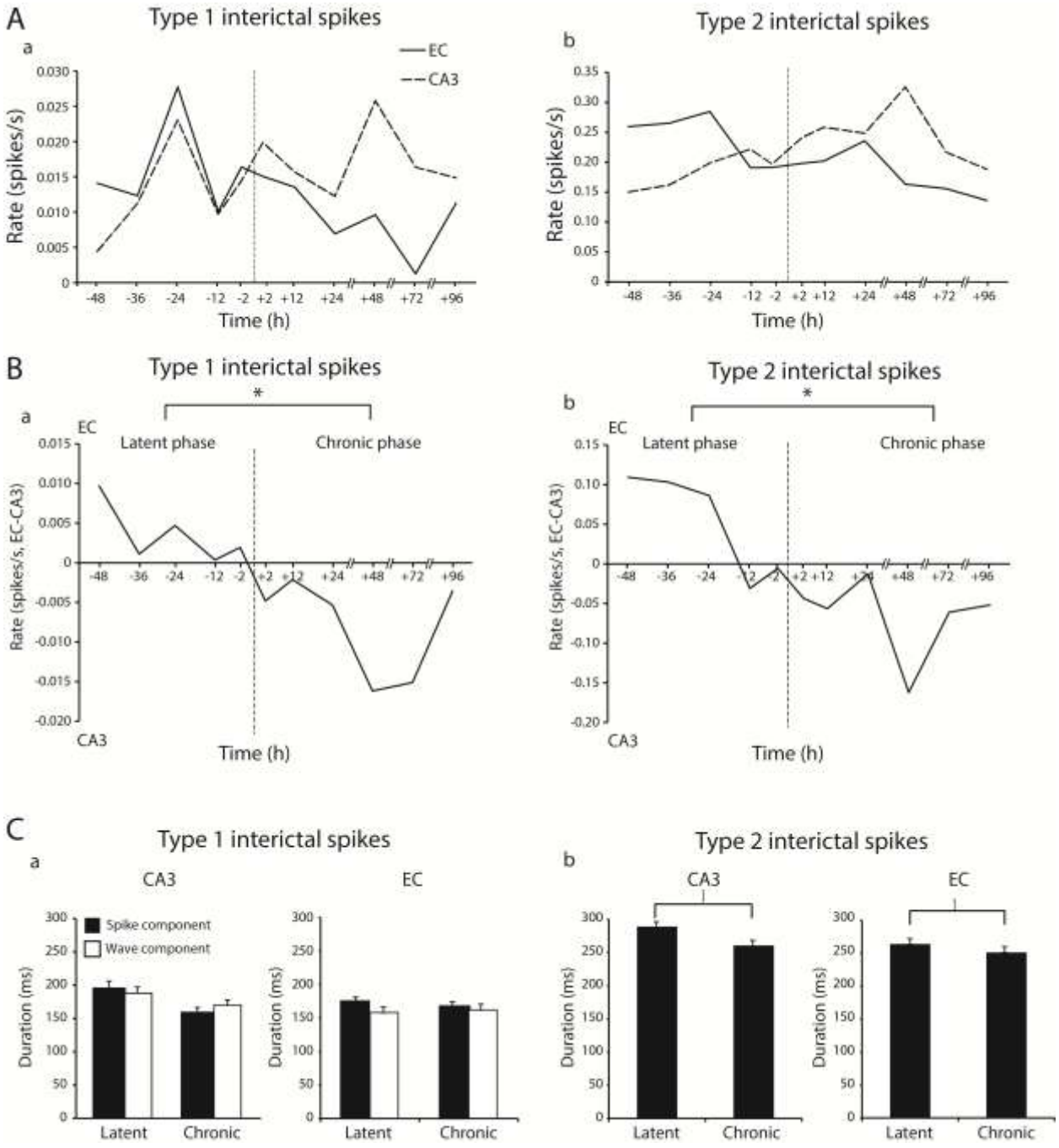
A
Type 1 interictal spikes
a
EC
CA3
Rate (spikes/s)
Time (h)
Type 2 interictal spikes
b
B
Type 1 interictal spikes
Latent phase
Chronic phase
Rate (spikes/s, EC-CA3)
Type 2 interictal spikes
C
Type 1 interictal spikes
CA3
EC
Spike component
Wave component
Duration (ms)
Latent
Chronic
Type 2 interictal spikes

Figure 6.4. Rates of occurrence of type 1 and type 2 interictal spikes during the latent and chronic phase. A. Average rates of occurrence of type 1 (**a**) and type 2 (**b**) spikes in CA3 and EC at different times before and after the occurrence of the first spontaneous seizure (dotted vertical lines at time 0). **B.** Over time difference of the rates of occurrence of type 1 (**a**) and type 2 (**b**) spikes between EC and CA3 (EC-CA3). Note that overall, rates of occurrence of type 1 and type 2 spikes are higher in EC compared to CA3 during the latent phase (-48 h to -2 h) compared to the chronic phase (+2 to +96 h) (* $p < 0.05$ in both cases). **C.** Bar graph showing the average duration of the *spike* and *wave* components of type 1 interictal spikes and of the *spike* component of type 2 interictal spikes during the latent and the chronic phases. Note the significant decrease in duration of type 2 spikes in both CA3 and EC from the latent to the chronic phase (* $p<0.05$).

Figure 6.5

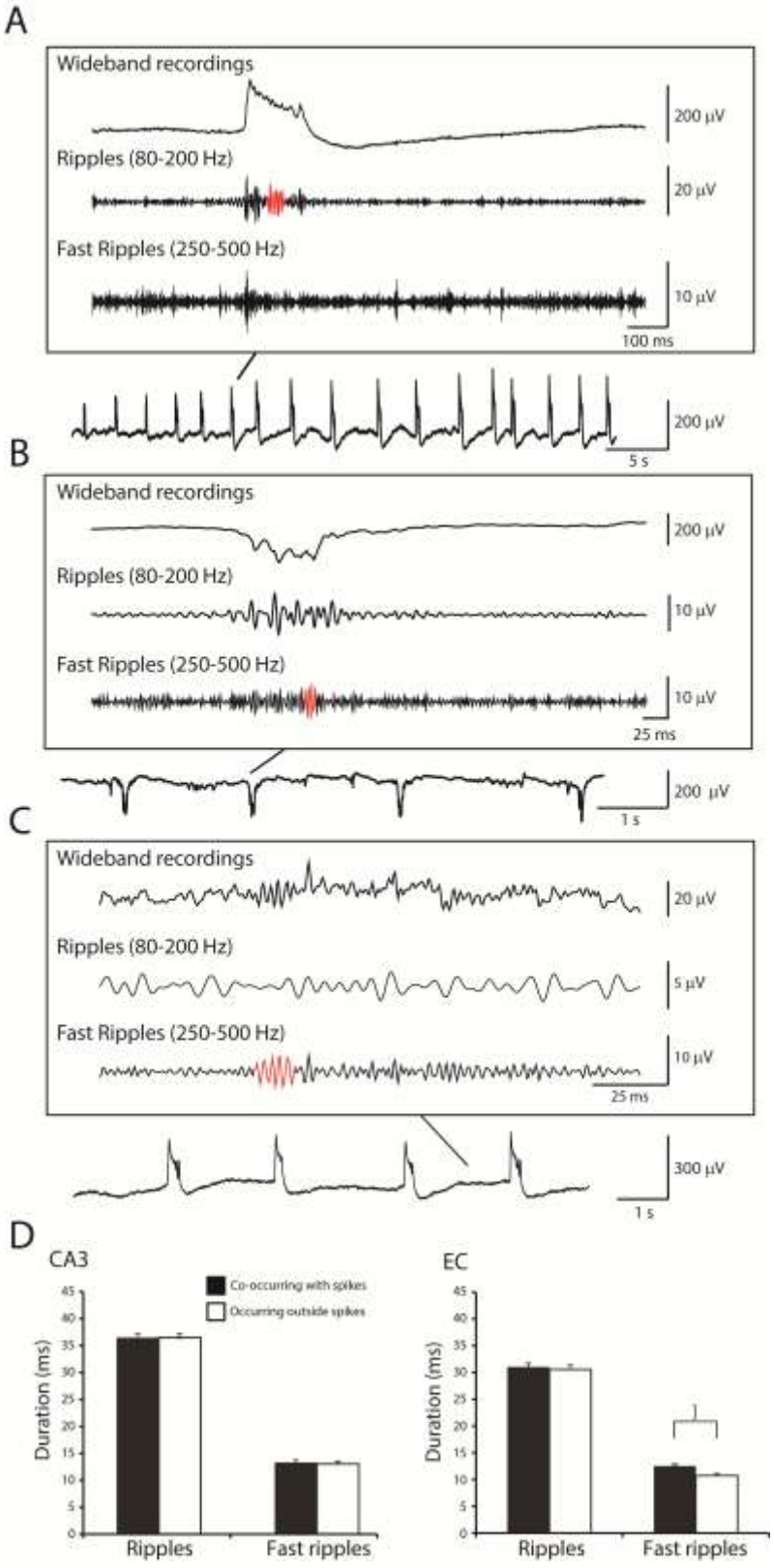
A
Wideband recordings
200 µV
Ripples (80-200 Hz)
20 µV
Fast Ripples (250-500 Hz)
10 µV
100 ms
200 µV
5 s
B
Wideband recordings
200 µV
Ripples (80-200 Hz)
10 µV
Fast Ripples (250-500 Hz)
10 µV
25 ms
200 µV
1 s
C
Wideband recordings
20 µV
Ripples (80-200 Hz)
5 µV
Fast Ripples (250-500 Hz)
10 µV
25 ms
300 µV
1 s
D
CA3
Co-occurring with spikes
Occurring outside spikes
Duration (ms)
Ripples
Fast ripples
EC
Duration (ms)
Ripples
Fast ripples

Figure 6.5. HFOs co-occurring with type 1 and type 2 spikes as well as outside of them. A. Example of a ripple co-occurring with a type 1 spike in the CA3 region of a pilocarpine-treated rat one day before the occurrence of the first spontaneous seizure. **B**. Example of a fast ripple co-occurring with a type 2 spike in the CA3 region of the same animal one day after the occurrence of the first seizure. **C.** Example of a fast ripple occurring in EC outside of interictal spikes on the day of the occurrence of the first seizure). HFOs in **A**, **B** and **C** are highlighted in red. **D.** Bar graph showing the average duration of ripples and fast ripples co-occurring with spikes and outside of spikes in CA3 and EC. Note that fast ripples occurring outside of spikes were significantly shorter in duration in EC (* $p < 0.05$).

Figure 6.6

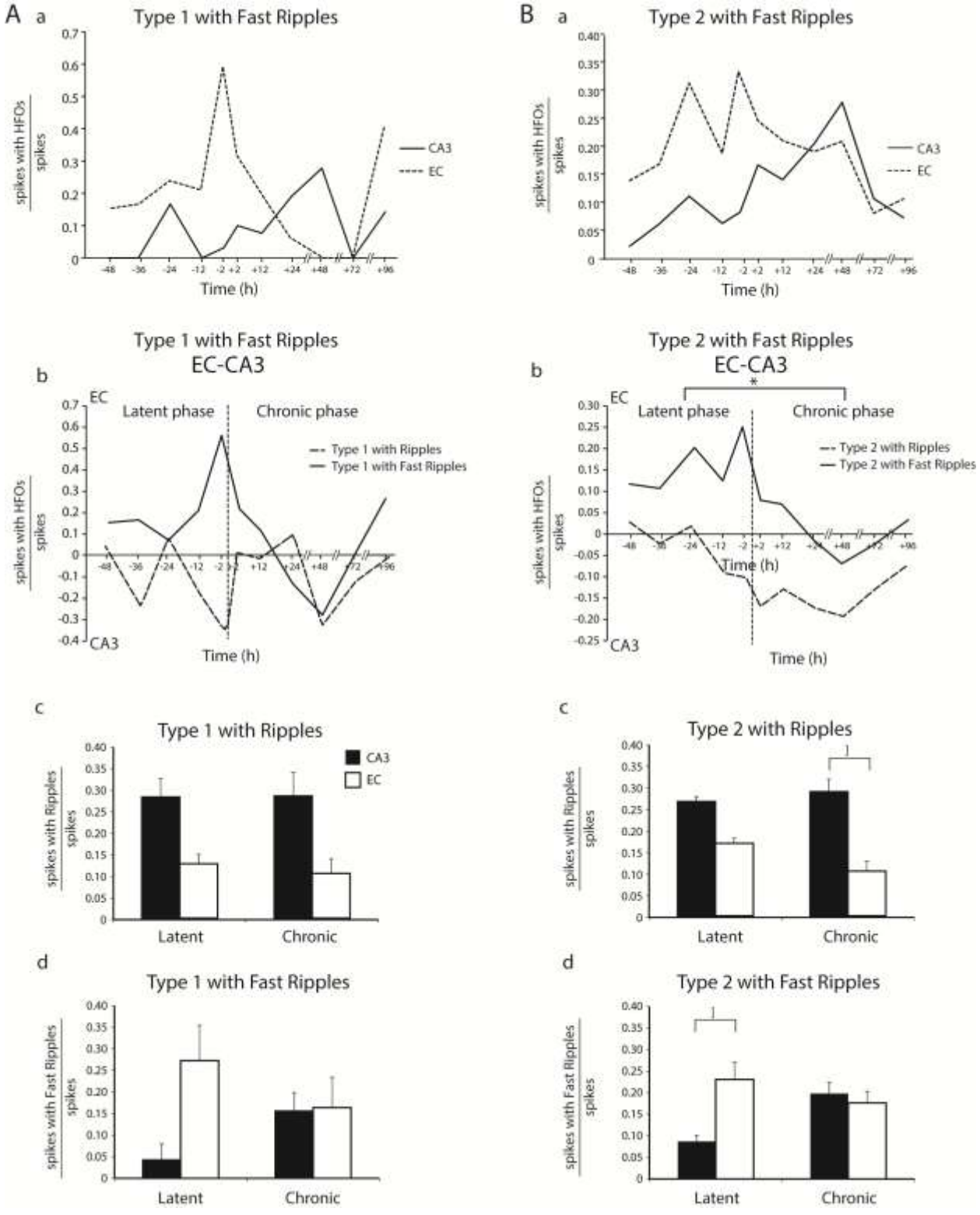
A a
Type 1 with Fast Ripples
spikes with HFOs / spikes
CA3
EC
Time (h)
B a
Type 2 with Fast Ripples
b
Type 1 with Fast Ripples
EC-CA3
EC
Latent phase
Chronic phase
Type 1 with Ripples
Type 1 with Fast Ripples
CA3
Type 2 with Fast Ripples
EC-CA3
Type 2 with Ripples
Type 2 with Fast Ripples
c
Type 1 with Ripples
spikes with Ripples / spikes
Latent
Chronic
Type 2 with Ripples
d
Type 1 with Fast Ripples
spikes with Fast Ripples / spikes
Type 2 with Fast Ripples

Figure 6.6. Rates of occurrence of type 1 and type 2 interictal spikes co-occurring with HFOs. Aa. Temporal changes of the ratio of occurrence of type 1 spikes with fast ripples. (The absolute values of the ratio of the type 1 spikes with ripples are not shown.) In this plot as well as in that shown in **Ba**, the ratio in each region was calculated by dividing the number of interictal spikes with ripples or fast ripples over the total number of interictal spikes. Note that there was no significant difference between the latent (-48 h to -2 h) and chronic phase (+2 h to +96 h). **Ab.** Over time differences between EC and CA3 of the ratios of type 1 spikes with ripples (dotted line) and fast ripples (continuous line). However, the difference between EC and CA3 reached its maximum value 2 h before the occurrence of the first seizure. The inset shows ratios of type 1 spikes with fast ripples in CA3 and EC. Note again the peak at 2 h before first seizure onset. **Ac.** Average ratios of type 1 spikes with ripples in CA3 and EC during latent and chronic phases. No significant differences were observed. **Ad.** Average ratios of type 1 spikes with fast ripples in CA3 and EC during latent and chronic phases. No significant differences were observed. **Ba.** Temporal changes of the ratio of occurrence of type 2 spikes with fast ripples. (The absolute values of the ratio of the type 2 spikes with ripples are not shown.) **Bb.** Difference over time between ratios of type 2 spikes with ripples and fast ripples between EC and CA3. Note that the difference between EC and CA3 for type 2 spikes with fast ripples is significantly higher in the latent phase compared to the chronic phase (* $p<0.05$) and it reaches its maximum value 2 h before the occurrence of the first seizure. **Bc.** Average ratio of type 2 spikes with ripples in CA3 and EC during latent and chronic phases. Type 2 spikes with ripples occurred at higher rates in CA3 compared to EC during the chronic phase. **Bd.** Average ratios of type 2 spikes with fast ripples in CA3 and EC during both latent and

chronic phases. Type 2 spikes with fast ripples occurred at higher rates in EC compared to CA3 during the latent phase (* $p<0.05$).

Figure 6.7

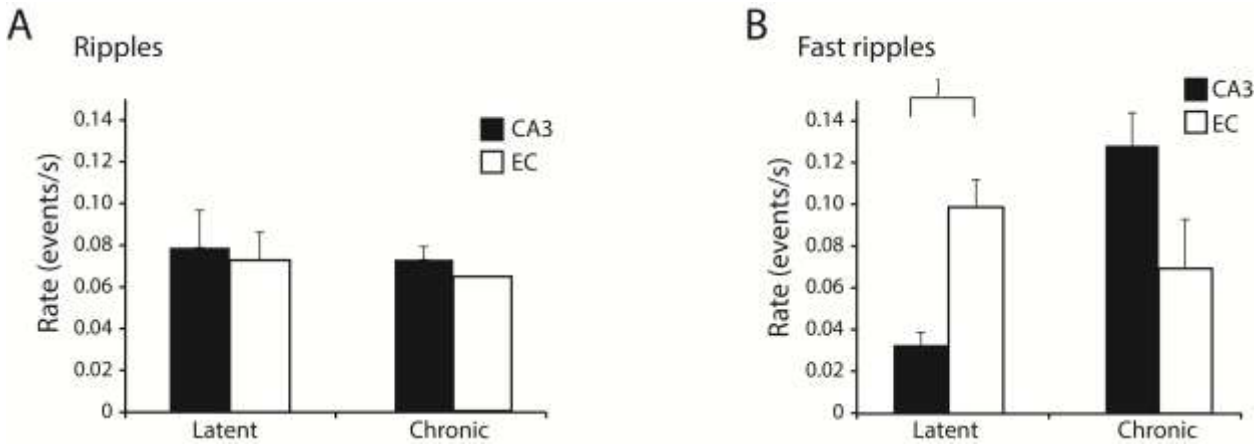

Figure 6.7. Average rates of occurrence of HFOs outside of spikes during the latent and chronic phases in CA3 and EC. A. Average rates of occurrence of ripples occurring outside of spikes in CA3 and EC during both latent and chronic phases. No significant differences were observed. **B.** Average rates of occurrence of fast ripples occurring outside of spikes in CA3 and EC during latent and chronic phases. Fast ripples outside of spikes occurred at higher rates in EC compared to CA3 during the latent phase ($p<0.05$). On the other hand during the chronic phase the average rate of occurrence of fast ripples is higher in CA3 compared to EC ($p=0.06$).

7. Chapter 7

General Discussion

In the last part of this thesis, I will summarize the main findings reported in the previous chapters. In addition, I propose possible directions for future studies while discussing the limitations of the experiments performed during my PhD research.

7.1. Summary of the findings

Fundamental brain research has contributed in many aspects to improve the understanding and the treatment of brain diseases. Mesial temporal lobe epilepsy (MTLE), one of the most frequent focal epilepsies, is often refractory to medications, and patients suffering from this disorder often become potential candidates for surgical removal of the epileptogenic zone. Depth electrode recordings in epileptic patients or in patients at risk of developing MTLE are greatly limited, and animal models have thus made it possible to understand this disorder better.

Successful surgical outcome depends mainly on the precise identification and removal of the epileptogenic area and various techniques and tools have been developed to help with the identification of epileptogenic area(s). More recently, the discovery of high frequency oscillations (HFOs: 80-500 Hz) have attracted the attention of epileptologists as a reliable biomarker of epileptogenic area. Understanding the mechanisms underlying HFOs and their association to ictogenesis and epileptogenesis not only could lead to a better identification of the epileptogenic area but may also provide new insights in our knowledge of epilepsy.

In this thesis, with the help of chronic and acute animal models of epilepsy, I addressed the role of HFOs during ictogenesis, and also identified their participation during epileptogenesis, along with that of interictal spikes, which are also electro-physiological biomarkers of focal epileptic disorders. The main findings of my studies can be summarized as follows:

1. There is a lack of a standardized reliable method of HFO detection - thus, in chapter 2, I developed an automated method for detecting HFOs during pre-ictal, ictal, and post-ictal periods. The suggested method, method 3, employs a reference period before the seizure onset for signal normalization. The results obtained with this method are more similar to visual analysis when detecting HFOs.

2. In chapter 3, I discovered that two main types of seizure onsets, namely low-voltage fast (LVF) and hypersynchronous (HYP) onset patterns, can be identified in pilocarpine treated rats. In addition, I demonstrated that these two onset patterns are associated with a different expression of HFOs proposing different mechanisms of generation.

3. In chapter 4, I investigated the features of seizures induced by 4-aminopyridine (4AP) *in vivo.* More specifically, I reported that systemic injection of 4AP results mainly in convulsive seizures and that most of these seizures are characterized by LVF onset patterns potentially implicating the role of GABAergic signaling in their generation.

4. In chapter 5, I confirmed that 4AP mostly induces LVF seizures and I found that picrotoxin induces HYP seizures; in addition, I discovered that 4AP-induced LVF seizures are mostly associated to ripples, whereas HYP seizures induced with picrotoxin are mostly associated to fast ripples.

5. Finally, in chapter 6, I identified specific changes in interictal spikes and HFOs, which are both electrophysiological biomarkers of focal epilepsy, during the transition from the latent to the chronic period; these changes may indeed reflect pathophysiological modifications occurring in limbic structures that are implicated in epileptogenesis.

Altogether, my findings demonstrated that: (i) there are specific changes in network excitability occurring during low-voltage fast-onset (LVF) and hypersynchronous-onset (HYP) seizures, and that these differences can be pinpointed *in vivo* by analyzing HFOs; (ii) these specific characteristics should mirror mechanisms that rest on inhibitory and excitatory signaling during LVF seizures, whereas HYP seizures should mainly result from the involvement of glutamatergic activity; (iii) epileptogenesis is associated to changes in synaptic plasticity and in the involvement of specific limbic structures as reflected by dynamic alterations in interictal spikes and HFOs occurring at the transition from latent to chronic period.

7.2. HFO analysis and seizure onset patterns

7.2.1. HFO detection

The identification of HFOs is a challenging process. Despite several efforts to improve the analysis of the EEG signals, there exists a lack of reliable standard method for detecting HFOs (Zelmann et al., 2012). Different groups are detecting and analyzing HFOs either with the help of their custom-made analyzing programs or the use of visual analysis, where the latter is still the gold standard for detecting HFOs. In chapter 2 of this thesis, I proposed an automated method that could be implemented and modified according to different systems in order to avoid the time-consuming visual analysis (Salami et al., 2012).

My method of automated analysis of HFOs, however, still needs visual verification to avoid artifacts. I propose the following directions for improving and developing better methods of HFO detection:

- In my automated method of HFO detection, visual analysis was necessary to a certain degree for further verification and noise or artifacts removal. Development of future methods with new parameters of removing noise and analyzing wavelet transforms can be of great interest for HFO identification in large data sets.
- Defining more universal criteria for HFO detection would also be helpful in developing more reliable methods for detecting HFOs. This indeed needs more investigation in distinguishing between physiological and pathological HFOs as well.
- As mentioned earlier, HFOs have been discovered recently on the scalp EEG of patients (Andrade-Valenca et al., 2011), but they were detected at lower rates. It should be taken into account that scalp HFOs may have a great clinical value. Thus, the new proposed automated methods should discover and take into account the criteria for detecting and analyzing the scalp HFOs as well as the HFOs recorded with the help of depth electrodes.

7.2.2. HFOs and seizure initiation

Earlier studies in the occurrence of HFOs during the seizures have demonstrated an increase in the HFOs at the initiation of the seizure, especially in seizure onset zones. These findings have proposed an important role for HFOs as a biomarker of seizure onset zone and epileptogenic areas (Jacobs et al., 2008, 2009b), but they mostly focused on the increase in the ripple or fast ripple rates at the seizure onset area, whereas the distribution of HFOs during different seizure onset patterns remained unidentified. In both animal models of MTLE and patients suffering from this disorder, seizures can often be classified into two groups termed LVF and HYP onset patterns (Velasco et al., 2000; Bragin et al.,

2005). My studies not only confirmed that these two types of seizure onset patterns can be identified in the pilocarpine model of MTLE, but also proposed an association between these onset patterns and HFOs (Lévesque et al., 2012). By analyzing the pilocarpine model of MTLE, I have determined that these two onset patterns are associated with different HFO patterns. More specifically I displayed an increase in the generation of ripples compared to fast ripples in seizures with LVF onset patterns while an increase in the fast ripples compared to ripples was identified at the initiation of seizures with HYP onset patterns. In addition, I demonstrated that this increase occurs in the seizure onset zone before its extension to the regions of secondary spread (Chapter 3).

My findings strongly indicate that different cellular or network mechanisms are responsible for initiating different seizure onset patterns; however, the underlying mechanism responsible for these differences remains to be identified. Our laboratory previously reported that the application of 4AP *in vitro* generates seizure-like events with the characteristics of LVF onset patterns. These i*n vitro* epileptiform activities are thought to be related to an enhancement in GABAergic signaling occurring at seizure onset (Avoli and de Curtis, 2011). We tested therefore the hypothesis that LVF and HYP onset patterns reflect enhanced GABAergic and glutamatergic mechanisms, respectively, with the systemic administration of 4AP (which enhances both GABAergic and glutamatergic signaling), and of picrotoxin, a drug that blocks $GABA_A$ receptor signaling. Specifically, we hypothesized that LVF seizures and higher number of ripples compared to fast ripples are associated with an increase in $GABA_A$ receptor signaling while HYP onset seizures and higher rates of fast ripples mostly occur when $GABA_A$ receptors are blocked. Interestingly, we detected mostly LVF seizures and a higher presence of ripples after the application of 4AP (Chapters

4 and 5) (Lévesque et al., 2013; Salami et al., 2015) whereas we found a predominance of fast ripples and occurrence of HYP seizures after the application of picrotoxin (Chapter 5) (Salami et al., 2015).

Recently in our laboratory, with the help of optogenetic techniques, the role of GABAergic signaling in the initiation of different seizure onset patterns was investigated. The results of this study suggested an involvement of interneuronal networks in the initiation of LVF onset seizures (Shiri et al., 2015). Similar to what we reported, Yekhlef and colleagues showed the involvement of different interneuronal subtypes in the generation of ictal events following the administration of 4AP, *in vitro* (Yekhlef et al., 2015).

My results are significant on two levels; first, I propose that distinguishing between seizure onset patterns can help us increase our knowledge about the basic mechanisms underlying epilepsy, and second, both ripples and fast ripples are of significant values in understanding these mechanisms since we could identify them separately at different seizure onset patterns.

Overall, I believe these findings to be a breakthrough in epilepsy research; however, more studies are needed to answer the following questions:

- We showed an association between seizure onset patterns and HFO occurrence at the initiation of seizures. We recorded from animals for two weeks and only seizures occurring at the first stage of chronic period were investigated. More investigation is of great interest to see if these results are also applied later on when the seizures are recorded after more progression into the disease, after few weeks or months in the animal model of MTLE.

- Similar to what is reported in patients, we could identify both types of seizures in the same animal. It would be important to establish whether seizures with different patterns occurring in the same individual originate from the same networks and/or regions. Investigations with the single cell recordings could bring answers to this issue as well as help us understanding the underlying mechanisms of ripples and fast ripples and their association with the seizure onset types.
- My experiments using 4AP or pictrotoxin proposed that HFOs with dominancy in different frequency bands are more specific to different seizure onset patterns. However, studies with different agents targeting a single mechanism could help validate these results.
- My studies have outlined differences in the occurrence of the two types of HFOs in LVF and HYP seizure onset patterns. It is interesting to find out if the networks involved in the generation of different seizures are started to get prepared long time before the onset of the seizure. Analyzing HFOs during interictal periods in the preceding minutes or hours before the onset of the seizures may answer this question. This analysis could bring new insights into the field and help us predict the occurrence of different seizures in advance.
- Investigating the interictal HFOs along with ictal HFOs can help us understand if the former is as informative as the latter. This could be of a great value as seizures are unpredictable and occur less frequently in some patients and it would make the assessment less time consuming and less costly.

- Since different mechanisms may be involved in the generation of different seizure onset patterns, these specific mechanisms should be further tested through different pharmacological treatments.

7.3. Epileptogenesis

Epileptogenesis is a process of paramount relevance in focal epileptic disorders but in spite of several studies, the mechanisms underlying it remain unclear. Patients who are at risk of developing epilepsy can only take advantage of non-invasive techniques, but there is a lack in associating those results to the progress of the disease. Over the past few years, improvements in experimental models have advanced our understanding of epilepsy and, in particular, of MTLE (Jefferys, 2010). Understanding the mechanisms during epileptogenesis can further help us to identify better biomarkers of epileptogenicity.

Interictal spikes have been used as biomarkers of epileptogenicity but their vague role in epileptogenesis makes it harder to benefit from them. The discovery of HFOs and their strong association with the epileptogenic area have indeed opened new insights. In addition, the association of HFOs with interictal spikes may also enlighten the exact role of interictal spikes. In chapter 6 of this thesis, I determined that the changes in the characteristics and morphology of interictal spikes and their associated HFOs are expressed differently in different structures (Salami et al., 2014). In addition, I identified a shift in the occurrence of both interictal spikes and HFOs between CA3 region of hippocampus and EC at the transition from the latent to the chronic period. This transition

may represent the dynamic activity and progressive pathological reorganization of limbic neuronal networks during epileptogenesis.

My observations suggest that interictal spikes, if classified properly, may play a more important role during epileptogenesis than previously thought. More specifically they should be classified in terms of their features such as their association with HFOs, their amplitude, morphology, as well as their duration. I have reported that the occurrence of fast ripples along with interictal spikes can act as a better biomarker of epileptogenicity.

Studies speculating mechanisms underlie HFO generation agree that the hyperexcitability of neurons is necessary for the generation of HFOs but this can be achieved through different mechanisms, some of which could be through pathologic networks while the rest can be involved in physiological mechanisms such as learning and memory. Indeed, more studies need to be done to distinguish between normal and pathological HFOs. As briefly described in the general introduction (chapter 1), diverse mechanisms have been proposed for the generation of HFOs (Jefferys et al., 2012b). It has also been reported that ripples and fast ripples may overlap in their mechanism of generation, suggesting that taking into consideration only frequency as a differentiating criterion may not be sufficient. Thus, more work is needed to investigate the mechanisms involved in the HFO generation, and HFOs should be classified using alternative parameters to their frequency range (e.g., their morphology, amplitude, and duration). The following investigations are therefore proposed to increase our understanding of epileptogenesis and the role of interictal spikes and HFOs in this process:

- Different potential mechanisms have been proposed to underlie ripples and fast ripples. Single cell recording could indeed represent a valuable technique to investigate the contribution of different mechanism in the generation of physiological and pathological HFOs. It is likely that there are overlaps in the mechanisms involved in the generation of both events; thus, discovering other criteria to differentiate between HFOs is required. This may also lead to identification of other biomarkers of epileptogenicity.
- Future studies should also emphasize the role of interneurons and principal cells in the generation of different types of spikes and of their associated HFOs thus identifying whether there are differences between spikes with ripples or with fast ripples in terms of interneuron participation.
- In chapter 6, different types of interictal spikes with and without HFOs are reported. The effects of antiepileptic drugs on the features of these spikes and its possible association to seizure frequency or latent period duration should be investigated.
- HFOs have been mainly analyzed in EEG signals obtained with depth electrodes. However, recent studies have demonstrated that HFOs can be identified in scalp EEG. This finding, along with the use of other non-invasive techniques such as fMRI might be important to help individuals at risk of developing epilepsy. More investigation to find the association between different HFOs and the results obtained with non-invasive tools, can be a great advantage for patients at risk of developing epilepsy.
- In chapter 6 of this thesis I focused on interictal periods during slow-wave sleep, as the occurrence of interictal spikes and HFOs is more frequent at this state. However,

it could be of great interest to see whether changes of interictal spikes and HFOs are similar during different brain states.

- Different methods, such as CT scan, SPECT scan, MRI, and X-rays, along with EEG recordings have been used for the precise localization of the epileptogenic area. It was shown that HFOs can also be seen in the non-lesional model of MTLE, thus their association to neuronal loss and brain damages has not been clearly identified. Imaging techniques could help the evaluation of the association of the HFOs to different possible neuronal damages.

7.4. Conclusive remarks

Despite all the work performed in epilepsy research, we still have scarce information regarding the mechanisms underlying the generation of seizures. During the course of my PhD studies, I have provided new insights into this field thus hoping to enrich our current understanding of epileptic disorders and in particular of MTLE. I anticipate that my findings will open new perspectives in epilepsy diagnostic and predictive approaches, as well as in developing new antiepileptic drugs for controlling epileptic seizures.

References

Akiyama T, McCoy B, Go CY, Ochi A, Elliott IM, Akiyama M, Donner EJ, Weiss SK, Snead OC, Rutka JT, Drake JM, Otsubo H. Focal resection of fast ripples on extraoperative intracranial EEG improves seizure outcome in pediatric epilepsy. *Epilepsia* 52: 1802–1811, 2011.

Alvarado-Rojas C, Huberfeld G, Baulac M, Clemenceau S, Charpier S, Miles R, de la Prida LM, Le Van Quyen M. Different mechanisms of ripple-like oscillations in the human epileptic subiculum. *Ann Neurol* 77: 281–290, 2015.

Andrade-Valenca LP, Dubeau F, Mari F, Zelmann R, Gotman J. Interictal scalp fast oscillations as a marker of the seizure onset zone. *Neurology* 77: 524–531, 2011.

André V, Dubé C, François J, Leroy C, Rigoulot M-A, Roch C, Namer IJ, Nehlig A. Pathogenesis and pharmacology of epilepsy in the lithium-pilocarpine model. *Epilepsia* 48 Suppl 5: 41–47, 2007.

Avanzini GG, Treiman DM, Engel J. Chapter 36: Animal Models of Acquired Epilepsies and Status Epilepticus. In: *Epilepsy: A Comprehensive Textbook*. Philadelphia: Lippincott Williams & Wilkins, p. 415:444, 2008.

Avoli M. Herbert H. Jasper and the Basic Mechanisms of the Epilepsies. In: *Jasper's Basic Mechanisms of the Epilepsies*, edited by Noebels JL, Avoli M, Rogawski MA, Olsen RW, Delgado-Escueta AV. Bethesda (MD): National Center for Biotechnology Information (US), 2012.

Avoli M. Mechanisms of epileptiform synchronization in cortical neuronal networks. *Curr Med Chem* 21: 653–662, 2014.

Avoli M, Barbarosie M, Lücke A, Nagao T, Lopantsev V, Köhling R. Synchronous GABA-mediated potentials and epileptiform discharges in the rat limbic system in vitro. *J Neurosci* 16: 3912–3924, 1996.

Avoli M, Biagini G, de Curtis M. Do interictal spikes sustain seizures and epileptogenesis? *Epilepsy Curr Am Epilepsy Soc* 6: 203–207, 2006.

Avoli M, de Curtis M. GABAergic synchronization in the limbic system and its role in the generation of epileptiform activity. *Prog Neurobiol* 95: 104–132, 2011.

Bagshaw AP, Jacobs J, LeVan P, Dubeau F, Gotman J. Effect of sleep stage on interictal high-frequency oscillations recorded from depth macroelectrodes in patients with focal epilepsy. *Epilepsia* 50: 617–628, 2009.

Ball AP, Hopkinson RB, Farrell ID, Hutchison JG, Paul R, Watson RD, Page AJ, Parker RG, Edwards CW, Snow M, Scott DK, Leone-Ganado A, Hastings A, Ghosh AC, Gilbert RJ. Human botulism caused by Clostridium botulinum type E: the Birmingham outbreak. *Q J Med* 48: 473–491, 1979.

Behr C, D'Antuono M, Hamidi S, Herrington R, Lévesque M, Salami P, Shiri Z, Köhling R, Avoli M. Chapter Four - Limbic Networks and Epileptiform Synchronization: The View from the Experimental Side. In: *International Review of Neurobiology*, edited by Premysl Jiruska M de C and JGRJ. Academic Press, p. 63–87, 2014.

Ben-Ari Y, Cossart R. Kainate, a double agent that generates seizures: two decades of progress. *Trends Neurosci* 23: 580–587, 2000.

Bénar CG, Chauvière L, Bartolomei F, Wendling F. Pitfalls of high-pass filtering for detecting epileptic oscillations: a technical note on "false" ripples. *Clin Neurophysiol* 121: 301–310, 2010.

Benini R, Avoli M. Rat subicular networks gate hippocampal output activity in an in vitro model of limbic seizures. *J Physiol* 566: 885–900, 2005.

Benini R, D'Antuono M, Pralong E, Avoli M. Involvement of amygdala networks in epileptiform synchronization in vitro. *Neuroscience* 120: 75–84, 2003.

Berger H. Über das Elektrenkephalogramm des Menschen - Siebente Mitteilung. *Arch Für Psychiatr Nervenkrankh* 100: 301–320, 1933.

Bortel A, Lévesque M, Biagini G, Gotman J, Avoli M. Convulsive status epilepticus duration as determinant for epileptogenesis and interictal discharge generation in the rat limbic system. *Neurobiol Dis* 40: 478–489, 2010.

Bragin A, Azizyan A, Almajano J, Engel J. The cause of the imbalance in the neuronal network leading to seizure activity can be predicted by the electrographic pattern of the seizure onset. *J Neurosci* 29: 3660–3671, 2009a.

Bragin A, Azizyan A, Almajano J, Wilson CL, Engel J. Analysis of chronic seizure onsets after intrahippocampal kainic acid injection in freely moving rats. *Epilepsia* 46: 1592–1598, 2005.

Bragin A, Benassi SK, Kheiri F, Engel J. Further evidence that pathologic high-frequency oscillations are bursts of population spikes derived from recordings of identified cells in dentate gyrus. *Epilepsia* 52: 45–52, 2011.

Bragin A, Engel J Jr, Wilson CL, Fried I, Buzsáki G. High-frequency oscillations in human brain. *Hippocampus* 9: 137–142, 1999a.

Bragin A, Engel J Jr, Wilson CL, Fried I, Mathern GW. Hippocampal and entorhinal cortex high-frequency oscillations (100--500 Hz) in human epileptic brain and in kainic acid--treated rats with chronic seizures. *Epilepsia* 40: 127–137, 1999b.

Bragin A, Engel J, Staba RJ. High-frequency oscillations in epileptic brain. *Curr Opin Neurol* 23: 151–156, 2010.

Bragin A, Engel J, Wilson CL, Vizentin E, Mathern GW. Electrophysiologic analysis of a chronic seizure model after unilateral hippocampal KA injection. *Epilepsia* 40: 1210–1221, 1999c.

Bragin A, Jandó G, Nádasdy Z, Hetke J, Wise K, Buzsáki G. Gamma (40-100 Hz) oscillation in the hippocampus of the behaving rat. *J Neurosci* 15: 47–60, 1995.

Bragin A, Wilson CL, Almajano J, Mody I, Engel J. High-frequency oscillations after status epilepticus: epileptogenesis and seizure genesis. *Epilepsia* 45: 1017–1023, 2004.

Bragin DE, Sanderson JL, Peterson S, Connor JA, Müller WS. Development of epileptiform excitability in the deep entorhinal cortex after status epilepticus. *Eur J Neurosci* 30: 611–624, 2009b.

Butuzova MV, Kitchigina VF. Repeated blockade of GABAA receptors in the medial septal region induces epileptiform activity in the hippocampus. *Neurosci Lett* 434: 133–138, 2008.

Buzsáki G. Theta oscillations in the hippocampus. *Neuron* 33: 325–340, 2002.

Buzsáki G, Draguhn A. Neuronal oscillations in cortical networks. *Science* 304: 1926–1929, 2004.

Buzsáki G, Horváth Z, Urioste R, Hetke J, Wise K. High-frequency network oscillation in the hippocampus. *Science* 256: 1025–1027, 1992.

Cavazos JE, Golarai G, Sutula TP. Mossy fiber synaptic reorganization induced by kindling: time course of development, progression, and permanence. *J Neurosci* 11: 2795–2803, 1991.

Châtillon C-É, Zelmann R, Bortel A, Avoli M, Gotman J. Contact size does not affect high frequency oscillation detection in intracerebral EEG recordings in a rat epilepsy model. *Clin Neurophysiol* 122: 1701–1705, 2011.

Chauvière L, Doublet T, Ghestem A, Siyoucef SS, Wendling F, Huys R, Jirsa V, Bartolomei F, Bernard C. Changes in interictal spike features precede the onset of temporal lobe epilepsy. *Ann Neurol* 71: 805–814, 2012.

Clifford DB, Olney JW, Maniotis A, Collins RC, Zorumski CF. The functional anatomy and pathology of lithium-pilocarpine and high-dose pilocarpine seizures. *Neuroscience* 23: 953–968, 1987.

Coetzee WA, Amarillo Y, Chiu J, Chow A, Lau D, McCormack T, Moreno H, Nadal MS, Ozaita A, Pountney D, Saganich M, Vega-Saenz de Miera E, Rudy B. Molecular diversity of K+ channels. *Ann N Y Acad Sci* 868: 233–285, 1999.

Cohen I, Navarro V, Clemenceau S, Baulac M, Miles R. On the origin of interictal activity in human temporal lobe epilepsy in vitro. *Science* 298: 1418–1421, 2002.

Crépon B, Navarro V, Hasboun D, Clemenceau S, Martinerie J, Baulac M, Adam C, Le Van Quyen M. Mapping interictal oscillations greater than 200 Hz recorded with intracranial macroelectrodes in human epilepsy. *Brain J Neurol* 133: 33–45, 2010.

Curia G, Longo D, Biagini G, Jones RSG, Avoli M. The pilocarpine model of temporal lobe epilepsy. *J Neurosci Methods* 172: 143–157, 2008.

de Curtis M, Avanzini G. Interictal spikes in focal epileptogenesis. *Prog Neurobiol* 63: 541–567, 2001.

Demont-Guignard S, Benquet P, Gerber U, Biraben A, Martin B, Wendling F. Distinct hyperexcitability mechanisms underlie fast ripples and epileptic spikes. *Ann Neurol* 71: 342–352, 2012.

Deutch C, Spencer S, Robbins R, Cicchetti D, Spencer D. Interictal spikes and hippocampal somatostatin levels in temporal lobe epilepsy. *Epilepsia* 32: 174–178, 1991.

Dingledine R, Gjerstad L. Reduced inhibition during epileptiform activity in the in vitro hippocampal slice. *J Physiol* 305: 297–313, 1980.

Draguhn A, Traub RD, Schmitz D, Jefferys JG. Electrical coupling underlies high-frequency oscillations in the hippocampus in vitro. *Nature* 394: 189–192, 1998.

Dreier JP, Heinemann U. Regional and time dependent variations of low Mg2+ induced epileptiform activity in rat temporal cortex slices. *Exp Brain Res* 87: 581–596, 1991.

Dudek FE, Clark S, Williams PA, Grabenstatter HL. Chapter 34 - Kainate-Induced Status Epilepticus: A Chronic Model of Accuired Epilepsy. In: *Models of Seizures and Epilepsy*, edited by Moshé APASL. Burlington: Academic Press, p. 415–432, 2006.

Dudek FE, Staley KJ. The Time Course and Circuit Mechanisms of Acquired Epileptogenesis. In: *Jasper's Basic Mechanisms of the Epilepsies*, edited by Noebels JL, Avoli M, Rogawski MA, Olsen RW, Delgado-Escueta AV. Bethesda (MD): National Center for Biotechnology Information (US), 2012.

Dzhala VI, Staley KJ. Mechanisms of fast ripples in the hippocampus. *J Neurosci* 24: 8896–8906, 2004.

El-Hassar L, Milh M, Wendling F, Ferrand N, Esclapez M, Bernard C. Cell domain-dependent changes in the glutamatergic and GABAergic drives during epileptogenesis in the rat CA1 region. *J Physiol* 578: 193–211, 2007.

Engel J. Introduction to temporal lobe epilepsy. *Epilepsy Res* 26: 141–150, 1996.

Engel J. Natural History of Mesial Temporal Lobe Epilepsy with Hippocampal Sclerosis. In: *Kindling 6*, edited by Corcoran ME, Moshé SL. Springer US, p. 371–384, 2005.

Engel J. Progress in epilepsy: reducing the treatment gap and the promise of biomarkers. *Curr Opin Neurol* 21: 150–154, 2008.

Engel J, Bragin A, Staba R, Mody I. High-frequency oscillations: what is normal and what is not? *Epilepsia* 50: 598–604, 2009.

Engel J, Schwartzkroin PA. Chapter 1 - What Should Be Modeled? [Online]. In: *Models of Seizures and Epilepsy*, edited by Moshé APASL. Academic Press, p. 1–14, 2006.

Engel J, da Silva FL. High-frequency oscillations - where we are and where we need to go. *Prog Neurobiol* 98: 316–318, 2012.

Fastier FN, McDOWALL MA. A comparison of the pharmacological properties of the three isomeric aminopyridines. *Aust J Exp Biol Med Sci* 36: 365–371, 1958.

Fisher RS, Webber WR, Lesser RP, Arroyo S, Uematsu S. High-frequency EEG activity at the start of seizures. *J Clin Neurophysiol* 9: 441–448, 1992.

Foffani G, Uzcategui YG, Gal B, Menendez de la Prida L. Reduced spike-timing reliability correlates with the emergence of fast ripples in the rat epileptic hippocampus. *Neuron* 55: 930–941, 2007.

Fragoso-Veloz J, Massieu L, Alvarado R, Tapia R. Seizures and wet-dog shakes induced by 4-aminopyridine, and their potentiation by nifedipine. *Eur J Pharmacol* 178: 275–284, 1990.

Fragoso-Veloz J, Tapia R. NMDA receptor antagonists protect against seizures and wet-dog shakes induced by 4-aminopyridine. *Eur J Pharmacol* 221: 275–280, 1992.

Gardner AB, Worrell GA, Marsh E, Dlugos D, Litt B. Human and automated detection of high-frequency oscillations in clinical intracranial EEG recordings. *Clin Neurophysiol* 118: 1134–1143, 2007.

Gloor P. *The Temporal Lobe and Limbic System*. New York: Oxford University Press, 1997.

Gotman J. Relationships between interictal spiking and seizures: human and experimental evidence. *Can J Neurol Sci J Can Sci Neurol* 18: 573–576, 1991.

Grasse DW, Karunakaran S, Moxon KA. Neuronal synchrony and the transition to spontaneous seizures. *Exp Neurol* 248: 72–84, 2013.

Gutman GA, Chandy KG, Grissmer S, Lazdunski M, McKinnon D, Pardo LA, Robertson GA, Rudy B, Sanguinetti MC, Stühmer W, Wang X. International Union of Pharmacology. LIII. Nomenclature and molecular relationships of voltage-gated potassium channels. *Pharmacol Rev* 57: 473–508, 2005.

Henderson Z, Lu CB, Janzsó G, Matto N, McKinley CE, Yanagawa Y, Halasy K. Distribution and role of Kv3.1b in neurons in the medial septum diagonal band complex. *Neuroscience* 166: 952–969, 2010.

Holden EW, Thanh Nguyen H, Grossman E, Robinson S, Nelson LS, Gunter MJ, Von Worley A, Thurman DJ. Estimating prevalence, incidence, and disease-related mortality for patients with epilepsy in managed care organizations. *Epilepsia* 46: 311–319, 2005.

Houser CR. Neuronal loss and synaptic reorganization in temporal lobe epilepsy. *Adv Neurol* 79: 743–761, 1999.

Houser CR, Miyashiro JE, Swartz BE, Walsh GO, Rich JR, Delgado-Escueta AV. Altered patterns of dynorphin immunoreactivity suggest mossy fiber reorganization in human hippocampal epilepsy. *J Neurosci* 10: 267–282, 1990.

Huberfeld G, Menendez de la Prida L, Pallud J, Cohen I, Le Van Quyen M, Adam C, Clemenceau S, Baulac M, Miles R. Glutamatergic pre-ictal discharges emerge at the transition to seizure in human epilepsy. *Nat Neurosci* 14: 627–634, 2011.

Huneau C, Demont-Guignard S, Benquet P, Martin B, Wendling F. Time-domain features of epileptic spikes as potential bio-markers of the epileptogenesis process. *Conf Proc Annu Int Conf IEEE Eng Med Biol Soc IEEE Eng Med Biol Soc Annu Conf* 2010: 6007–6010, 2010.

Ibarz JM, Foffani G, Cid E, Inostroza M, Menendez de la Prida L. Emergent dynamics of fast ripples in the epileptic hippocampus. *J Neurosci* 30: 16249–16261, 2010.

Jacobs J, LeVan P, Chander R, Hall J, Dubeau F, Gotman J. Interictal high-frequency oscillations (80-500 Hz) are an indicator of seizure onset areas independent of spikes in the human epileptic brain. *Epilepsia* 49: 1893–1907, 2008.

Jacobs J, Levan P, Châtillon C-E, Olivier A, Dubeau F, Gotman J. High frequency oscillations in intracranial EEGs mark epileptogenicity rather than lesion type. *Brain J Neurol* 132: 1022–1037, 2009a.

Jacobs J, Staba R, Asano E, Otsubo H, Wu JY, Zijlmans M, Mohamed I, Kahane P, Dubeau F, Navarro V, Gotman J. High-frequency oscillations (HFOs) in clinical epilepsy. *Prog Neurobiol* 98: 302–315, 2012.

Jacobs J, Zelmann R, Jirsch J, Chander R, Dubeau C-ECF, Gotman J. High frequency oscillations (80-500 Hz) in the preictal period in patients with focal seizures. *Epilepsia* 50: 1780–1792, 2009b.

Jacobs J, Zijlmans M, Zelmann R, Chatillon C-E, Hall J, Olivier A, Dubeau F, Gotman J. High-frequency electroencephalographic oscillations correlate with outcome of epilepsy surgery. *Ann Neurol* 67: 209–220, 2010.

Jefferys JGR. Advances in understanding basic mechanisms of epilepsy and seizures. *Seizure* 19: 638–646, 2010.

Jefferys JGR, Jiruska P, de Curtis M, Avoli M. Limbic Network Synchronization and Temporal Lobe Epilepsy [Online]. In: *Jasper's Basic Mechanisms of the Epilepsies*, edited by Noebels JL, Avoli M, Rogawski MA, Olsen RW, Delgado-Escueta AV. National Center for Biotechnology Information (US), 2012a.

Jefferys JGR, Menendez de la Prida L, Wendling F, Bragin A, Avoli M, Timofeev I, Lopes da Silva FH. Mechanisms of physiological and epileptic HFO generation. *Prog Neurobiol* 98: 250–264, 2012b.

Jensen MS, Yaari Y. The relationship between interictal and ictal paroxysms in an in vitro model of focal hippocampal epilepsy. *Ann Neurol* 24: 591–598, 1988.

Jirsch JD, Urrestarazu E, LeVan P, Olivier A, Dubeau F, Gotman J. High-frequency oscillations during human focal seizures. *Brain J Neurol* 129: 1593–1608, 2006.

Jiruska P, Csicsvari J, Powell AD, Fox JE, Chang W-C, Vreugdenhil M, Li X, Palus M, Bujan AF, Dearden RW, Jefferys JGR. High-frequency network activity, global increase in neuronal activity, and synchrony expansion precede epileptic seizures in vitro. *J Neurosci* 30: 5690–5701, 2010a.

Jiruska P, Finnerty GT, Powell AD, Lofti N, Cmejla R, Jefferys JGR. Epileptic high-frequency network activity in a model of non-lesional temporal lobe epilepsy. *Brain J Neurol* 133: 1380–1390, 2010b.

Jiruska P, Powell AD, Chang W-C, Jefferys JGR. Electrographic high-frequency activity and epilepsy. *Epilepsy Res* 89: 60–65, 2010c.

Jones RS, Lambert JD. The role of excitatory amino acid receptors in the propagation of epileptiform discharges from the entorhinal cortex to the dentate gyrus in vitro. *Exp Brain Res* 80: 310–322, 1990.

Khosravani H, Pinnegar CR, Mitchell JR, Bardakjian BL, Federico P, Carlen PL. Increased high-frequency oscillations precede in vitro low-^{Mg} seizures. *Epilepsia* 46: 1188–1197, 2005.

Kitchigina VF, Butuzova MV. Theta activity of septal neurons during different epileptic phases: the same frequency but different significance? *Exp Neurol* 216: 449–458, 2009.

Klausberger T. GABAergic interneurons targeting dendrites of pyramidal cells in the CA1 area of the hippocampus. *Eur J Neurosci* 30: 947–957, 2009.

Kobayashi K, Oka M, Akiyama T, Inoue T, Abiru K, Ogino T, Yoshinaga H, Ohtsuka Y, Oka E. Very fast rhythmic activity on scalp EEG associated with epileptic spasms. *Epilepsia* 45: 488–496, 2004.

Köhling R, Lücke A, Straub H, Speckmann EJ, Tuxhorn I, Wolf P, Pannek H, Oppel F. Spontaneous sharp waves in human neocortical slices excised from epileptic patients. *Brain J Neurol* 121 (Pt 6): 1073–1087, 1998.

Köhling R, Staley K. Network mechanisms for fast ripple activity in epileptic tissue. *Epilepsy Res* 97: 318–323, 2011.

Le Gal La Salle G, Cavalheiro EA. Stimulation of septal and amygdaloid nuclei: EEG and behavioral responses during early development of kindling with special reference to wet dog shakes. *Exp Neurol* 74: 717–727, 1981.

Lerner-Natoli M, Rondouin G, Baldy-Moulinier M. Evolution of wet dog shakes during kindling in rats: comparison between hippocampal and amygdala kindling. *Exp Neurol* 83: 1–12, 1984.

Leung LS, Shen B. Hippocampal partial kindling decreased hippocampal GABAB receptor efficacy and wet dog shakes in rats. *Behav Brain Res* 173: 274–281, 2006.

Lévesque M, Avoli M. The kainic acid model of temporal lobe epilepsy. *Neurosci Biobehav Rev* 37: 2887–2899, 2013.

Lévesque M, Bortel A, Gotman J, Avoli M. High-frequency (80-500 Hz) oscillations and epileptogenesis in temporal lobe epilepsy. *Neurobiol Dis* 42: 231–241, 2011.

Lévesque M, Salami P, Behr C, Avoli M. Temporal lobe epileptiform activity following systemic administration of 4-aminopyridine in rats. *Epilepsia* 54: 596–604, 2013.

Lévesque M, Salami P, Gotman J, Avoli M. Two seizure-onset types reveal specific patterns of high-frequency oscillations in a model of temporal lobe epilepsy. *J Neurosci* 32: 13264–13272, 2012.

Lieb JP, Engel J, Brown WJ, Gevins AS, Crandall PH. Neuropathological findings following temporal lobectomy related to surface and deep EEG patterns. *Epilepsia* 22: 539–549, 1981.

Lopantsev V, Avoli M. Laminar organization of epileptiform discharges in the rat entorhinal cortex in vitro. *J Physiol* 509 (Pt 3): 785–796, 1998a.

Lopantsev V, Avoli M. Participation of GABAA-mediated inhibition in ictallike discharges in the rat entorhinal cortex. *J Neurophysiol* 79: 352–360, 1998b.

Löscher W. Animal models of epilepsy for the development of antiepileptogenic and disease-modifying drugs. A comparison of the pharmacology of kindling and post-status epilepticus models of temporal lobe epilepsy. *Epilepsy Res* 50: 105–123, 2002.

Martin BS, Kapur J. A combination of ketamine and diazepam synergistically controls refractory status epilepticus induced by cholinergic stimulation. *Epilepsia* 49: 248–255, 2008.

Martín ED, Pozo MA. Valproate suppresses status epilepticus induced by 4-aminopyridine in CA1 hippocampus region. *Epilepsia* 44: 1375–1379, 2003.

Matsumoto A, Brinkmann BH, Matthew Stead S, Matsumoto J, Kucewicz MT, Marsh WR, Meyer F, Worrell G. Pathological and physiological high-frequency oscillations in focal human epilepsy. *J Neurophysiol* 110: 1958–1964, 2013.

Medina-Ceja L, Cordero-Romero A, Morales-Villagrán A. Antiepileptic effect of carbenoxolone on seizures induced by 4-aminopyridine: a study in the rat hippocampus and entorhinal cortex. *Brain Res* 1187: 74–81, 2008.

Medina-Ceja L, Ventura-Mejía C. Differential effects of trimethylamine and quinine on seizures induced by 4-aminopyridine administration in the entorhinal cortex of vigilant rats. *Seizure* 19: 507–513, 2010.

Melani F, Zelmann R, Dubeau F, Gotman J. Occurrence of scalp-fast oscillations among patients with different spiking rate and their role as epileptogenicity marker. *Epilepsy Res* 106: 345–356, 2013.

Menendez de la Prida LM, Totterdell S, Gigg J, Miles R. The subiculum comes of age. *Hippocampus* 16: 916–923, 2006.

Menendez de la Prida L, Trevelyan AJ. Cellular mechanisms of high frequency oscillations in epilepsy: on the diverse sources of pathological activities. *Epilepsy Res* 97: 308–317, 2011.

Mihály A, Bencsik K, Solymosi T. Naltrexone potentiates 4-aminopyridine seizures in the rat. *J Neural Transm Gen Sect* 79: 59–67, 1990.

Miller RD. Recent developments with muscles relaxants and their antagonists. *Can Anaesth Soc J* 26: 83–93, 1979.

Ogren JA, Bragin A, Wilson CL, Hoftman GD, Lin JJ, Dutton RA, Fields TA, Toga AW, Thompson PM, Engel J, Staba RJ. Three-dimensional hippocampal atrophy maps distinguish two common temporal lobe seizure-onset patterns. *Epilepsia* 50: 1361–1370, 2009a.

Ogren JA, Wilson CL, Bragin A, Lin JJ, Salamon N, Dutton RA, Luders E, Fields TA, Fried I, Toga AW, Thompson PM, Engel J, Staba RJ. Three-dimensional surface maps link local atrophy and fast ripples in human epileptic hippocampus. *Ann Neurol* 66: 783–791, 2009b.

Ono T, Galanopoulou AS. Epilepsy and epileptic syndrome. *Adv Exp Med Biol* 724: 99–113, 2012.

Panuccio G, Sanchez G, Lévesque M, Salami P, de Curtis M, Avoli M. On the ictogenic properties of the piriform cortex in vitro. *Epilepsia* 53: 459–468, 2012.

Park YD, Murro AM, King DW, Gallagher BB, Smith JR, Yaghmai F. The significance of ictal depth EEG patterns in patients with temporal lobe epilepsy. *Electroencephalogr Clin Neurophysiol* 99: 412–415, 1996.

Paxinos G, Watson C. *The Rat Brain in Stereotaxic Coordinates, Fourth Edition*. 4 edition. San Diego: Academic Press, 1998.

Perucca P, Dubeau F, Gotman J. Intracranial electroencephalographic seizure-onset patterns: effect of underlying pathology. *Brain J Neurol* 137: 183–196, 2014.

Pitkänen A, Schwartzkroin PA, Moshé SL. *Models of Seizures and Epilepsy*. Academic Press, 2005.

Pitkänen A, Sutula TP. Is epilepsy a progressive disorder? Prospects for new therapeutic approaches in temporal-lobe epilepsy. *Lancet Neurol* 1: 173–181, 2002.

Popova IY, Sinelnikova VV, Kitchigina VF. Disturbance of the correlation between hippocampal and septal EEGs during epileptogenesis. *Neurosci Lett* 442: 228–233, 2008.

Racine RJ. Modification of seizure activity by electrical stimulation. II. Motor seizure. *Electroencephalogr Clin Neurophysiol* 32: 281–294, 1972.

Rutecki PA, Grossman RG, Armstrong D, Irish-Loewen S. Electrophysiological connections between the hippocampus and entorhinal cortex in patients with complex partial seizures. *J Neurosurg* 70: 667–675, 1989.

Salami P, Lévesque M, Benini R, Behr C, Gotman J, Avoli M. Dynamics of interictal spikes and high-frequency oscillations during epileptogenesis in temporal lobe epilepsy. *Neurobiol Dis* 67: 97–106, 2014.

Salami P, Lévesque M, Gotman J, Avoli M. A comparison between automated detection methods of high-frequency oscillations (80-500 Hz) during seizures. *J Neurosci Methods* 211: 265–271, 2012.

Salami P, Lévesque M, Gotman J, Avoli M. Distinct EEG seizure patterns reflect different seizure generation mechanisms. *J. Neurophysiol* 113:2840-2844, 2015.

Salanova V, Markand ON, Worth R. Clinical characteristics and predictive factors in 98 patients with complex partial seizures treated with temporal resection. *Arch Neurol* 51: 1008–1013, 1994.

Schwam E. Severe accidental overdose of 4-aminopyridine due to a compounding pharmacy error. *J Emerg Med* 41: 51–54, 2011.

Schwartzkroin PA, Prince DA. Changes in excitatory and inhibitory synaptic potentials leading to epileptogenic activity. *Brain Res* 183: 61–76, 1980.

Shiri Z, Manseau F, Lévesque M, Williams S, Avoli M. Interneuron activity leads to initiation of low-voltage fast-onset seizures. *Ann Neurol* 77: 541–546, 2015.

Smart SL, Lopantsev V, Zhang CL, Robbins CA, Wang H, Chiu SY, Schwartzkroin PA, Messing A, Tempel BL. Deletion of the K(V)1.1 potassium channel causes epilepsy in mice. *Neuron* 20: 809–819, 1998.

Smith KL, Swann JW. Carbamazepine suppresses synchronized afterdischarging in disinhibited immature rat hippocampus in vitro. *Brain Res* 400: 371–376, 1987.

Spencer SS, Kim J, Spencer DD. Ictal spikes: a marker of specific hippocampal cell loss. *Electroencephalogr Clin Neurophysiol* 83: 104–111, 1992.

Spencer SS, Spencer DD. Entorhinal-hippocampal interactions in medial temporal lobe epilepsy. *Epilepsia* 35: 721–727, 1994.

Staba RJ, Bragin A. High-frequency oscillations and other electrophysiological biomarkers of epilepsy: underlying mechanisms. *Biomark Med* 5: 545–556, 2011.

Staba RJ, Frighetto L, Behnke EJ, Mathern GW, Fields T, Bragin A, Ogren J, Fried I, Wilson CL, Engel J. Increased fast ripple to ripple ratios correlate with reduced hippocampal volumes and neuron loss in temporal lobe epilepsy patients. *Epilepsia* 48: 2130–2138, 2007.

Staba RJ, Stead M, Worrell GA. Electrophysiological biomarkers of epilepsy. *Neurother J Am Soc Exp Neurother* 11: 334–346, 2014.

Staba RJ, Wilson CL, Bragin A, Fried I, Engel J. Quantitative analysis of high-frequency oscillations (80-500 Hz) recorded in human epileptic hippocampus and entorhinal cortex. *J Neurophysiol* 88: 1743–1752, 2002.

Staba RJ, Wilson CL, Bragin A, Jhung D, Fried I, Engel J. High-frequency oscillations recorded in human medial temporal lobe during sleep. *Ann Neurol* 56: 108–115, 2004.

Staley KJ, White A, Dudek FE. Interictal spikes: harbingers or causes of epilepsy? *Neurosci Lett* 497: 247–250, 2011.

Stringer JL, Lothman EW. Reverberatory seizure discharges in hippocampal-parahippocampal circuits. *Exp Neurol* 116: 198–203, 1992.

Sutula T, Cavazos J, Golarai G. Alteration of long-lasting structural and functional effects of kainic acid in the hippocampus by brief treatment with phenobarbital. *J Neurosci*12: 4173–4187, 1992.

Szente M, Pongrácz F. Aminopyridine-induced seizure activity. *Electroencephalogr Clin Neurophysiol* 46: 605–608, 1979.

Toyoda I, Bower MR, Leyva F, Buckmaster PS. Early activation of ventral hippocampus and subiculum during spontaneous seizures in a rat model of temporal lobe epilepsy. *J Neurosci* 33: 11100–11115, 2013.

Traub RD, Duncan R, Russell AJC, Baldeweg T, Tu Y, Cunningham MO, Whittington MA. Spatiotemporal patterns of electrocorticographic very fast oscillations (> 80 Hz) consistent with a network model based on electrical coupling between principal neurons. *Epilepsia* 51: 1587–1597, 2010.

Traub RD, Whittington MA, Buhl EH, LeBeau FE, Bibbig A, Boyd S, Cross H, Baldeweg T. A possible role for gap junctions in generation of very fast EEG oscillations preceding the onset of, and perhaps initiating, seizures. *Epilepsia* 42: 153–170, 2001.

Traub RD, Wong RK. Cellular mechanism of neuronal synchronization in epilepsy. *Science* 216: 745–747, 1982.

Tuff LP, Racine RJ, Mishra RK. The effects of kindling on GABA-mediated inhibition in the dentate gyrus of the rat. II. Receptor binding. *Brain Res* 277: 91–98, 1983.

Turski WA, Cavalheiro EA, Schwarz M, Czuczwar SJ, Kleinrok Z, Turski L. Limbic seizures produced by pilocarpine in rats: behavioural, electroencephalographic and neuropathological study. *Behav Brain Res* 9: 315–335, 1983.

Urrestarazu E, Chander R, Dubeau F, Gotman J. Interictal high-frequency oscillations (100-500 Hz) in the intracerebral EEG of epileptic patients. *Brain J Neurol* 130: 2354–2366, 2007.

Urrestarazu E, Jirsch JD, LeVan P, Hall J, Avoli M, Dubeau F, Gotman J. High-frequency intracerebral EEG activity (100-500 Hz) following interictal spikes. *Epilepsia* 47: 1465–1476, 2006.

Velasco AL, Wilson CL, Babb TL, Engel J. Functional and anatomic correlates of two frequently observed temporal lobe seizure-onset patterns. *Neural Plast* 7: 49–63, 2000.

Velíšek L. Chapter 11 - Models of Chemically- Induced Acute Seizures [Online]. In: *Models of Seizures and Epilepsy*. Academic Press, p. 127–152, 2006.

Vicedomini JP, Nadler JV. A model of status epilepticus based on electrical stimulation of hippocampal afferent pathways. *Exp Neurol* 96: 681–691, 1987.

Világi I, Dobó E, Borbély S, Czégé D, Molnár E, Mihály A. Repeated 4-aminopyridine induced seizures diminish the efficacy of glutamatergic transmission in the neocortex. *Exp Neurol* 219: 136–145, 2009.

Wang H-L, Xiang X-H, Guo Y, Wu W-R, Cao D-Y, Wang H-S, Zhao Y. Ionotropic glutamatergic neurotransmission in the ventral tegmental area modulates DeltaFosB expression in the nucleus accumbens and abstinence syndrome in morphine withdrawal rats. *Eur J Pharmacol* 527: 94–104, 2005.

Wang S, Wang IZ, Bulacio JC, Mosher JC, Gonzalez-Martinez J, Alexopoulos AV, Najm IM, So NK. Ripple classification helps to localize the seizure-onset zone in neocortical epilepsy. *Epilepsia* 54: 370–376, 2013.

Wickenden AD. Potassium channels as anti-epileptic drug targets. *Neuropharmacology* 43: 1055–1060, 2002.

Worrell GA, Jerbi K, Kobayashi K, Lina JM, Zelmann R, Le Van Quyen M. Recording and analysis techniques for high-frequency oscillations. *Prog Neurobiol* 98: 265–278, 2012.

Wu JY, Sankar R, Lerner JT, Matsumoto JH, Vinters HV, Mathern GW. Removing interictal fast ripples on electrocorticography linked with seizure freedom in children. *Neurology* 75: 1686–1694, 2010.

Yao JA, Tseng GN. Modulation of 4-AP block of a mammalian A-type K channel clone by channel gating and membrane voltage. *Biophys J* 67: 130–142, 1994.

Yekhlef L, Breschi GL, Lagostena L, Russo G, Taverna S. Selective activation of parvalbumin- or somatostatin-expressing interneurons triggers epileptic seizure like activity in mouse medial entorhinal cortex. *J Neurophysiol* 113: 1616–1630, 2015.

Ylinen A, Bragin A, Nádasdy Z, Jandó G, Szabó I, Sik A, Buzsáki G. Sharp wave-associated high-frequency oscillation (200 Hz) in the intact hippocampus: network and intracellular mechanisms. *J Neurosci* 15: 30–46, 1995.

Zelmann R, Mari F, Jacobs J, Zijlmans M, Dubeau F, Gotman J. A comparison between detectors of high frequency oscillations. *Clin Neurophysiol* 123: 106–116, 2012.

Zhang L, McBain CJ. Potassium conductances underlying repolarization and after-hyperpolarization in rat CA1 hippocampal interneurones. *J Physiol* 488 (Pt 3): 661–672, 1995.

Zijlmans M, Jacobs J, Kahn YU, Zelmann R, Dubeau F, Gotman J. Ictal and interictal high frequency oscillations in patients with focal epilepsy. *Clin Neurophysiol* 122: 664–671, 2011.

Zijlmans M, Jacobs J, Zelmann R, Dubeau F, Gotman J. High-frequency oscillations mirror disease activity in patients with epilepsy. *Neurology* 72: 979–986, 2009a.

Zijlmans M, Jacobs J, Zelmann R, Dubeau F, Gotman J. High frequency oscillations and seizure frequency in patients with focal epilepsy. *Epilepsy Res* 85: 287–292, 2009b.

Zijlmans M, Jiruska P, Zelmann R, Leijten FSS, Jefferys JGR, Gotman J. High-frequency oscillations as a new biomarker in epilepsy. *Ann Neurol* 71: 169–178, 2012.